Summer 2010

Solid oxide fuel cell electrode characterization and improvement for fuel flexibility and supplemental power production

Isaiah D. Kellogg

Department: Mechanical and Aerospace Engineering

SOLID OXIDE FUEL CELL ELECTRODE CHARACTERIZATION AND IMPROVEMENT FOR FUEL FLEXIBILITY AND SUPPLEMENTAL POWER PRODUCTION

by

ISAIAH DANIEL KELLOGG

A DISSERTATION

Presented to the Faculty of the Graduate School of the

MISSOURI UNIVERSITY OF SCIENCE AND TECHNOLOGY

In Partial Fulfillment of the Requirements for the Degree

DOCTOR OF PHILOSOPHY

in

MECHANICAL ENGINEERING

2010

Approved by

Umit O. Koylu, Advisor
Fatih Dogan, Advisor
Kelly O. Homan
William G. Fahrenholtz
Matthew J. O'Keefe

ABSTRACT

Solid oxide fuel cells (SOFC) were fabricated and the electrodes tested for their individual catalytic effectiveness in various fuels by exposing each electrode to mixed gas while the opposite electrode was exposed to its respective pure gas. Mixed hydrogen and oxygen gas was successfully utilized as fuel in a single chamber SOFC (SC-SOFC). The conditions at which the porous nickel-yttria-stabilized zirconia (Ni-YSZ) cermet anode performed well did not significantly overlap the conditions at which the $La_{0.8}Sr_{0.2}Fe_{0.8}Co_{0.2}$ oxide (LSCF) cathode performed well, but there was significant catalytic activity at both electrodes which increased the open circuit voltage (OCV) beyond that predicted by the Nernst equation. The results of these tests, and future tests of similar format, could be useful in the development of SC-SOFC electrode catalysts.

Pyrolytic carbon was used as fuel in a SOFC with a YSZ electrolyte and a bi-layer anode composed of nickel gadolinia-doped ceria (Ni-GDC) and Ni-YSZ. The common problems of bulk shrinkage and emergent porosity in the YSZ layer adjacent to the GDC/YSZ interface were avoided by using an interlayer of porous Ni-YSZ as a buffer anode layer between the electrolyte and the Ni-GDC primary anode. Cells were fabricated from commercially available component powders so that unconventional production methods suggested in the literature were avoided. A cell of similar construction was used with externally applied acetylene flame soot as fuel so that soot captured at the exhaust of a diesel engine could be utilized for secondary power generation in a SOFC while decreasing particulate pollution without the need for filter regeneration.

ACKNOWLEDGMENTS

The author would like to express his gratitude for the guidance, support, and patience of his advisors, Dr. Umit O. Koylu, and Dr. Fatih Dogan. The author is also grateful for the experience and assistance of his advisory committee, Dr. Kelly O. Homan, Dr. William G. Fahrenholtz, and Dr. Matthew J. O'Keefe.

Gratitude is extended as well to Dr. Vladimir Petrovsky and Dr. Piotr Jasinski for their depth of knowledge and to Ayhan Sarikaya for his SEM assistance and materials experience.

Thanks are also due the U. S. Department of Education for financial support through the Graduate Assistance in Areas of National Need (GAANN) Fellowship.

TABLE OF CONTENTS

LIST OF ILLUSTRATIONS

LIST OF TABLES

NOMENCLATURE

Term	Description
SOFC	solid oxide fuel cell
OCV	open-circuit voltage
F	Faraday constant
R	universal gas constant
pO_2	oxygen partial pressure
SC-SOFC	single-chamber solid oxide fuel cell
EMF	electromotive force
LSCF	$La_{0.8}Sr_{0.2}Fe_{0.8}Co_{0.2}$
redox	reduction/oxidation
YSZ	yttria-stabilized zirconia
GDC	gadolinia-doped ceria
DPF	diesel particulate filter
$\Delta G°$	standard Gibbs free energy
K	equilibrium constant
OCV_{mga}	open circuit voltage with mixed gas on the anode
OCV_{mgc}	open circuit voltage with mixed gas on the cathode
OCV_{DC}	open circuit voltage in double chamber configuration
$OCV_{SCestimate}$	open circuit voltage estimate for single-chamber
PM	particulate material

1. INTRODUCTION

Internal combustion engines have powered transportation by an overwhelming majority in the last century, but both dwindling fossil fuel reserves and rising awareness of pollution are increasing interest in technologies which use renewable energy sources or more efficiently utilize current fossil fuels. A solid oxide fuel cell (SOFC) is a solid state device to convert chemical energy from a wide variety of liquid and gaseous fuels directly into electrical energy, without the efficiency limits imposed by the thermodynamic heat cycles of an internal combustion engine, such as the idealized Carnot cycle. SOFCs are uniquely suited to use both hydrogen, which can be generated from many sustainable "green" energy sources such as solar or wind, or to scavenge energy from unburned fuel in the exhaust of an internal combustion engine [1].

1.1. BACKGROUND AND MOTIVATION

This research is part of the continuing research at the Missouri University of Science and Technology which is intended to improve the performance and evaluation techniques for fuel cells. These goals include enhancing catalytic effectiveness of anodes and cathodes, increasing ionic conductivity and physical strength of electrolytes, improving fabrication methods for better physical strength and electrochemical performance, and improved characterization of fuel cell performance; all of which lead toward increasing the economic and practical viability of fuel cells in the transportation and electrical generation market.

While SOFCs have the potential for high efficiency and extraordinary fuel flexibility, there are several hurdles which prevent them from being widely

commercially-viable in their current state. In order to understand and overcome some of these shortcomings, background information on the construction and function of SOFCs is given below, followed by the objectives of the studies presented here.

1.1.1. Solid Oxide Fuel Cell. A SOFC uses an oxygen-conducting electrolyte to separate fuel and oxygen, which creates a difference in oxygen partial pressure across the electrolyte. A double-chamber SOFC, which uses the electrolyte to physically separate the gases into two distinct chambers as shown in Figure 1.1, is the most common configuration. Because the SOFC is composed of metal oxides that contain oxygen as O^{2-} ions in a crystal matrix, the oxygen partial pressure is expressed as oxygen ion activity. The difference in negatively-charged oxygen ion (O^{2-}) concentration across the electrolyte is expressed as the open-circuit voltage (OCV) in equation 1, known as the Nernst equation, where F is the Faraday constant, R is the universal gas constant, T is the temperature in Kelvin, and pO_2 is the oxygen partial pressure.

$$OCV = \frac{1}{4F} RT \ln\left(\frac{pO_2^{cathode}}{pO_2^{anode}}\right) \quad (1)$$

Part of the anode, which is exposed to fuel, readily gives up its O^{2-} ions to the fuel and reduces to its component metal while the O^{2-} oxidizes the fuel, freeing its two electrons and creating an oxygen vacancy in the crystal lattice. More O^{2-} ions diffuse through the crystal lattice from the electrolyte, which can be alternatively considered as oxygen vacancies diffusing from the anode to the electrolyte. Equation 2 gives the example of the anode reaction in a SOFC using hydrogen as fuel. As oxygen vacancies

diffuse into the cathode, the cathode material begins to reduce by giving up O^{2-} from its crystal matrix to the electrolyte, but because it is exposed to oxygen gas and electrons, it quickly converts oxygen gas into O^{2-} ions to re-oxidize itself, as shown in equation 3. This process provides continuous electrical power as long as the fuel and oxygen are supplied to the cell.

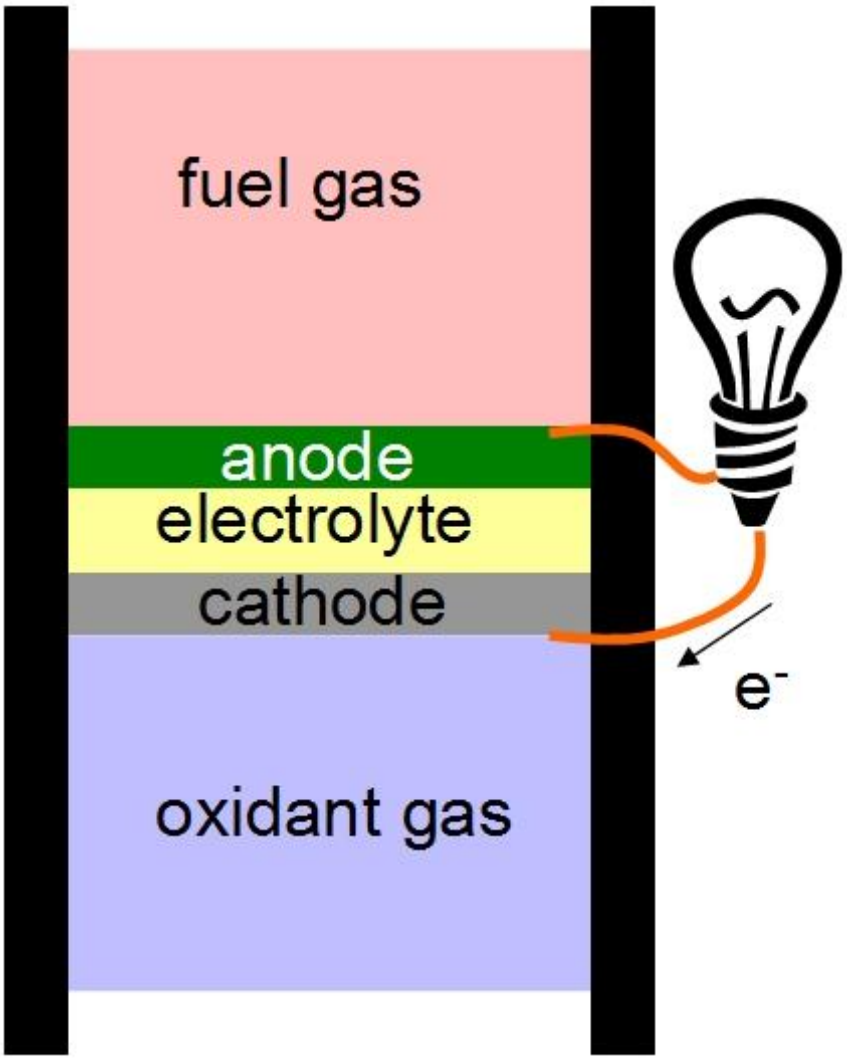

Figure 1.1. Main components of a solid oxide fuel cell

$$H_2 + O^{2-} \rightarrow H_2O + 2e^- \quad (2)$$

$$\tfrac{1}{2}O_2 + 2e^- \rightarrow O^{2-} \quad (3)$$

1.1.2. Single-Chamber SOFC. While a traditional double chamber SOFC uses the electrolyte to physically separate the fuel and oxygen, a single chamber SOFC (SC-SOFC), illustrated in Figure 1.2, is immersed in a single flow of mixed fuel and oxygen, and relies on catalytic selectivity of the anode and cathode to provide the difference in oxygen ion activity. An anode for a SC-SOFC which uses hydrogen for fuel must have high catalytic activity for the reaction in equation 2 but not catalyze equation 3, and likewise the cathode must catalyze the reaction in equation 3 but not equation 2.

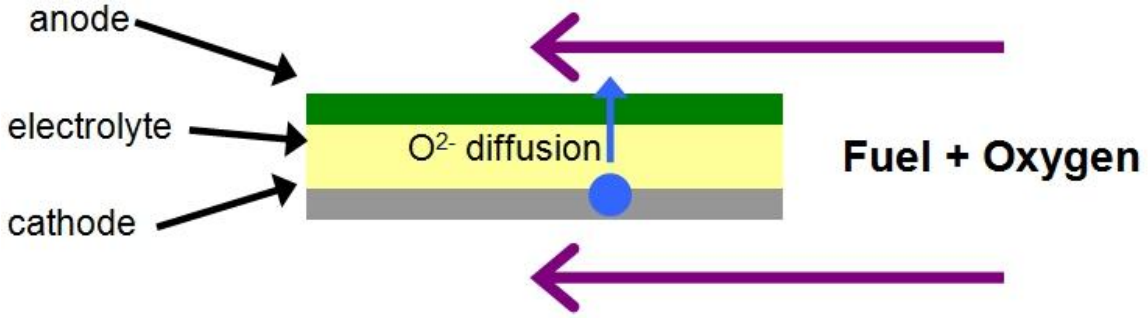

Figure 1.2. Schematic of a single chamber SOFC

A single chamber solid oxide fuel cell provides several advantages over the conventional double chamber SOFC, such as simplified cell structure with no sealing

required and direct use of hydrocarbon fuel [2,3]. The oxygen activity at the electrodes of the SC-SOFC is not fixed and the anode has a higher electrocatalytic activity for the oxidation of the fuel than the cathode. Oxidation reactions of a hydrocarbon fuel can be represented with a simplified multistep, quasi-general mechanism as follows in equations 4-6.

$$C_n H_m + \tfrac{n}{2} O_2 \rightarrow nCO + \tfrac{m}{2} H_2 \quad (4)$$

$$H_2 + O^{2-} \rightarrow H_2O + 2e^- \quad (5)$$

$$CO + O^{2-} \rightarrow CO_2 + 2e^- \quad (6)$$

These reactions lead to a low oxygen partial pressure at the anode locally, while the oxygen partial pressure at the cathode remains relatively high. As a result, an electromotive force (EMF) between two electrodes is generated using a mixed gas of fuel and air. Another advantage of SC-SOFC is that it converts hydrocarbon fuels into hydrogen and other reaction products in addition to electrical power generation. Hence, SC-SOFC has a potential for co-generation of hydrogen and electrical power simultaneously by controlling the reaction in equation 4.

If the electrode materials are not sufficiently selective, a parasitic reaction creates mixed potentials at the electrodes that reduces the efficiency of the cell. The electrode materials must not only be selective but also impede unwanted fuel reactions [4]. Compared to traditional double chamber fuel cells, parasitic reactions in a single chamber

fuel cell have historically decreased the open circuit voltage (OCV) by about half [5]. This is analogous to a leak that allows the fuel to seep into the oxidizer side of a double chamber fuel cell. Another concern is that the SC-SOFC operates in a narrow range of oxygen partial pressures that are near the ranges where both Ni-based anodes and $La_{0.8}Sr_{0.2}Fe_{0.8}Co_{0.2}$ oxide (LSCF) based cathodes may undergo undesirable oxidation/reduction reactions, although new research is directed towards creating more reduction/oxidation (redox) stable electrodes [6,7]. While the current choices of selective electrode materials are relatively poor, recent advances in materials have helped narrow the performance gap between double and single chamber fuel cells.

An ideal SC-SOFC has the same OCV and current-voltage discharge profile (I-V) as a double chamber cell, given a uniform oxygen partial pressure. A difference in catalytic properties of the electrodes must be sufficient to cause a substantial difference in oxygen partial pressure between the electrodes. For the ideal SC-SOFC, one electrode would be reversible toward oxygen adsorption and inert to fuel, while the other electrode would be reversible toward fuel adsorption and completely inert to oxygen [8]. Advances in electrode catalyst materials are needed for SC-SOFC to have the same performance as conventional double chamber SOFC with a significant reduction in complexity and cost.

1.2. LITERATURE REVIEW

A large amount of research has been focused into solid oxide fuel cells, and the most relevant literature is discussed here, divided into three sections corresponding to the three research areas discussed in this thesis; single chamber SOFC, SOFC for use with

solid carbon fuel, and a solid carbon fuelled SOFC for potentially generating auxiliary power while decreasing particulate pollution from various combustion systems.

1.2.1. Single-Chamber Solid Oxide Fuel Cells. In order to increase the effectiveness of SC-SOFC, previous research has explored various possibilities including quantification of electrode catalytic activity [9,10] and detailed studies of oxygen reduction in the cathode [11] as well as enhancing electrode performance by adding new dopants [12,13,14].

Other studies have investigated improved measurement techniques for impedance [15], temperature [16], electrolyte characterization [17], fabrication at lower temperatures [18], and simpler fabrication processes [19]. Some groups have pursued novel configurations such as electrolyte supported cells in different configurations [20,21] sharing a common electrolyte, or different electrolyte materials for lower temperature use such as ceria instead of zirconia [2]. One way to make the electrolyte thinner and less resistive is to use a thin electrolyte film on a structurally supportive anode [22,23,24], while the less reducing mixed-gas environment opens up alternative electrolyte materials [25,26]. Some research has looked into improving existing electrolyte materials with added oxide layers [27], or an entirely different class of electrolyte that conducts protons instead of negatively charged oxygen ions [28]. Efficiency could be significantly improved with a thermally self-sustaining cell heated only by the exothermic reaction at the anode [29,3].

Significant research has focused on characterizing and improving Ni anodes, including determining stability in a wide range of gas mixtures, current loads [30], and temperatures [31], calculations of oxidation/reduction kinetics [7], improved processing

methods such as backfilling a yttria-stabilized zirconia (YSZ) [32] or gadolinia-doped ceria (GDC) [33] skeleton with a Ni precursor for co-firing the anode with the electrolyte, while others have methodically varied anode thickness and sintering techniques [34]. Some research has taken a different direction with attempts to eliminate Ni entirely to avoid issues with redox instability [6].

Other research has focused on the catalytic ability of the electrodes specifically for single chamber use, where the selectivity of the electrodes is particularly important [4] and found that traditional cathode materials are better than they should be at oxidizing fuel [35,36], and not as good as they should be at reducing oxygen [37]; attempts to remedy this have included backfilling a common cathode with mixtures of different perovskite oxides [38].

1.2.2. SOFC for Utilization of Solid Carbon Fuel. With the push for fuel flexibility, many groups worked on the ability of a SOFC to directly utilize hydrocarbons [39] without the necessity of reforming the fuel into hydrogen, which even if done internally can leave carbon deposits [40]. Some groups studied how to decrease carbon deposition with direct use of hydrocarbon fuel [41,42], or where the deposition takes place [43] while others focused on using the carbon as fuel [44].

With the possibility of solid carbon as fuel, research commenced into better catalysts such as Ni and GDC [45,46] which works almost nine times better than the more traditional Ni and YSZ. With a solid understanding of the reaction mechanism [47], and how the anode works [48], cells can be made to draw significant amounts of power from solid carbon [49]. Kinetics research [43] helps determine areas to focus future research for cell improvement.

However, new materials present new challenges, and GDC is not compatible with YSZ, while there are methods to make it possible, none are both simple and effective [50], though mass production can make some methods practical [51].

1.2.3. Diesel Particulate Filter Improvement. Much of the research on transportation energy is focused on short-term goals such as decreasing pollution with existing internal-combustion energy technology, and diesel particulate filters (DPF) are a large part of that vision due to the number of diesel engines in use now and in the foreseeable future. Research on DPFs has focused on three main areas; characterization of particulates, improved filtering, and improved regeneration.

In order to better understand the requirements for a filter, the particulate in question must be well understood. Soot has been characterized by size and mobility [52,53] and this characterization continues for newer, cleaner engines [54] which output less particulate mass but more smaller particles that are more harmful to human health. Other research has focused on how the exhaust flow changes the loading of a filter [55] or the character of particulates [56] or other pollutants [57] released during regeneration.

The high temperatures of a diesel engine exhaust limits the selection of materials, but some studies have looked at using high temperature metal foam [58] or contamination-resistant ceramics like mullite [59]. The requirement for minimal exhaust backpressure spurs research into new structures, such as whisker-shaped growths of cordierite [60], or simulations of fluid flow through a clogged filter [61].

Cleaning a DPF clogged with soot is accomplished by a process called regeneration, usually achieved by dumping fuel into the exhaust which burns and raises the temperature high enough to burn off the carbon, but that requires higher temperature

materials, wastes fuel, and releases other pollutants [56,57]. Research has found that the microstructure of the soot affects the regeneration capabilities, while regeneration changes the microstructure as a result of the oxidation process [62]. Alternate regeneration methods being researched include microwave heating of the DPF to save fuel [63], injection of plasma-generated highly reactive ozone into the DPF to oxidize the soot at lower temperature [64], and direct injection of non-thermal plasma [65]. Other research subjects include addition of a catalyst directly to the diesel fuel itself [66].

1.3. THESIS OBJECTIVES

This study is composed of three parts, each leading toward the goal of improved electrode design and use, with each part summarized below. The first part is a new method for electrode characterization, the second part is a new application method for anodes incompatible with a YSZ electrolyte, and the third part is a new use for a SOFC capable of use with solid carbon fuel.

1.3.1. Evaluation of Individual Electrode Effectiveness in Single-Chamber SOFC with Hydrogen/Air Feed Gas. In a SOFC, the difference in electrode potential is created by separating fuel gas from oxygen gas to create a difference in oxygen ion activity across the ion-conducting electrolyte, but unlike a double-chamber SOFC which provides physical separation between the gases, a SC-SOFC operates in a uniform mixture of fuel and oxygen.

Therefore, the generation of voltage relies on the catalytic effectiveness of each electrode to change the oxygen ion activity; the cathode must increase the oxygen ion

activity at the cathode/electrolyte interface, while the anode is required to decrease the oxygen ion activity at the anode/electrolyte interface.

However, directly measuring the catalytic effectiveness of a material for a particular reaction is very difficult and the results may not be applicable outside the scope of the experiment itself. Therefore a method to determine the effectiveness of electrode catalysts in situ is necessary, but the performance of a cell is affected by both electrodes simultaneously. This study isolates the electrodes by only exposing one at a time to mixed gas, which minimizes the catalytic contribution necessary for the opposing electrode. The measured results are supported by a prediction of voltage in single-chamber configuration which is closely matched by tests. A new explanation for a phenomenon, which is detected in an environment in which the commonly accepted mechanism is impossible, is presented.

1.3.2. Fabrication of a SOFC with a Gadolinia-Doped Ceria Anode on Yttria-Stabilized Zirconia Electrolyte and Use of Solid Carbon Fuel. One of the primary advantages of a SOFC is the ability to use a wide variety of fuels ranging from hydrogen to hydrocarbons, up to and including solid carbon. The ability to use solid carbon fuel makes the use of hydrocarbons more reasonable because any carbon which is deposited on the anode from pyrolytic decomposition may be consumed as fuel rather than clogging the anode.

Yttria-stabilized zirconia does not have sufficient catalytic activity for the carbon oxidation reaction, but is necessary for an electron blocking electrolyte. Gadolinia-doped ceria is more than eight times more catalytically effective than YSZ, but is too electrically conductive to be used for an electrolyte. The most obvious solution of a YSZ

electrolyte with GDC anode presents its own problems including excess diffusion of yttrium ions into the GDC which causes bulk shrinkage, leading in turn to voids and cracking. However, the available literature does not discuss any simple, effective methods to prevent this negative interaction, and therefore this study presents a simple method using easily available materials and simple laboratory equipment, which is completely effective at preventing the negative interaction at the YSZ/GDC interface. The integrity of the SOFC fabricated by this method is verified with Scanning Electron Microscope photography, as well as operation with several fuels including hydrogen and pyrolytically deposited solid carbon.

1.3.3. Use of Externally Applied Simulated Diesel Engine Soot as Fuel for SOFC. Applications of SOFCs capable of using solid carbon as fuel include coal power plants, cells rechargeable by repeated pyrolytic decomposition of hydrocarbon fuel, and cells fueled by soot from the exhaust of other combustion systems. Diesel engines are particularly sooty, in widespread use, and the subject of increasing regulation regarding exhaust particulates, which makes them a prime subject for a SOFC which can harvest additional energy from unburned solid fuel particles in the exhaust stream.

Pyrolytic solid carbon fuel has been used in a SOFC, as has small amounts of leftover gasoline and air in the exhaust of a motorcycle engine, but there is no instance in literature of soot or any other form of solid carbon from engine exhaust used as fuel for a SOFC. A diesel engine could benefit from supplemental electrical power generation by decreasing the electrical load on the alternator, and by removing the necessity of fuel-consuming regeneration of the particulate filter. This study presents a SOFC which uses acetylene flame soot to simulate diesel engine exhaust soot as fuel.

1.4. BROADER IMPACTS

Solid oxide fuel cells are an integral part of the effort to secure many energy-related objectives related to environmental protection and energy security. SOFCs have the potential to increase the efficiency with which existing fuels such as gasoline are used, as well as the flexibility to use many renewable or sustainable fuels such as bio-generated ethanol or hydrogen from solar-powered electrolysis. These sustainable fuels are often made locally which further decreases dependence on foreign energy sources whose price and availability are subject to ever-changing international politics. The use of SOFCs in the exhaust of other engines can both generate secondary electricity and decrease the pollution from these engines by removing unburned hydrocarbons or even particulates from the exhaust gas. This can provide both a small increase in efficiency and a reduction in emissions of unburned fuel.

To help develop SOFC technology toward the goal of commercial and practical viability, this research presents a simple and effective method to evaluate the ability of any material to function as a SOFC electrode. New research into SOFC materials selection can focus on improved cathodes and anodes by using this method to directly determine whether a material is an appropriate selection. This study may also help direct the development of SOFC toward the use of unburned particulates in the exhaust of sooty internal combustion engines.

1.5. EXPERIMENTAL APPARATUS

In order to perform measurements on the cells in these tests, a test stand was fabricated to hold a cell and provide access for electronic measurements. Such a test stand is required to secure the cell, provide a gas seal to separate the anode and cathode chambers, as well as allow access to both the anode and cathode for electronic measurements.

Figure 1.3 is a schematic of the double chamber sample holder, showing the separate tube for cathode feed gas, and the anode exhaust tube concentric with the smaller anode feed gas tube, all of which fits inside the outer furnace tube. The furnace tube is made of mullite, and the feed gas tubes are polycrystalline aluminum oxide (alumina). All of the alumina tubes passed through Swagelok fittings mounted in holes drilled through a single aluminum plate, which was secured to the end of the furnace tube as a single unit.

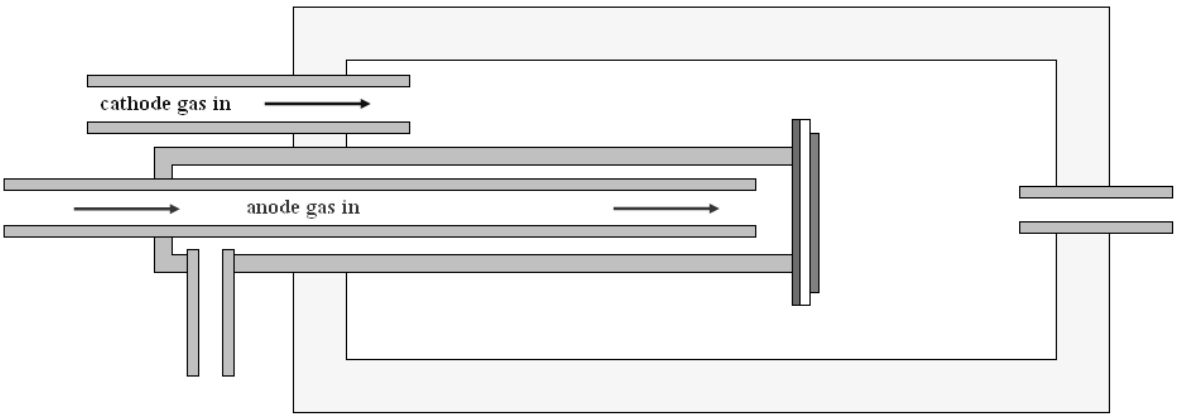

Figure 1.3. Double chamber sample holder.

Figure 1.4 is a photograph showing the tip of the sample holder, where the cell is mounted between the end of the anode gas exhaust tube and a short aluminum oxide ring of identical diameter which distributes force from the tensioning U-bar. The pressure from the U-bar helps provide a gas seal between the cell and the anode gas exhaust tube. A gasket of gold foil is pressed between the cell and the face of the tube, and also provides electrical contact with the anode. Two additional aluminum oxide tubes carry wires for electrical tests, including two wires for a thermocouple, and four wires for a four point electronic probe.

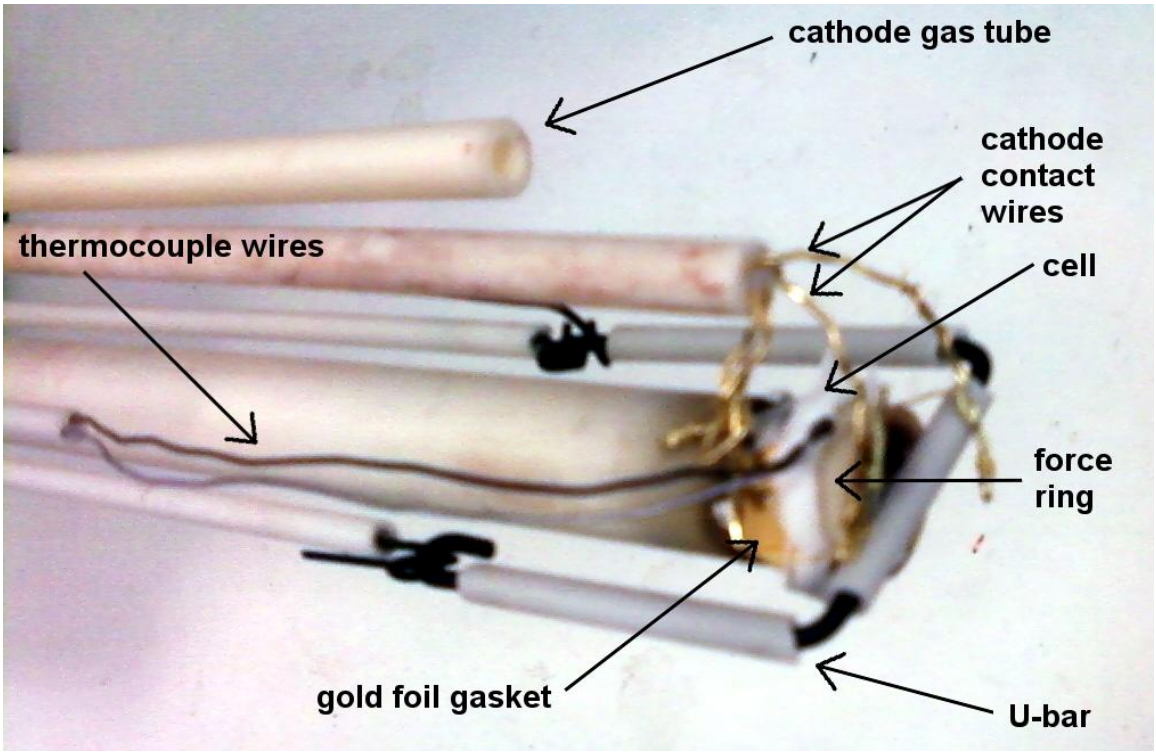

Figure 1.4. Photograph of cell in sample holder.

2. INDIVIDUAL ELECTRODE TESTS

2.1. BACKGROUND

Single chamber solid oxide fuel cells (SC-SOFC) are immersed in a flow of mixed fuel and oxygen, relying on the selectivity of the respective electrode catalysts to create a difference in oxygen ion activity across the thickness of the electrolyte [67,68]. In a traditional double chamber SOFC, the fuel and oxygen are separated by the electrolyte. The oxygen ions (O^{2-}) diffuse through the electrolyte due to the high O^{2-} activity on the cathode side and low O^{2-} activity on the anode side. The fuel simply prevents a buildup of O^{2-} on the anode side by consuming the O^{2-}. In a single chamber SOFC, the same mixed gas is flowing over both electrodes, so the anode must decrease the O^{2-} activity by effectively catalyzing the consumption of O^{2-} by the fuel without catalyzing the ionization of O_2. Likewise, the cathode must have the opposite catalytic effects [68]. The ability of the electrode to create or sustain a difference in O^{2-} activity across the electrolyte is measured by the open circuit voltage (OCV).

More effective electrode catalysts would increase both the voltage and the power produced by a SC-SOFC, but catalytic effectiveness is difficult to measure directly in this setting. Therefore, in order to separately observe the catalytic effectiveness of the anode in a single chamber fuel cell, the OCV of an SOFC was measured with the anode exposed to varying gas compositions while the cathode was exposed to a standard double chamber oxidizing environment. Hydrogen was used as a fuel for simulating a single chamber SOFC. Although there is no substantial improvement in cell design or operation in this study, it may be one of the first studies in which the effectiveness of the individual electrodes have been measured in this way, and it contributes to the understanding of the

way in which the anode reacts to its environment. Future studies may enable better design and selections of anode materials to further increase power density.

2.2. EXPERIMENTAL METHODS

2.2.1. Sample Fabrication. Samples were fabricated from a dense 300 μm thick 8% yttria-stabilized zirconia (YSZ) electrolyte substrate with tape cast porous NiO-YSZ anode and painted with 25% $La_{0.8}Sr_{0.2}Fe_{0.8}Co_{0.2}$ (LSCF) / 75% Ag porous cathode. This cell composition was chosen because similar cells have been successfully tested in single chamber configuration with other fuels [29]. The sample for use in double chamber configuration had an effective area of 0.8 cm^2 while the sample for use in single chamber configuration was smaller with a rectangular effective area of 0.4 cm^2. NiO in the anodes was reduced to Ni during operation.

2.2.2. Measurement Methods. The double chamber sample holder was constructed so that both anode and cathode gas compositions could be controlled separately. As illustrated in Figure 1.1, the double chamber sample holder consisted of two concentric tubes within a tubular furnace. The anode experienced stagnation flow with significantly higher gas velocity than the cathode, which experienced a mostly stationary diffusing gas environment.

The single chamber sample holder illustrated in Figure 2.1 was significantly simpler than the double chamber, with a single tube holding the cell edgewise in a flow of mixed gases. In the single chamber configuration, both electrodes experienced the same flat-plate type flow at the same velocity.

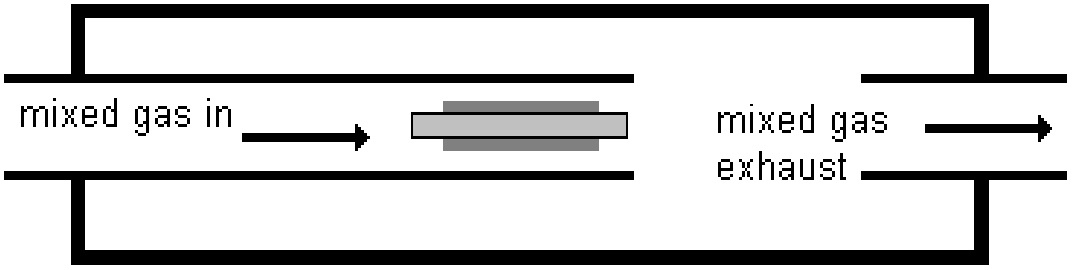

Figure 2.1. Single chamber sample holder.

In double chamber configuration, the anode was exposed to a mixed fuel-oxidizer gas while the cathode was exposed to pure oxidizer. This was to simulate a single chamber configuration for the anode while the cathode was operated in the well-characterized double chamber configuration. A similar test was conducted with the cathode exposed to mixed gases and while the anode was exposed to pure fuel. The fuel selected was dry hydrogen, and in order to avoid the explosion limits, all gases were diluted with 95% argon. All gas mixtures are stated as a percentage of the remaining 5% of reactive gas. The anode gas compositions were varied from pure fuel (double chamber configuration) through the stoichiometric mixture (66% H_2 / 33% O_2) to being slightly oxygen rich (60% H_2 / 40% O_2), while the cathode gas compositions were varied from pure oxygen through stoichiometric to slightly fuel rich mixtures (87% H_2 / 13% O_2), as noted in Table 2.1. The single chamber experiments were performed with a stoichiometric mixture of hydrogen and oxygen (diluted with 95% argon). No gases were bubbled through water.

All measurements were taken for the furnace temperature range from 400 °C to 700 °C in 50 °C increments. Note that the actual cell temperature was in most cases 5 °C

to 10 °C higher due to the exothermic reactions taking place on the surface of the electrodes, and exceptions to this are discussed in section 2.3.3.

Table 2.1. Gas mixtures for individual electrode tests

	Anode Gas, %		Cathode Gas, %	
	Fuel	Oxidizer	Fuel	Oxidizer
Double Chamber	100	0	0	100
Anode gas mix A	93	7	0	100
Anode gas mix B	87	13	0	100
Anode gas mix C	80	20	0	100
Anode gas mix D	73	27	0	100
Anode gas mix E	67	33	0	100
Anode gas mix F	60	40	0	100
Cathode gas mix A	100	0	87	13
Cathode gas mix B	100	0	73	27
Cathode gas mix C	100	0	60	40
Cathode gas mix D	100	0	47	53
Cathode gas mix E	100	0	34	67
Cathode gas mix F	100	0	20	80
Cathode gas mix G	100	0	7	7

For each gas composition, impedance and open circuit voltage (OCV) were measured at each temperature in order to determine the effectiveness of the anode. The OCV was measured for 20 minutes at each condition to ensure that a stable voltage was achieved. All data were recorded with a commercial data collection software (CorrWare) and analyzed with the corresponding analysis software (CorrView or Zview).

2.2.3. Error Analysis. The present voltage measurements were accurate to within 1% and area specific resistance measurements were accurate to within 11%, estimated with a 95% confidence interval. Details on uncertainty analysis can be found in the appendix.

2.3. RESULTS AND DISCUSSION

2.3.1. Anode Test Results. The open circuit voltage for the double chamber cell with mixed gas on the anode is shown in Figure 2.2. Based on a comparison of single and double chamber SOFC performance in the available literature, a standard double chamber SOFC performs better at higher temperatures around 700 °C to 900 °C and offers at least double the open circuit voltage and area specific power compared to a single chamber SOFC. As expected, the anode was most effective when tested closest to double chamber configuration and at higher temperatures.

When compared to the predicted Nernst voltage in Figure 2.3, which assumes no anode catalytic activity, the voltage is significantly higher, more than an order of magnitude in most cases, indicating that the Ni does exhibit significant catalytic activity to decrease the effective oxygen pressure at the electrolyte/anode interface, increasing the driving force for O^{2-} ions beyond that provided by the simple gas mixture.

In gas mixtures of less than 87% fuel (Figure 2.2.c-f), at furnace temperatures below 450 °C, the reaction between O^{2-} from the electrolyte and the increasingly dilute fuel was occurring too slowly to remove the O^{2-} which had diffused through the electrolyte, leading to a lower OCV. As the temperature or fuel concentration was increased, the reaction at the anode occurred faster, decreasing the oxygen activity at the

anode and causing the increase in OCV between 400 °C and 550 °C, as seen in Figure 2.2.c-f.

It is known that mixed hydrogen and oxygen gases in the absence of a catalyst react to complete consumption of reactants at temperatures above 500 °C with a residence time of several minutes [69], but the mixed gas in this study was only exposed to high temperatures for a time on the order of five seconds before reaching the cell. However, Ni is known to be a catalyst for this reaction [6], and above 600 °C in the 60% fuel mixture (Figure 2.2.f), the Ni allowed the oxygen gas to consume a significant portion of the H_2 before it was able to diffuse farther into the anode to reach the O^{2-} ions from the electrolyte. This led to a buildup of O^{2-} ions which further decreased the OCV and also increased the overpotential.

In these lean gas mixtures at temperatures above 600 °C, the equilibrium gases contained water vapor and oxygen, which readily oxidized the part of the Ni anode to which it was exposed. The partially oxidized Ni anode lowered the available catalytic surface area and did not allow the anode to make effective use of what fuel remained in the gas under these conditions [30]. The oxidized portion of the anode also decreased in porosity [7], slowing the diffusion of fuel into the anode. The Ni anode did not completely oxidize as complete oxidation of the anode would decrease its conductivity by more than three orders of magnitude [32,33]. However, enough of the anode had oxidized to decrease the OCV by two orders of magnitude.

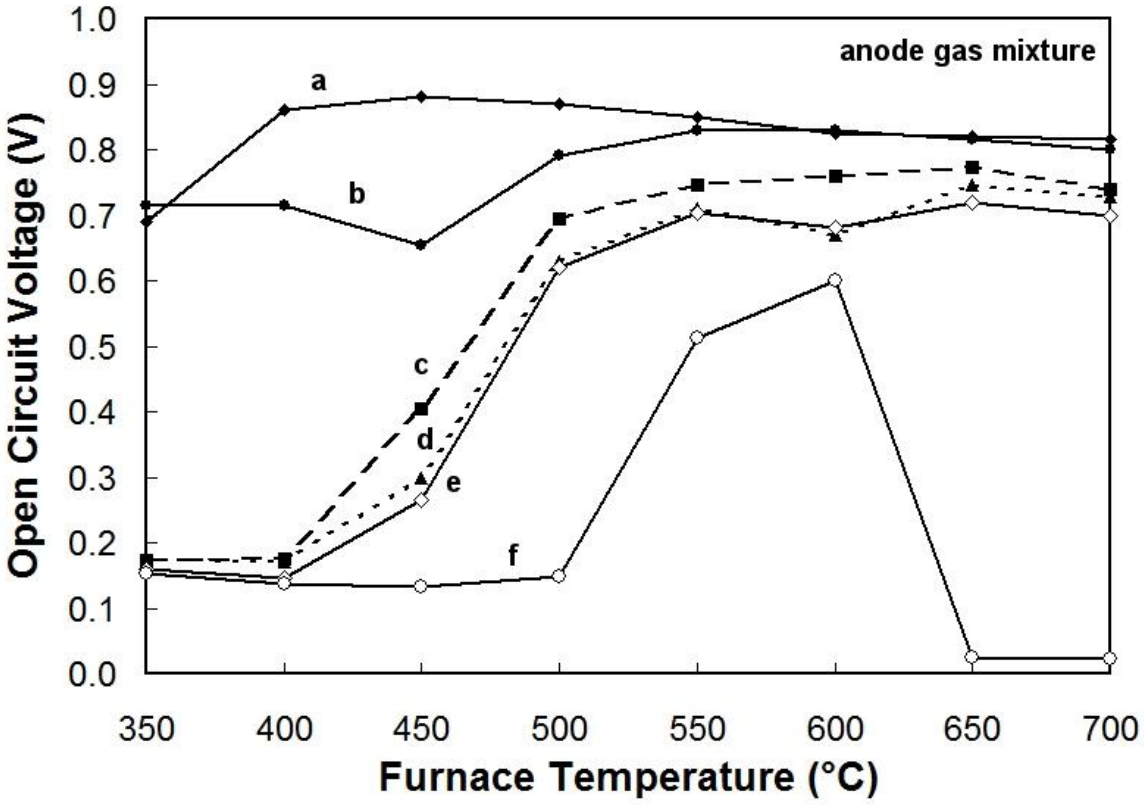

Figure 2.2. Open Circuit Voltage, Anode exposed to various mixtures of fuel and oxidizer gases (diluted with 95% Ar – mixtures stated as percentage of remainder) in double chamber configuration: (a) 93% fuel (balance oxidizer), (b) 87%, (c) 80%, (d) 73%, (e) 67% (stoichiometric), (f) 60%, while cathode was exposed to constant oxidizer gas.

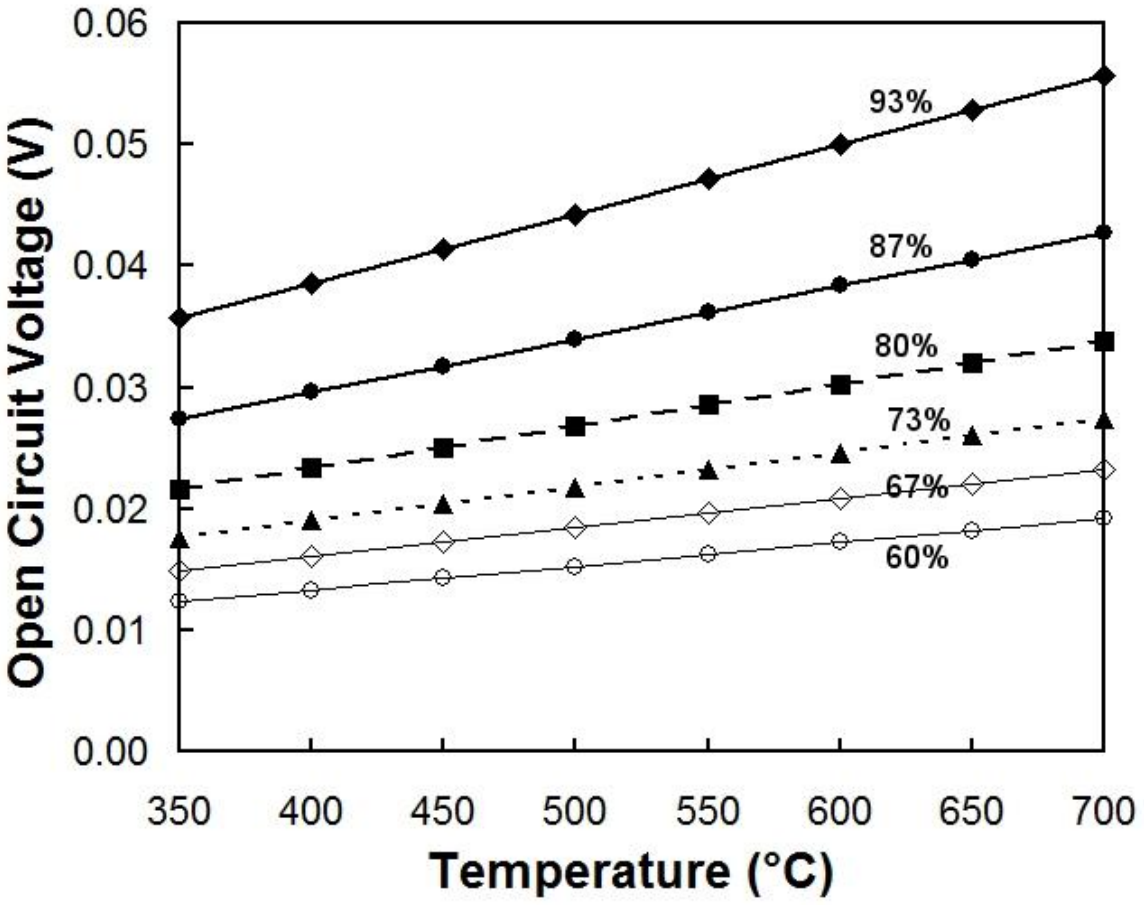

Figure 2.3. Predicted Nernst voltage for anode mixed gas test, assuming no anode catalytic activity.

The impedance spectra of the sample was measured from 10^{6} to 10^{-1} Hz and analyzed with both Bode and Nyquist plots, then the data was fitted to an equivalent circuit (Figure 2.4). The electrolyte is represented by a resistor while the anode and cathode are each represented by a resistor and constant phase element (CPE) in parallel (a Cole-Element), with all three in series. The resistance of the individual electrolyte, cathode, and anode can be determined by the equivalent circuit approach.

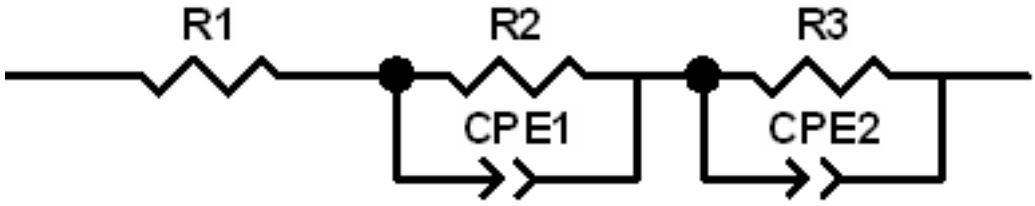

Figure 2.4. Equivalent circuit diagram representing the electrolyte (R1), cathode (R2 and CPE1 in parallel) and anode (R3 and CPE2 in parallel).

Zview software was used to calculate values for each component of the equivalent circuit based on the measured spectra to determine the electrical properties under each tested condition. The impedance spectrum of the equivalent circuit was calculated and compared to the measured spectrum. Figure 2.5 shows the impedance spectrum of the cell at 700 °C with the anode exposed to 93% fuel, as well as the spectrum of the equivalent circuit based on the calculated values of the components. Two Cole-Element semicircles are visible. Although there was no reference electrode for this experiment, de-convolution of the impedance spectra was achieved by a method similar to that used by Boillot et al. [70] for a PEM fuel cell. As the anode gas mixture changed, features on the Bode plot which corresponded to the higher frequency semicircle (R2) remained unchanged. However, features on the Bode plot which corresponded to the low frequency semicircle (R3) experienced significant phase shift, indicating that the anode reaction corresponds to the semicircle labeled R3 in Figure 2.5. Similar tests performed by changing conditions on the cathode side while keeping the anode conditions constant showed that cathode effects on the R3 semicircle were minimal. Changes in cathode

conditions showed changes in the R2 semicircle while the R3 semicircle remained the same.

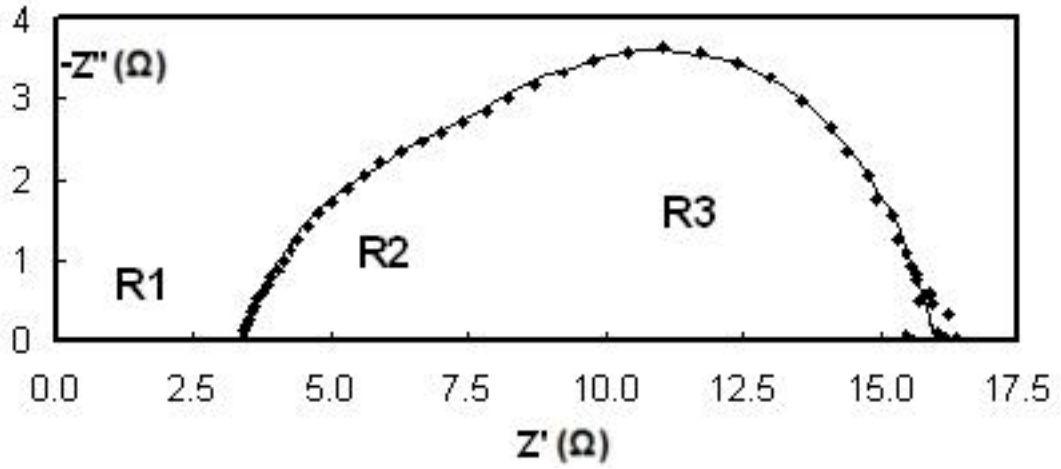

Figure 2.5. An example of impedance spectra: (♦) experimental data (—) line fitting by equivalent circuit which gives the following values: R1 = 3.4, R2 = 4.3, R3 = 8.3 Ohms

The calculated values for the resistance of the anode were used to calculate the area specific resistance (ASR) of the anode, shown in Figure 2.6 for the different gas mixtures. Note the significantly higher resistance for 60% fuel at 650 and 700 °C. The low frequency semicircle in this case represented by R3 is typically associated with gas transport in an electrode. However, in this case the increase is likely due to oxidation of part of the Ni within the anode rather than a change in gas transport as the gas flow conditions and anode porosity were constant.

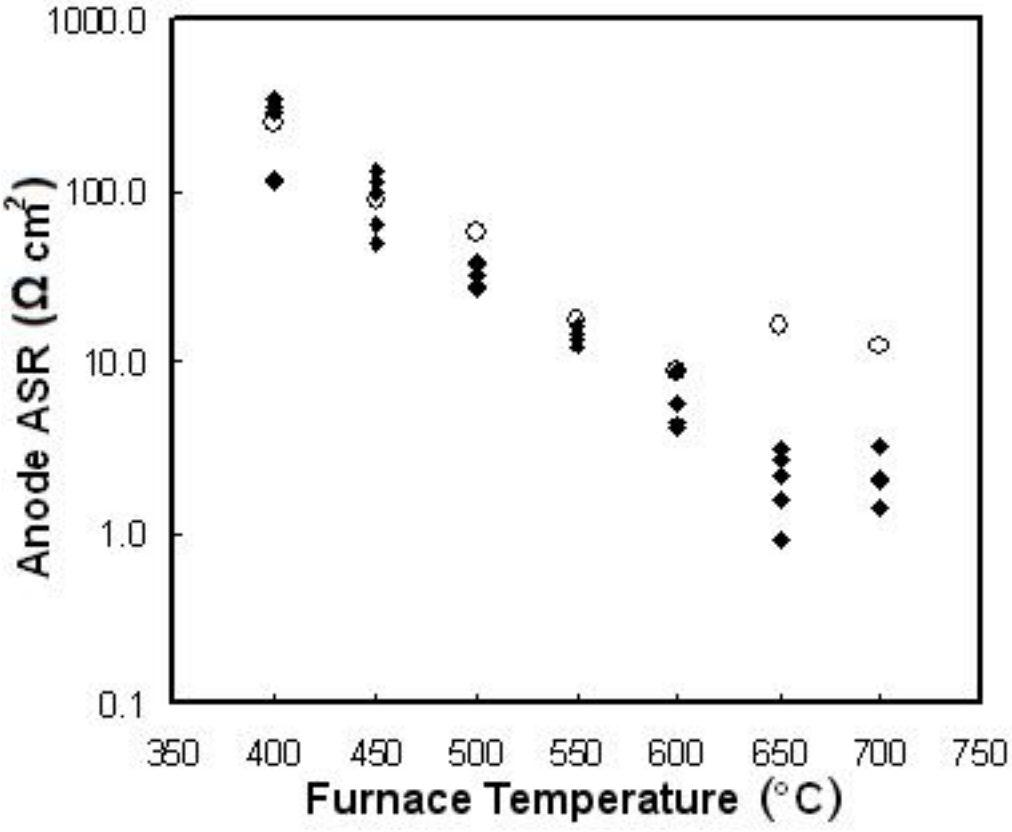

Figure 2.6. Area specific resistance of the anode when it was exposed to gas mixtures; (○) 60% fuel mixture, (♦) all other mixtures.

Some open circuit voltage (OCV) measurements also showed significant periodic voltage oscillations, an example of which is shown in Figure 2.7. These voltage oscillations appeared to coincide with lower power curves and the higher ASR measurements in Figure 2.6. Impedance measurements for these gas mixtures were taken during intervals with stable voltage. These oscillations were detected in various gas mixtures but were most pronounced and most frequent in the stoichiometric mixture of 66% fuel.

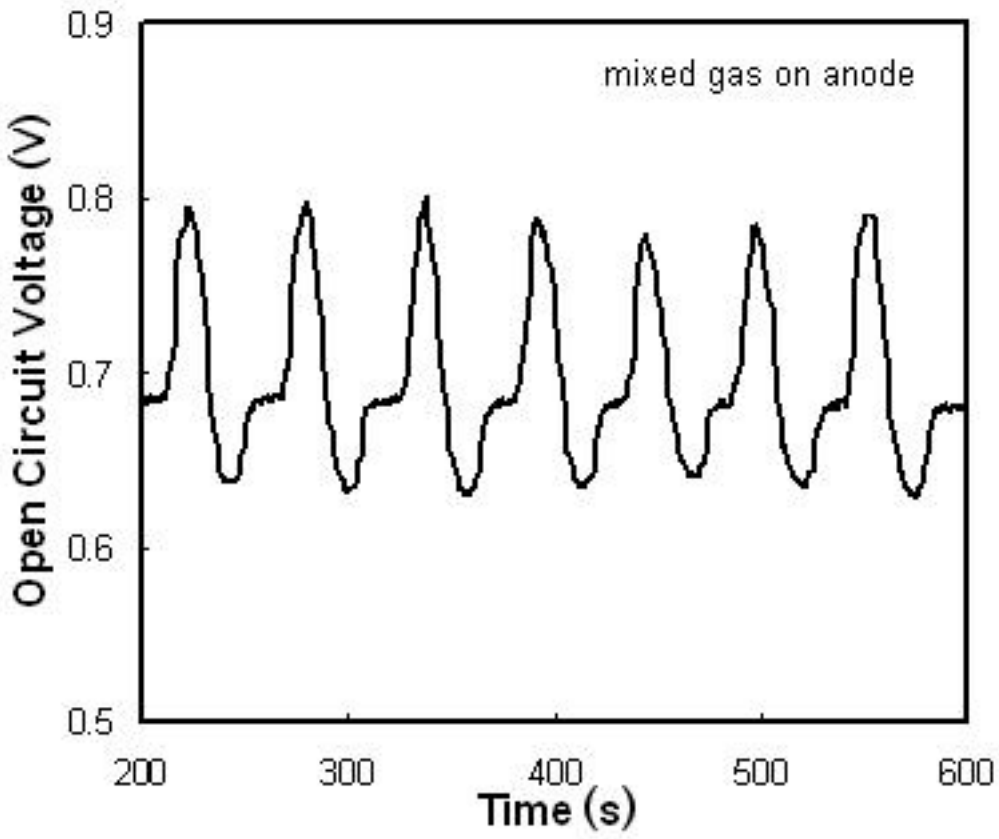

Figure 2.7. Typical open circuit voltage oscillations detected at 600 ℃ in double chamber with stoichiometric gas mixture (66% H_2 / 33% O_2 diluted with 95% Ar) on the anode, and pure diluted oxidizer (O_2 diluted with 95% Ar) on the cathode.

Carbon deposition has been previously studied for its role in anode degradation [40] both by blocking pores and by volume expansion to create micro-cracks [41]. However, based on a survey of relevant literature, carbon has not been found to act in a cyclic manner which could cause voltage oscillations. More importantly, hydrogen was

exclusively used as fuel in these tests; the lack of any hydrocarbon in the system precludes the possibility of any carbon deposition.

A more plausible mechanism by which the cell generates voltage oscillations is proposed here: The Ni anode consumes fuel during normal operation, leading to a locally oxygen rich atmosphere, moving the oxygen partial pressure from (a) to (b) in Figure 2.8. The Ni anode then oxidizes in this local atmosphere, lowering its catalytic effectiveness which lowers the voltage. The decrease in fuel concentration would also increase the anode overpotential, further contributing to lowering of cell power. Partial oxidation of the anode also significantly decreases its conductivity. While the oxidized anode is not consuming fuel, more mixed gas diffuses into the porous anode which restores the concentration of fuel, while the surplus oxygen simultaneously diffuses out of the anode, moving the pO_2 from (b) back down to (a) in Figure 2.8. The anode is now exposed to a reducing atmosphere and reduces to Ni and becomes catalytically effective once again, while the restored fuel concentration decreases the anode overpotential. The anode is in the same condition as when the cycle began, except for micro-cracking due to volume changes [6].

The $H_2/O_2/H_2O$ and Ni/NiO system equilibria were calculated separate from each other using the data from Table 2.2 according to equation 7, where $\Delta G°$ is the standard free energy, R is the universal gas constant, and K is the equilibrium constant. The activities of the gases were assumed to be their partial pressures, and the activities of both Ni and NiO were assumed to be 1 because the anode is never completely oxidized or reduced during operation, and both materials are assumed to be always exposed due to

the more active areas of the anode nearest the electrolyte consuming fuel faster than the outer areas and likely oxidizing first, beginning the cycle.

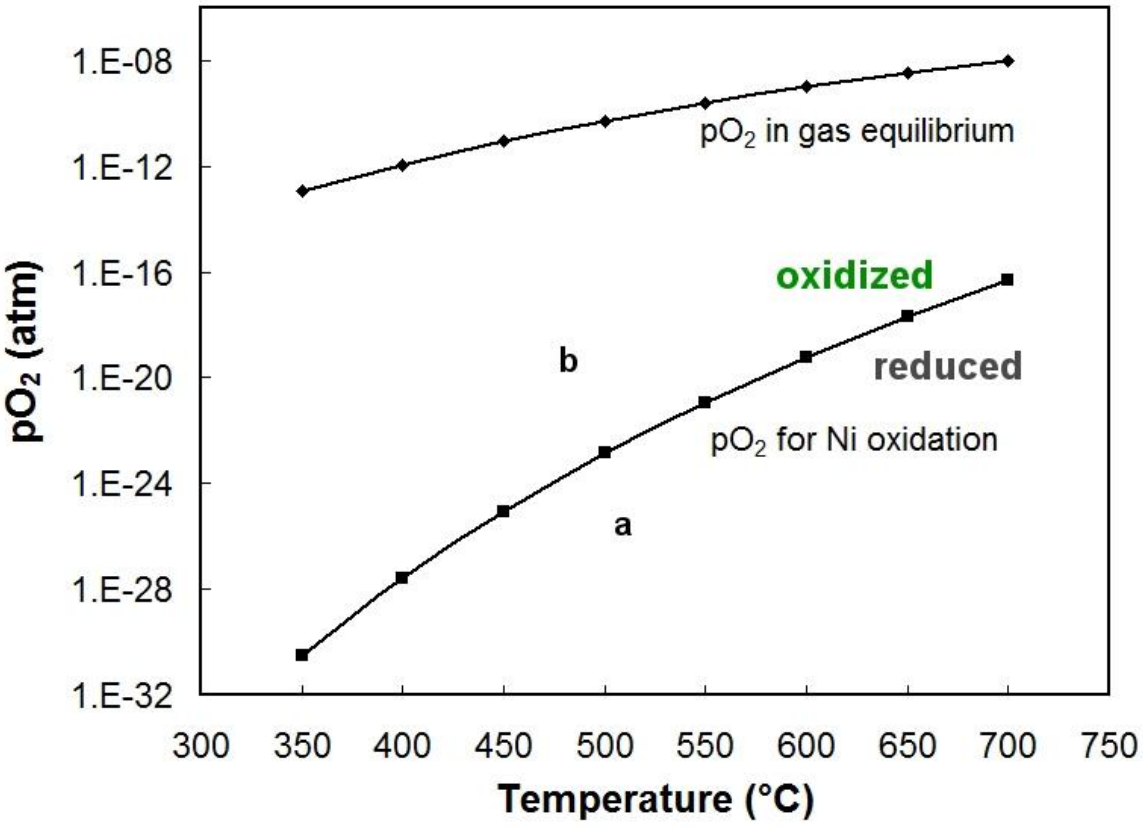

Figure 2.8. Graph of oxygen partial pressure necessary for Ni oxidation/reduction; (a) reduced Ni metal and (b) oxidized NiO.

Due to the high flow rate which would constantly flush the cell with gas, it was assumed that the small amount of oxygen which was bound in the NiO did not change the concentration of the oxygen. The equilibrium partial pressures of the gases are shown in Table 2.3 along with the equilibrium partial pressure of oxygen necessary to completely

oxidize the Ni anode. Of note is that without considering any interactions with hydrogen, the little oxygen left in the system is sufficient to completely oxidize the Ni anode. The Ellingham Diagram, a plot of the free energy of a reaction, is shown for these reactions in Figure 2.9.

$$-\Delta G^{\circ} = RT \ln K \tag{7}$$

Table 2.2. Standard Gibbs free energy of relevant reactions

	Reaction	$\Delta_r G^{\circ}$, J
gas	$H_2+1/2O_2 = H_2O$	-247500 + 55.85T
nickel	$2Ni+O_2 = 2NiO$	-471200 + 172T
oxidation	$2Ni+H_2+3/2O_2 = H_2O+2NiO$	-718700 + 227.58T
reduction	$2NiO+H_2 = 2Ni+H_2O+1/2O_2$	223700 - 116.42T

Table 2.3. Equilibrium of separate Ni/NiO and $O_2/H_2/H_2O$ systems

	equilibrium pO_2 for	equilibrium concentrations of gas, atm		
Temp °C	complete Ni oxidation, atm	pO_2	pH_2	pH_2O
350	3.00E-31	1.10E-13	2.21E-13	5.00E-02
400	2.59E-28	1.18E-12	2.35E-12	5.00E-02
450	8.75E-26	9.04E-12	1.81E-11	5.00E-02
500	1.39E-23	5.34E-11	1.07E-10	5.00E-02
550	1.20E-21	2.54E-10	5.08E-10	5.00E-02
600	6.18E-20	1.01E-09	2.02E-09	5.00E-02
650	2.08E-18	3.46E-09	6.92E-09	5.00E-02
700	4.88E-17	1.04E-08	2.09E-08	5.00E-02

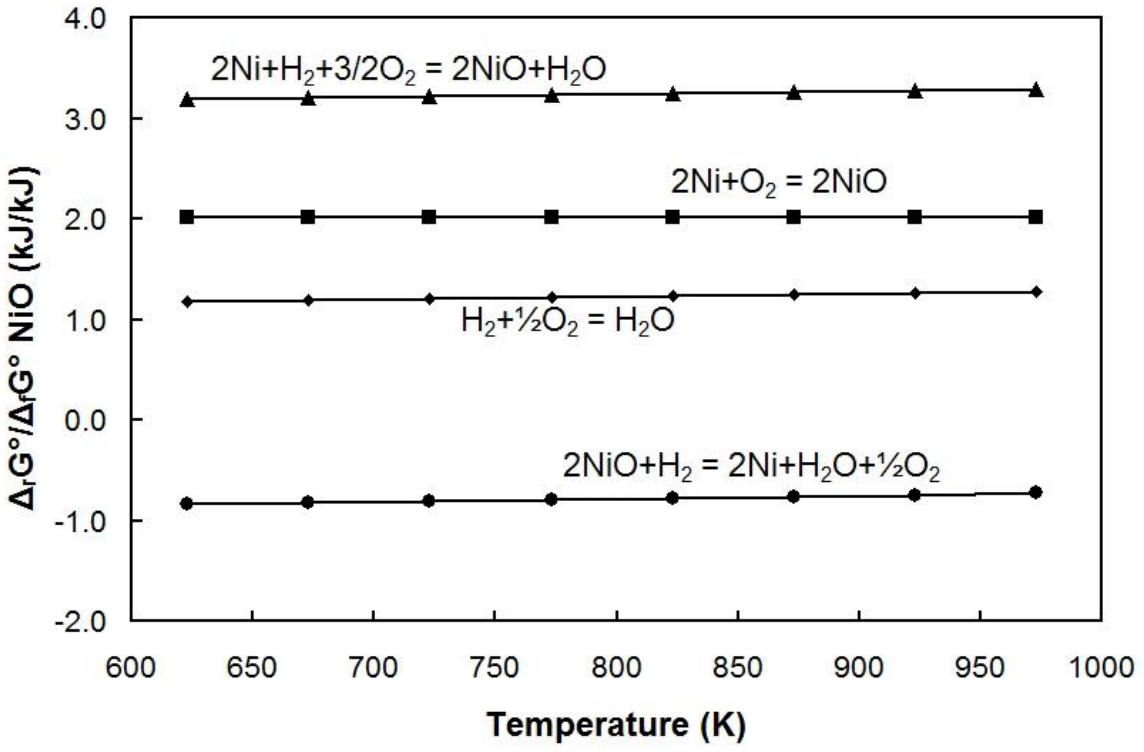

Figure 2.9. Ellingham diagram of relevant reactions, normalized to the standard Gibbs free energy of formation for NiO.

The proposed mechanism was not completely modeled due to the certainty of certain steps taking place under normal operating conditions in this gas mixture, such as fuel consumption, gas diffusion, and anode oxidation. Only the final step, anode reduction after diffusion of fresh mixed gas into the anode, was questionable and therefore analyzed. Equilibrium was calculated assuming the activities of gases are the partial pressures of the respective gases, the activities of Ni and NiO are 1, and the concentration of oxygen was not changed by its interaction with the Ni. Equilibrium concentrations of the gases are shown in Table 2.4 for the reduction of NiO in the final step of the proposed mechanism. The oxygen concentration of the unreacted gas is sufficiently low to reduce the anode from NiO to Ni during operation.

Table 2.4. Equilibrium concentrations of gas for NiO reduction.

Equilibrium concentrations, atm		
pO_2	pH_2	pH_2O
1.67E-02	3.33E-02	5.46E-14
1.67E-02	3.33E-02	1.35E-12
1.67E-02	3.33E-02	2.15E-11
1.67E-02	3.33E-02	2.38E-10
1.67E-02	3.33E-02	1.97E-09
1.67E-02	3.33E-02	1.28E-08
1.67E-02	3.33E-02	6.82E-08
1.67E-02	3.33E-02	3.05E-07

In order to experimentally determine whether the Ni anode was experiencing a cyclic change in oxidation state, the resistance of the Ni anode was measured during normal fuel cell operating conditions by laying two Au sensing wires along opposing edges of the anode (Figure 2.10). The entire width of the anode was measured in this method.

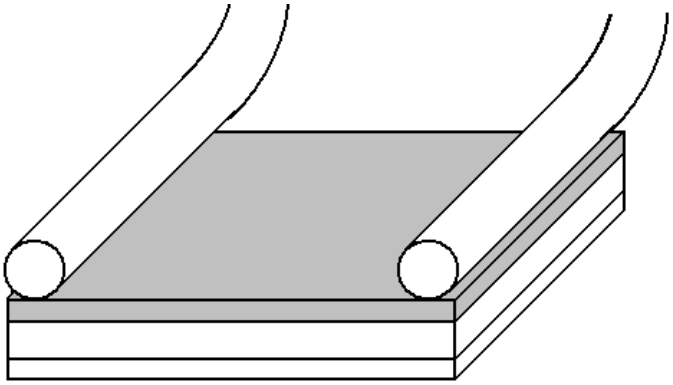

Figure 2.10. Au sensing wires mounted on the anode (gray layer) for measuring ASR.

An oscillation in the resistance of the anode was detected during operation of the cell (Figure 2.11). This indicates a cyclic change in the oxidation state of the anode, as NiO is around 17 orders of magnitude less conductive than Ni. These oscillations, with a period of around 70 seconds, were in the same period range as the voltage oscillations recorded under the same conditions, which varied from 45 to 90 seconds. The anode resistance oscillations were of only a few percent in magnitude compared to the voltage oscillation with magnitudes of about 20 percent. However, due to the large measured area and multiple conduction paths through the porous agglomeration of sintered Ni particles, the change in resistance signifies a large change in the volume of oxidized Ni within the anode. This would cause a correspondingly large change in the catalytic ability of the anode, further increasing the change in voltage beyond the scale of the change in resistance.

An oxidized Ni anode would lower the voltage of a SC-SOFC due to both a decreased available catalytic surface area and an increased internal resistance of the cell as a whole. This mechanism is further supported by the OCV oscillations which were detected when the anode was exposed to a single chamber atmosphere, including single chamber tests, but not when the anode was exposed to a pure fuel environment. No OCV oscillations were detected when the test was reversed and the cathode was exposed to mixed gases while the anode was exposed to only fuel.

Tikekar et al [7] determined that the oxidation kinetics of a porous Ni-YSZ anode are governed by gas diffusion into the pores, therefore the rate limiting mechanism for the voltage oscillation cycle is probably gas diffusion into the porous anode. The linear gas velocity in these tests was 70.7 cm/s, fast enough to ensure that the gas immediately

outside of the anode was constantly flushed and replaced with fresh gas. The anode particles were on the order of 1 μm as measured by SEM micrography, likely small enough that oxidation and reduction occur more quickly than the period of the oscillations.

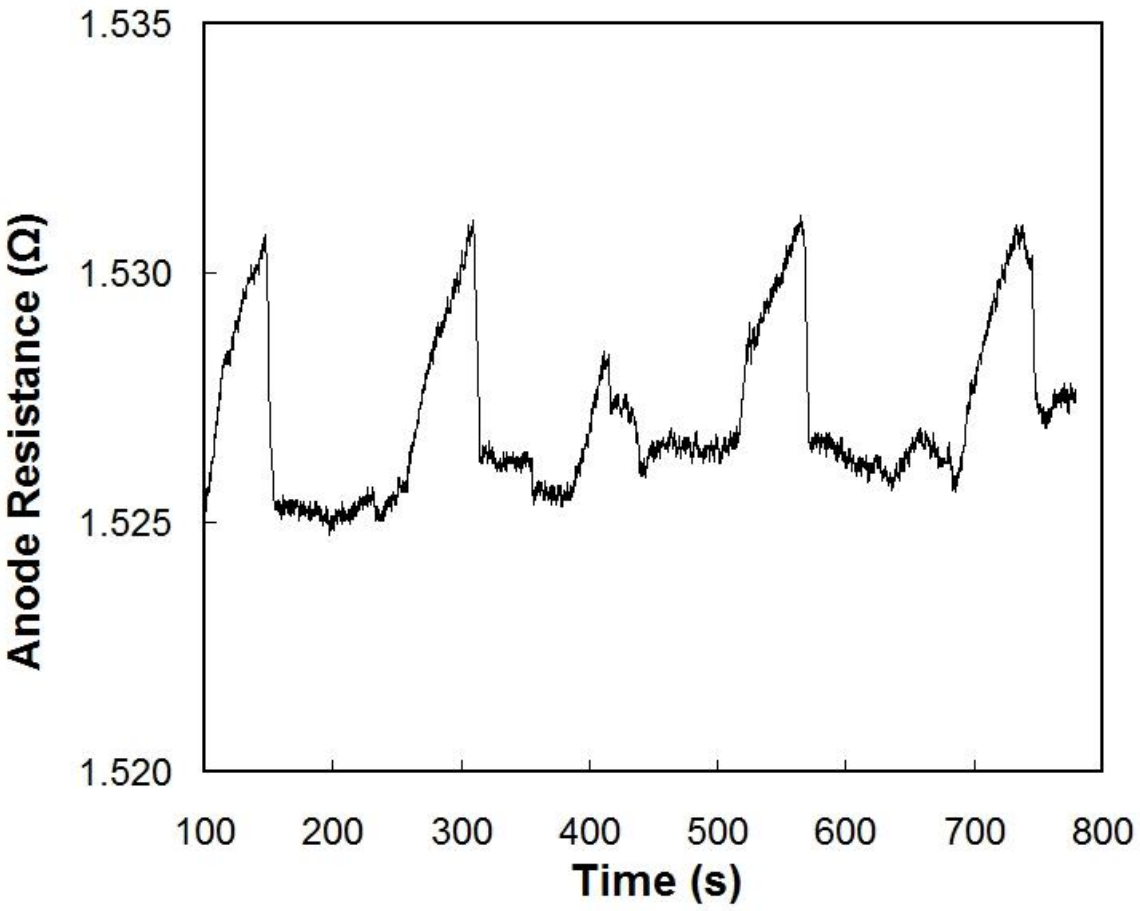

Figure 2.11. Typical anode resistance oscillations detected at 550 °C in single chamber conditions with stoichiometric gas mixture (66% H_2 / 33% O_2 diluted with 95% Ar).

2.3.2. Cathode Test Results. The cathode OCV in Figure 2.12 is up to four times higher than the Nernst predicted voltage in Figure 2.13, and showed little temperature dependence at mixtures closer to double chamber configuration (pure oxidizer for cathode), but at stoichiometric and lower oxygen concentration there was a drop of about 80% in voltage at higher temperatures due to the decrease in oxygen activity of several orders of magnitude in the product gases.

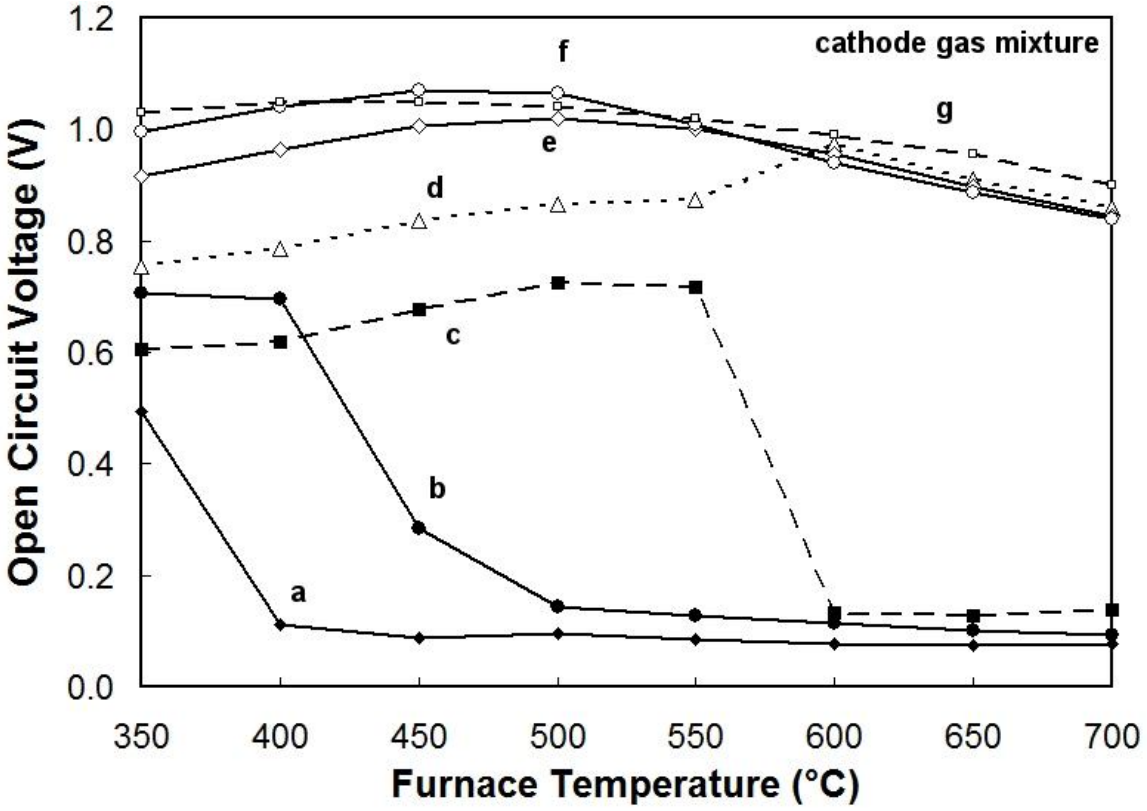

Figure 2.12. OCV, Cathode exposed to various gas mixtures in double chamber cell configuration: (a) 7% oxidizer (oxidizer is 5% O_2 in Ar), (b) 20%, (c) 33% (stoichiometric), (d) 47%, (e) 60%, (f) 73%, (g) 87%, while anode was exposed to constant fuel gas.

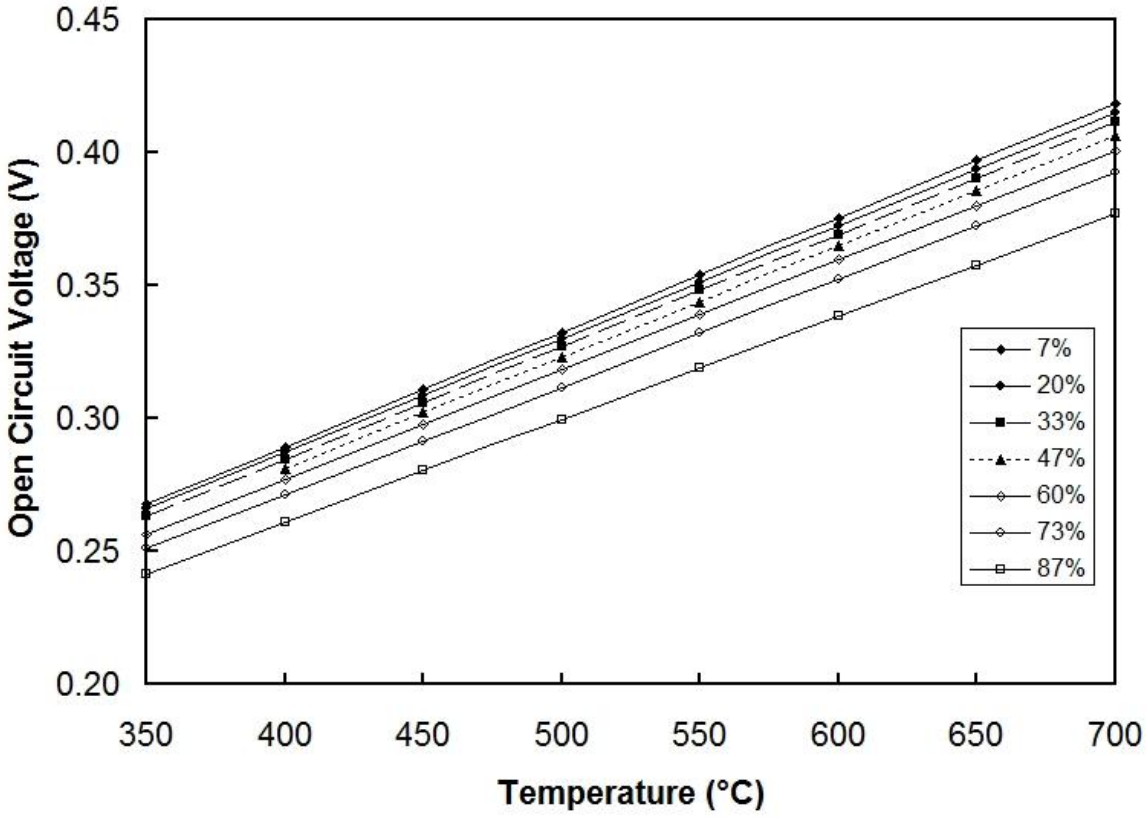

Figure 2.13. Predicted Nernst voltage for cathode mixed gas test, assuming no cathode catalytic activity.

The varying cathode gas mixtures OCV decreased by an order of magnitude in gas mixtures with less than stoichiometric oxygen at temperatures high enough that the gas mixture reacted and consumed the oxygen, which decreased the oxygen activity by several orders of magnitude. As the amount of excess fuel increased, the OCV dropped off at lower temperatures, most likely due to a reaction taking place in the gas phase which consumed the available oxygen, and increasing fuel allowed this reaction to consume the oxygen at lower temperatures. In addition to this, the LSCF cathode material has been shown to have significant catalytic activity towards fuel oxidation,

which is more pronounced at higher temperatures and at higher concentrations of fuel [35]. Other cathode materials, such as $Sm_{0.5}Sr_{0.5}CoO_{3-x}$ tend to show much less catalytic activity towards fuel oxidation and may be a better choice for SC-SOFC, although more suitable for use with Sm-doped ceria (SDC) electrolytes [71].

2.3.3. Single Chamber Test Results. The results of the double chamber tests with each electrode in varying gas compositions were used to predict the voltage and power that could be expected in a single chamber test. Data from previous double chamber tests were used as a baseline for comparison, and the predictions were made using equation 8, where the subscripts *mga*, *mgc*, *DC*, and *SCestimate* are respectively "mixed gas on anode," "mixed gas on cathode," "double chamber," and "single-chamber estimate."

The predictions were the result of normalizing the values from each electrode with respect to the values for the same cell in double chamber configuration. The results of these predictions are illustrated in Figure 2.14 and compared to the open circuit measurements taken in single chamber mode. The measured voltage was for the most part higher than the predicted voltage, indicating that some of the decrease in performance was due to the decreased difference in oxygen activity across the electrolyte in addition to the individual electrode inefficiencies in a mixed gas.

$$\left(\frac{OCV_{mga}}{OCV_{DC}}\right)\left(\frac{OCV_{mgc}}{OCV_{DC}}\right)OCV_{DC} = OCV_{SCestimate} \tag{8}$$

The performance envelopes of the anode and cathode at 550 °C are illustrated in Figure 2.15 with the predicted voltage from equation 8. The gas mixtures at which the Ni anode performed well, generating 0.8 V above 80% fuel, did not overlap the gas mixtures at which the LSCF cathode performed well, generating 1.0 V below 47% fuel. A stoichiometric mixture at a temperature range of 500-550 °C provided a middle ground where both electrodes performed marginally, generating more than 50% of the voltage generated within its respective envelope.

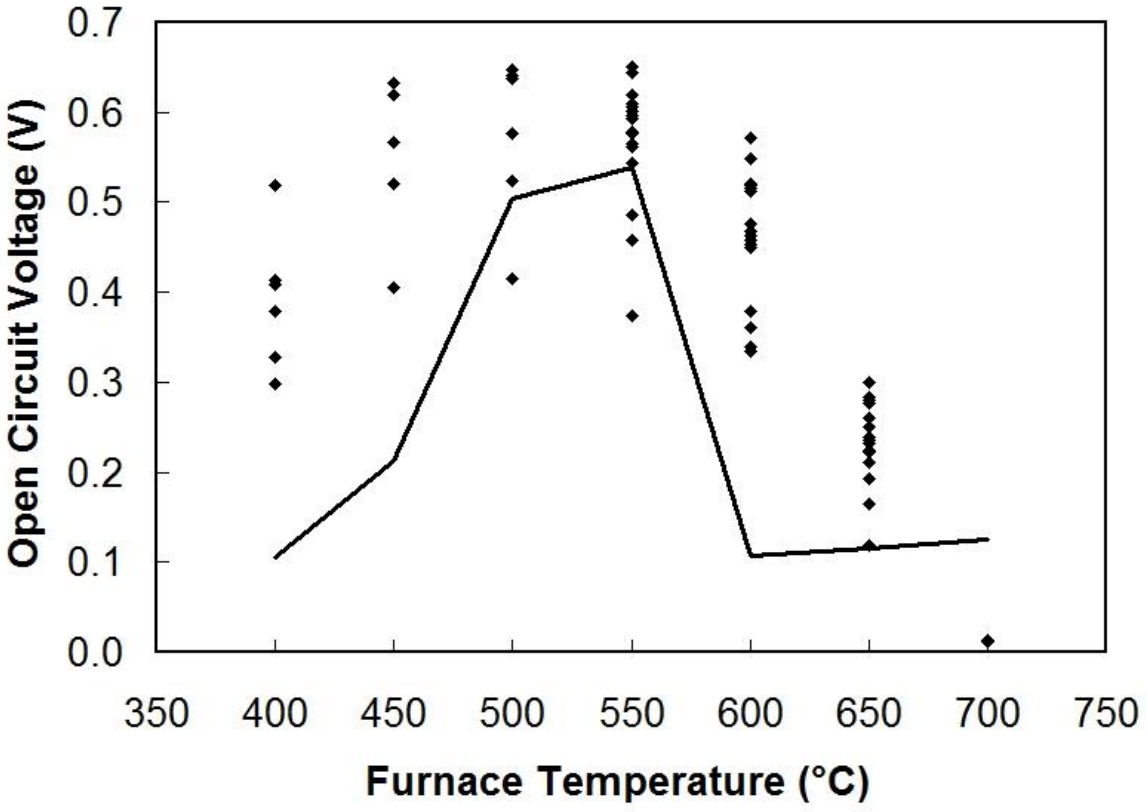

Figure 2.14. Temperature dependence of OCV, predicted from double chamber tests (solid line) and experimentally measured in single chamber configuration with stoichiometric gas mixture (66% H_2 / 33% O_2 diluted with 95% Ar) (♦).

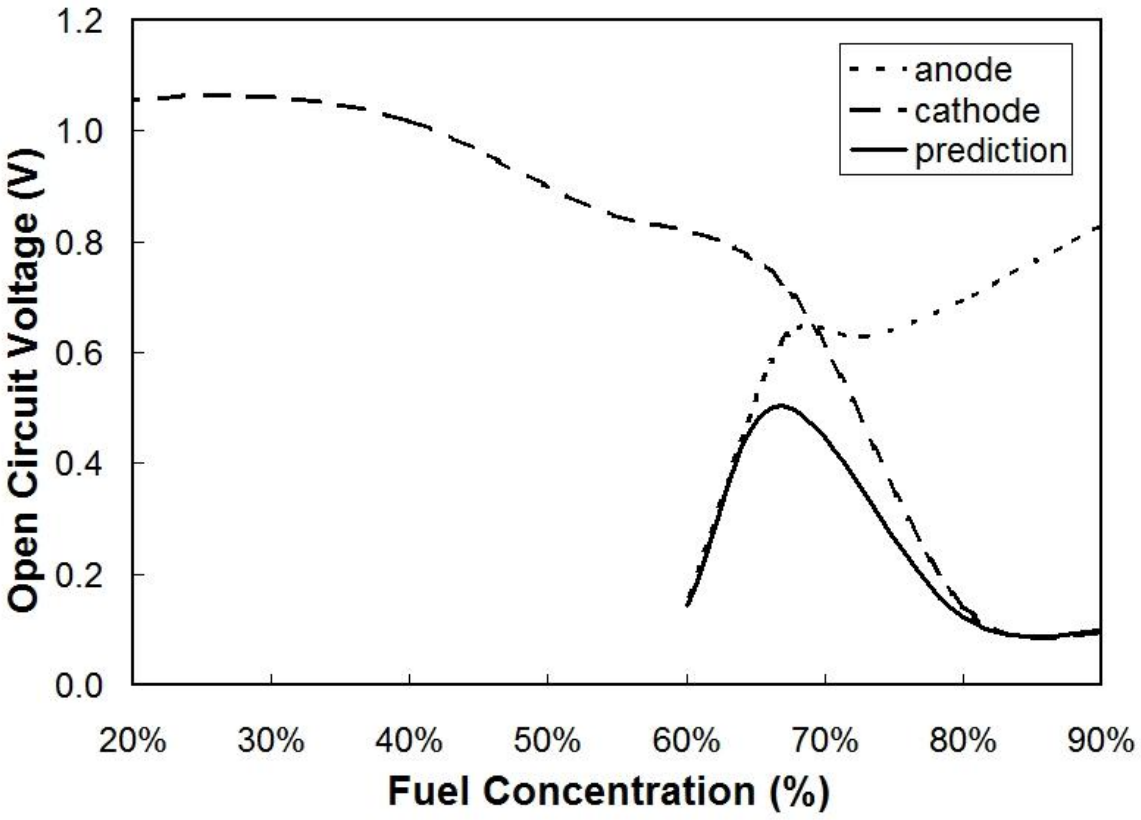

Figure 2.15. OCV of cell at 550 °C with mixed gas on anode, with mixed gas on cathode, and prediction for single chamber.

At 500 °C the cell generated about 0.8 volts when the anode was exposed to gas mixtures with as little as 87% fuel, but the voltage began to drop sharply as the fuel concentration decreased. Similarly at 500 °C the cell generated about 1.0 volts when the cathode was exposed to gas mixtures with as much as 40% fuel, but the voltage began to drop sharply as the fuel concentration increased. The performance envelopes at 500 °C would then be 87% and greater fuel for the anode and 40% and lower fuel for the cathode. When the anode was exposed to a stoichiometric gas mixture at 500 °C, the voltage generated was about 0.65 volts, or a drop of 24% from the voltage generated

from a gas that was within the anode's performance envelope. When the anode was exposed to a gas mixture within the performance envelope of the cathode (40% or lower fuel) the voltage generated was about 0.1 volt, or a performance drop of 88%. Likewise, when the cathode was exposed to a stoichiometric mixture of gas at 500 °C, the voltage was about 0.7 volts, or a drop of 30% from the voltage generated from a gas that was within the cathode's performance envelope. When the cathode was exposed to a gas mixture that was within the performance envelope of the anode (87% or greater fuel) the voltage generated was about 0.1 volt, or a performance drop of 90%.

The power generated by this cell in single chamber configuration is shown in Figure 2.16, with two distinct curves; a lower power curve recorded during operation when the anode was experiencing oscillations as detailed in section 2.3.1, and a higher power curve recorded during operation with the anode reduced. Although the power generated by this cell was low compared to other SC-SOFC in the literature [10] due to the highly diluted gases and thick electrolyte, the purpose of these tests was not to directly increase the power density of a cell. The present tests were designed to study the ability of the anode to create and sustain a difference in oxygen activity across the electrolyte in a single chamber environment. With a greater understanding of the way in which the individual electrodes behave, cells with higher power density may be achieved.

The cell temperature was measured and compared to the furnace temperature, as a measure of the exothermic reaction taking place at the cell electrodes. Figure 2.17 shows the temperature differential with the cell in operation and the anode in various states of oxidation. When the cell was first inserted into the furnace, before the anode had reduced from NiO to the more catalytically effective Ni, the exothermic reaction provided less

heat generation than the convective cooling effect of the incoming gases, resulting in a cell temperature up to 12 °C lower than the furnace temperature. Once the anode had reduced during operation and become catalytically active, the temperature of the cell was consistently higher than the furnace temperature, 5 °C to 15 °C depending on the operating temperature, but when voltage oscillations were present the cell temperature was very inconsistent, from 5 °C below the furnace temperature to 15 °C higher. The inconsistency was likely due to the anode being alternately catalytically active and ineffective, with some temperatures higher than the reduced anode due to the added reaction heat from the oxidation of the Nickel anode itself.

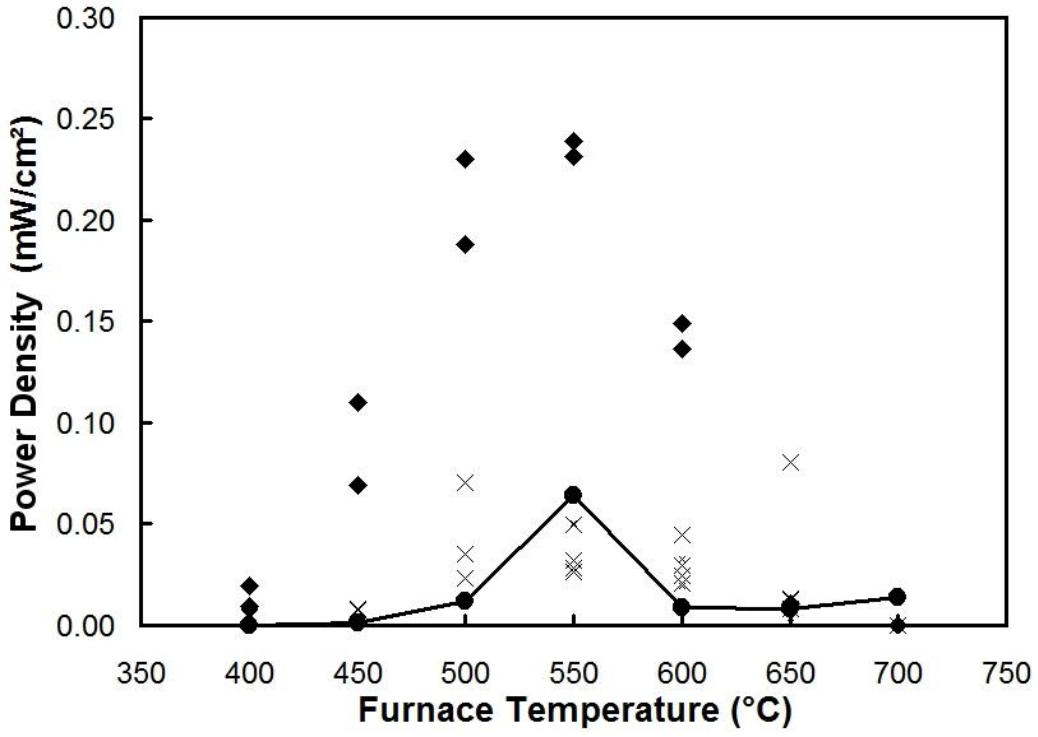

Figure 2.16. Power curves with anode oxidized (♦) and anode reduced (X), compared to predicted single chamber power (line).

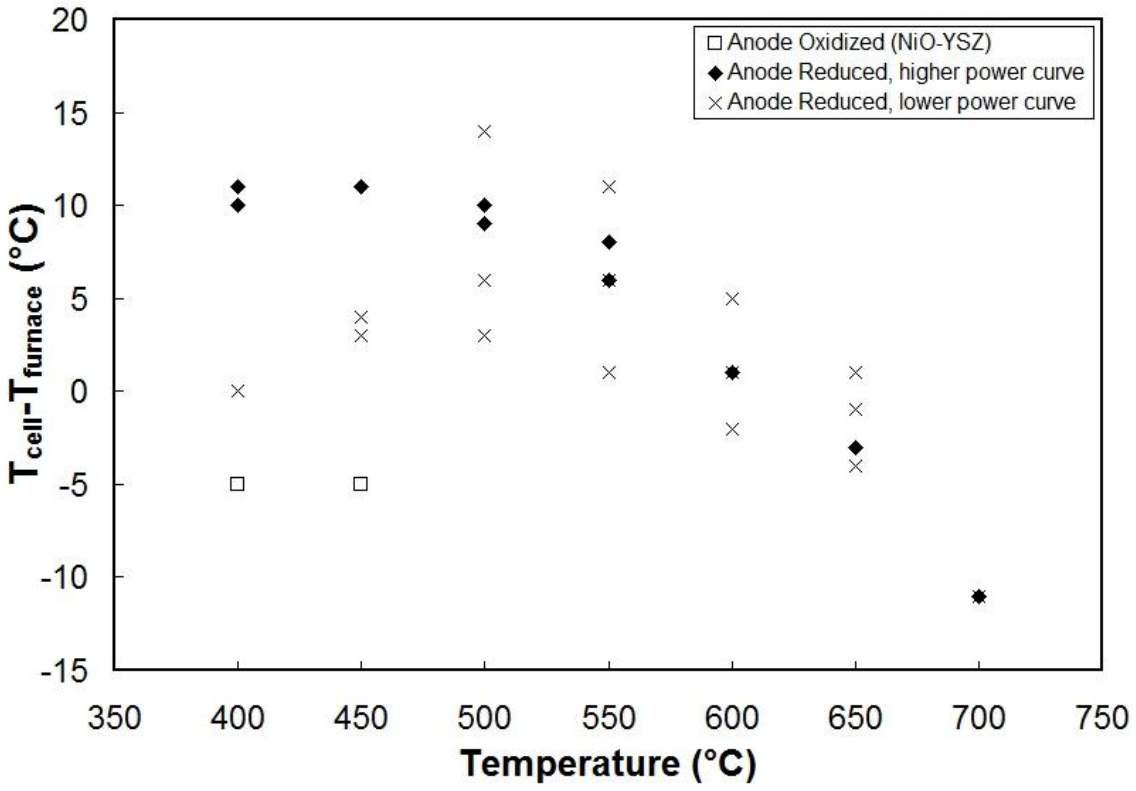

Figure 2.17. Temperature differential between cell and furnace of single chamber SOFC.

2.4. SUMMARY AND CONCLUSIONS

The effect of different hydrogen-oxygen gas compositions on the individual abilities of the anode and cathode to effect and sustain a decrease in O^{2-} activity across the electrolyte of a SC-SOFC was investigated. A dense YSZ electrolyte supported SOFC with NiO-YSZ anode and Ag-LSCF cathode was tested with mixed gas on the anode. The Ni anode was unable to sufficiently lower the O^{2-} activity in fuel-lean mixtures to create a voltage above 0.2 V except at intermediate temperatures of 550 °C to 600 °C where the temperature was high enough that the anode was catalytic enough to utilize the small amount of fuel in the gas mixture, but low enough that the gas did not

react to completion leaving no fuel in the oxygen-bearing product gas. These tests and future tests of similar format may aid in the development of new electrodes which would be better suited for single chamber use.

The hydrogen-oxygen mixture may have reacted before reaching the active area of the anode, and fuel-lean mixtures then caused the Ni anode to partially oxidize to NiO which is both less catalytic and less conductive. The lower voltage and conductivity resulted in lowered power density when a single chamber SOFC with this anode was operated in a stoichiometric gas mixture. The NiO anode was able to reduce again to Ni upon exposure to a gas mixture richer in fuel, with only a miniscule drop in performance, detectable only after several cycles, due to known volume expansion cracking issues in the porous Ni-YSZ matrix.

Voltage oscillations were observed in several of the tests, which could not have been caused by a carbon deposition/burnoff cycle due to the absence of carbon in the hydrogen/oxygen system. These oscillations were not detected when the anode was exposed only to fuel. A redox cycle in the Ni anode was proposed which is believed to cause a periodic change in the catalytic effectiveness and resistance of the cell, leading to voltage oscillations that corresponded to lower power densities. This redox cycle was measured under SC-SOFC operating conditions where carbon-based reactions and related mechanisms did not exist. Future research on development of more redox-stable anode materials may help resolve this issue.

3. ANODE WITH GADOLINIA-DOPED CERIA FOR SOLID CARBON FUEL

3.1. BACKGROUND

In addition to gas fuels such as hydrogen and propane and liquid fuels such methanol and aviation fuel, the high temperature necessary to enable oxygen ion diffusion through the ceramic electrolyte in a SOFC makes the direct use of solid carbon fuel possible [39,44]. Solid carbon may come from internal pyrolysis of hydrocarbon fuel or from the exhaust gas of an internal combustion engine. Diesel engine exhaust soot has been removed from an exhaust filter with an electrochemical reaction [72] but it may be possible to recover energy rather than expend energy while consuming the unwanted particulate pollution, similar to carbon particulate filter regeneration downstream from thermal partial oxidation reformers intended to feed hydrogen to a SOFC [73]. SOFCs capable of using solid carbon fuel could have the potential to recover a significant amount of unused energy while simultaneously decreasing particulate pollution from exhaust streams of various fossil-fueled combustion sources. The amount of electricity recovered from this solid carbon can reduce the load on the alternator and remove the need for filter regeneration, both of which would increase fuel efficiency.

Utilization of solid carbon fuel may be by direct oxidation or by Boudouard gasification [47], which are both made more practical by the correct choice of anode material to catalyze the carbon oxidation reaction [47,51,46], which in turn makes hydrocarbon fuels more practical by oxidizing the deposited solid carbon before it builds up to the point of hindering cell performance.

An SOFC requires the use of an ion conducting ceramic both as the electrolyte and as one component of a cermet (ceramic/metal composite) anode. High ionic

conductivity is necessary to allow oxygen ion transport and minimize internal cell resistance, and for the electrolyte a low electronic conductivity is necessary to minimize electron leakage. When the ionic conductor is used as part of the anode cermet, it should also have high catalytic activity toward oxidation of the selected fuel.

Two ceramic materials commonly used as ion conductors in SOFCs are yttria-stabilized zirconia (YSZ) and gadolinia-doped ceria (GDC). GDC is more catalytically active than YSZ, performing more than eight times better as a catalyst for oxidation of solid carbon than does YSZ [45], and the reaction zone in a GDC anode extends 10 μm to 20 μm beyond the three phase boundary [48]. These characteristics make GDC more favorable as the anode ion conductor for the use of solid carbon fuel in a SOFC [47,49]. YSZ provides the low electrical conductivity which is desirable in an electrolyte material, but as an anode material, it suffers from lower catalytic activity for fuel oxidation than ceria. GDC has higher ionic conductivity than YSZ but suffers from higher electronic conductivity, which makes it less suitable for use as an electrolyte; however YSZ has been used as a thin layer to block electronic conduction with a GDC electrolyte [74].

An SOFC composed of a YSZ electrolyte combined with a GDC anode would have less electron leakage and higher catalytic activity. GDC also shows increased electronic conductivity in the low oxygen partial pressure environment of the anode, further decreasing anode resistance. However, when GDC and YSZ are sintered as adjacent layers, there are significant chemical compatibility problems, [50] including excessive diffusion of Y ions into the GDC causing bulk shrinkage and voids which lead to decreased overall cross sectional area and lower ionic conductivity, as well as lower mechanical strength. Adding Ni to the anode somewhat suppresses the undesirable solid

state reaction, [50] but does not eliminate the problem, as illustrated in Figure 3.1, which shows voids and a crack caused by a Ni-GDC anode sintered onto a YSZ electrolyte. An interlayer of $Ce_{0.43}Zr_{0.43}Gd_{0.10}Y_{0.04}O_{1.93}$ can be used to slow the solid state reaction so a GDC anode can be sintered onto a YSZ electrolyte [50] but this cannot be done with commercially available materials, requiring combustion synthesis or other unconventional methods.

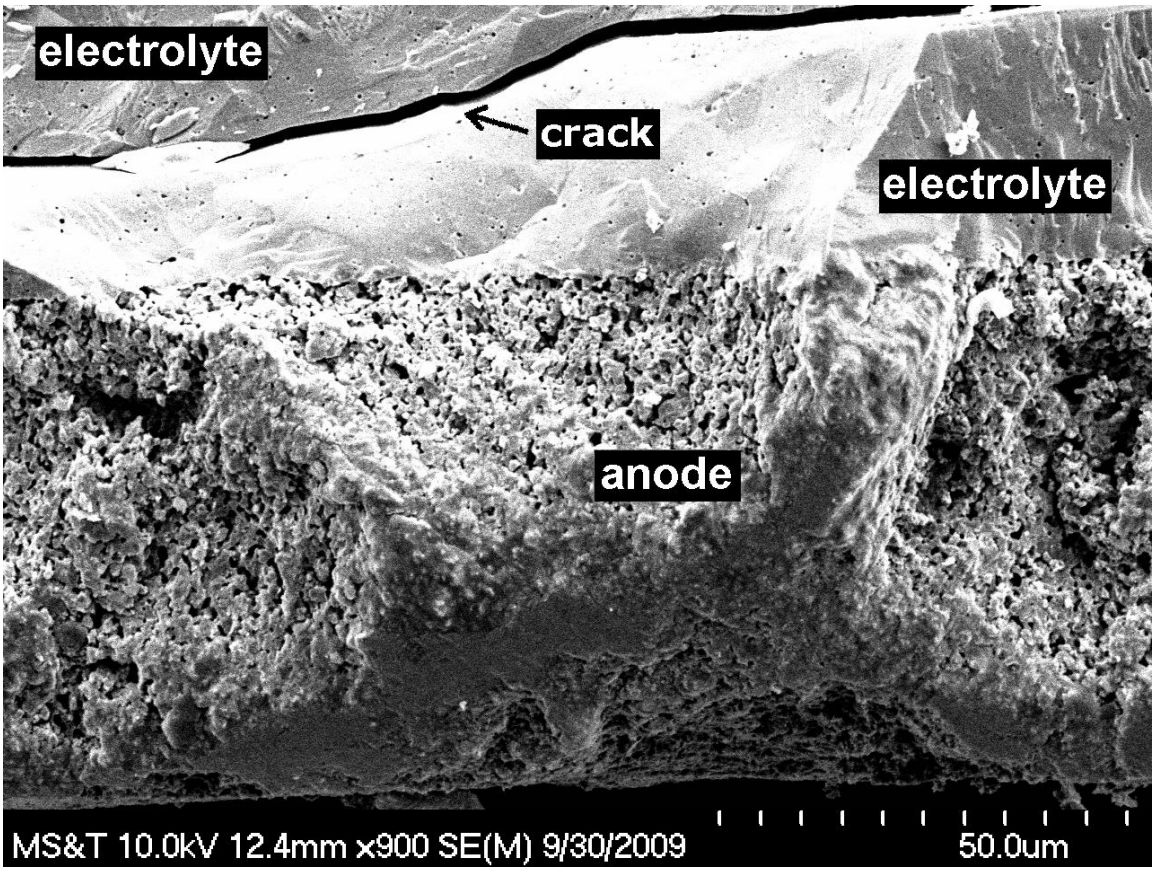

Figure 3.1. YSZ electrolyte (top) and Ni-GDC porous anode (bottom) showing voids and a crack within the electrolyte.

Previous cell construction using GDC anode directly applied to the YSZ electrolyte revealed several problems after sintering, consistent with results from other groups [75][50]. Excess diffusion of Y from the YSZ electrolyte into the GDC anode caused void formation and bulk shrinkage, which in turn led to subsurface cracking. Figure 3.2.a shows the surface of the electrolyte after the anode flaked off. Figure 3.2.b shows some of the anode flakes on both the front and the rear where a thin layer of electrolyte is still visible.

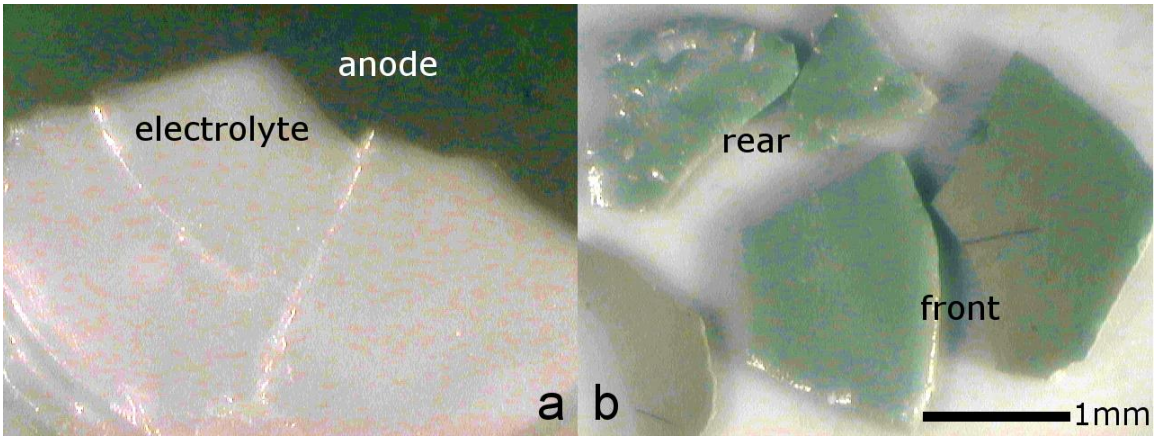

Figure 3.2. (a) YSZ electrolyte surface after GDC anode flaked off, and (b) GDC anode flakes showing a thin layer of electrolyte remaining on the rear surface.

Commercial cells with a YSZ electrolyte and GDC anode are available and do well in testing, both in terms of power production and resistance to carbon fouling, [51] while experimental cells of similar compositions have successfully used solid carbon as fuel [49]. Nevertheless, few researchers have discussed the methods used to overcome

the difficulties in applying a GDC anode to a YSZ electrolyte. The methods which have been presented are less than completely effective, decreasing but not eliminating negative interactions, or require specialty multicomponent oxide materials or unconventional synthesis methods such as glycine-nitrate combustion synthesis [50]. The first objective of the experiments conducted here is to present a simple and effective method to fabricate a functional SOFC using a GDC cermet anode and a YSZ electrolyte using only the commercially available oxide powders necessary to make either a YSZ or a GDC based anode. The second objective is to successfully demonstrate the utilization of not only hydrogen and a hydrocarbon fuel but also solid carbon fuel and this bi-layer SOFC anode for their applications in power generation and pollution control.

3.2. EXPERIMENTAL METHODS

3.2.1. Sample Fabrication. Several cells were fabricated for testing. Electrolytes were 300 μm thick, fully-dense 8 mol% YSZ disks tape cast from Tosoh TZ-8Y powder. In order to promote oxidation of solid carbon as well as to increase anode conductivity, GDC was chosen as the ionic conductor for the anode.

Two anode inks were prepared, denoted as Anode 1 and Anode 2. Each anode ink was mixed from commercial off-the-shelf component powders; NiO (Aldrich, USA), GDC (Praxair, USA), and YSZ (TZ-8Y, Tosoh, Japan); then combined with an equal amount by weight of Ferro B-75000, a commercial pre-prepared screen printing binder

and mixed in mortar and pestle. Anode compositions are given in Table 3.1 by weight percent.

Table 3.1. Bi-layer anode compositions by weight

Layer	NiO	YSZ	GDC
Anode 1	60 wt%	40 wt%	0 wt%
Anode 2	55 wt%	15 wt%	30 wt%

Anode 1 ink was first painted onto an electrolyte disk and allowed to dry at room temperature. Anode 2 ink was then painted over Anode 1 and also allowed to dry at room temperature. The anodes were then sintered in air at 1350 °C for 4 hours, resulting in a sintered anode with a thickness of between 25 and 30 μm, as measured with SEM micrography. A diagram of this configuration is shown in Figure 3.3.

Figure 3.3. Layers of bi-layer SOFC anode.

This anode fabrication method is much simpler or less expensive than many of the methods mentioned in the literature. No combustion synthesis or chemical vapor deposition was necessary, and no equipment more complicated than a simple sintering

furnace was used for fabrication of the anode. Commercial samples by this method could be manufactured with a simple screen printing or inkjet process, which would be both simpler and much less expensive than vapor deposition, while laboratories can make effective fuel cell samples without the cost of specialty multicomponent oxides.

Cathode ink was prepared by combining $La_{0.8}Sr_{0.2}Fe_{0.8}Co_{0.2}$ oxide powder with screen printing binder and mixing in mortar and pestle. The cathode was painted onto each electrolyte disk opposite the anode and sintered in air at 900 °C for one hour.

3.2.2. Test Procedures. Cells were mounted in a furnace and heated to 800 °C at a rate of 5 °C/min, and all measurements were taken at this furnace temperature. The actual cell temperatures were measured by thermocouple to be 5-15 °C higher than the furnace temperature due to the exothermic reactions taking place at the electrodes. The actual temperature increase depended on the type of test being performed. The cathode was exposed to a flow of preheated air at 300 mL/min, and the anode was exposed to various preheated fuel gases at 300 mL/min, including 5% H_2 in Ar, 10% H_2 in N_2, and propane. All gas flows unless otherwise specified were at a rate of 300 mL/min.

When operated with propane fuel, solid carbon was deposited on the anode by pyrolysis of this hydrocarbon fuel. Any remaining fuel gas was flushed from the test chamber with Ar for sufficiently long times to ensure no gaseous fuels remained in the system [45,47]. The solid carbon remaining on the anode was used as indirect fuel by flowing CO_2 gas, which is a major component of hydrocarbon combustion exhaust and found with soot in diesel engine exhaust, over the anode to gasify the carbon via the Boudouard reaction, converting it to CO, according to equation 9, which can be directly utilized by the anode as fuel.

$$C + CO_2 \rightarrow 2CO \quad (9)$$

Temperature measurements were taken with a type R thermocouple. Gas flow was measured with Cole-Parmer 112-02-N ball flow meters calibrated for nitrogen. Correction factors for the ball flow meters were determined by flowing gas through a Tylan FC-260 electronic mass flow controller and then through the ball flow meters. Electrical tests were taken by four-point probe with a Solartron CellTest 1470 system, and recorded by CorrWare and Zplot software. Impedance was measured from 1 Hz to $1x10^6$ Hz at an amplitude of 20 mV AC. SEM micrography was performed with a Hitachi S-4700 scanning electron microscope.

3.2.3. Error Analysis. Voltage measurements are accurate to within 1%, current density and impedance measurements to within 5%, for a 95% confidence interval. Details on uncertainty analysis can be found in the appendix.

3.3. RESULTS AND DISCUSSION

A representative sample SOFC identical to the ones used in the present tests was fractured and examined under SEM. Figure 3.4 shows the cross section, with a thin porous bi-layer anode on the bottom firmly bonded to the dense electrolyte on the top of each picture, revealing that the electrolyte was intact and had no voids. If detrimental interactions between the GDC and YSZ had occurred, there would have been significant bulk shrinkage evidenced by voids or cracking in the electrolyte layer near the porous anode, as shown in Figure 3.1. The adjacency of the GDC and YSZ was located in the

anode, where porosity is necessary for gas transport, and where bulk shrinkage normally takes place during sintering.

Figure 3.5 shows the results of the open circuit voltage (OCV) tests with the anode exposed to various fuels, including 5% H_2 in Ar and 10% H_2 in N_2, which produce identical voltage around 1.0 V, both represented on trace (a), revealing that the SOFC was capable of producing about 1 V in hydrogen which is consistent with values recorded by other groups [22]. Trace (b) in Figure 3.5 shows the OCV as the cell is first exposed to propane after operating with H_2 fuel, and trace (c) shows the voltage in propane after an hour of propane operation and then 300 seconds of potentiostatic operation at 0.5 V, which allows oxide ion current to flow through the electrolyte and consume the solid carbon which clogged the anode porosity. Trace (d) shows the voltage recorded when the gas was switched to argon at 0 seconds, after 420 seconds of open-circuit operation in propane to pyrolytically deposit solid carbon on the anode.

It is interesting to note that after operating the sample in propane for less than sixty seconds, the OCV had dropped by about 0.075 V from its initial value, but after increasing the current and operating in potentiostatic mode, recording current at a constant 0.5 V, and then again measuring the open circuit voltage, the voltage increased initially and then slowly decreased. This is consistent with results reported by other groups [47] that the open circuit condition tends to allow carbon buildup which decreases the OCV, while an increased current consumes some of the deposited carbon and restores some porosity to the anode, restoring the high OCV.

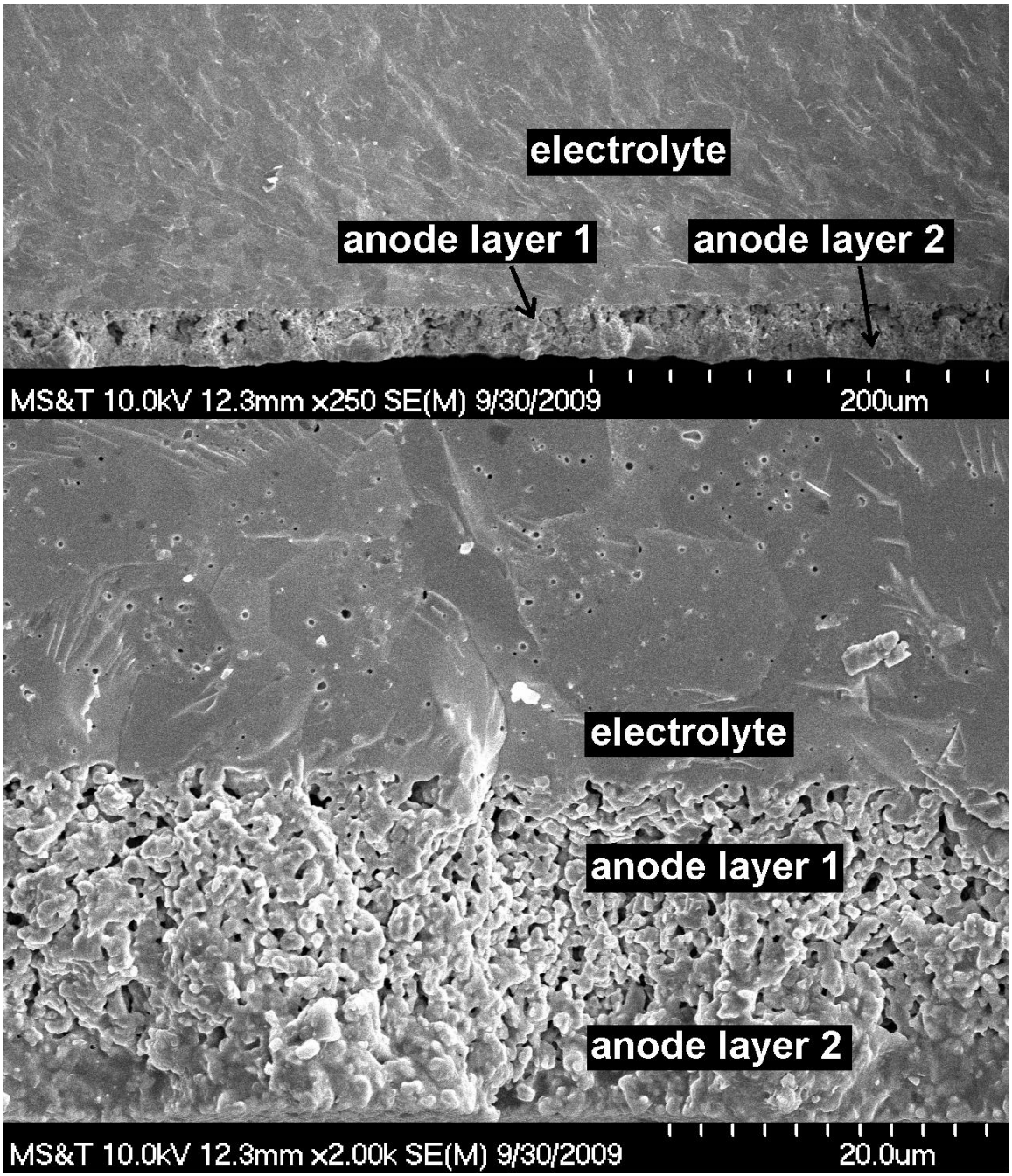

Figure 3.4. SEM photos of the bi-layer anode SOFC cross-section showing the anode and proximate electrolyte.

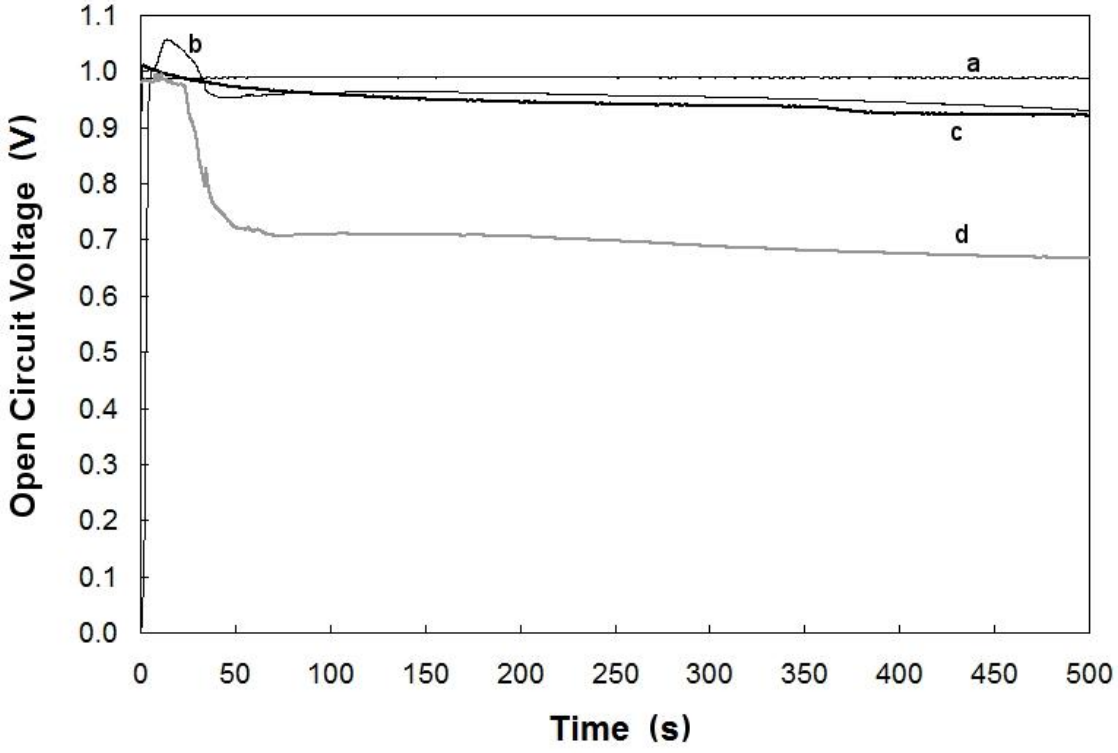

Figure 3.5. OCV of the bi-layer anode SOFC when operated with (a) 5% H_2 and 10% H_2 (b) initial propane, (c) propane after 1h of propane and 5 min of potentiostatic operation at 0.5 V, (d) Ar after 7 minutes of propane on a new cell.

The cell initially produced a maximum power of about 65.6 mW/cm^2 using 5% H_2 as fuel, but after about an hour, the cell degraded slightly and only produced 61.6 mW/cm^2 with 10% H_2 fuel, and subsequently 61.8 mW/cm^2 with propane fuel. This amount of power is lower than current thin-electrolyte technology cells capable of

producing up to 500 mW/cm^2 [22], but it is quite respectable when the 60 times thicker 300 μm electrolyte and diluted 5% fuel is taken into account.

A new identical cell was exposed to propane fuel gas stream at 300 mL/min for 420 seconds, achieving identical voltage performance to (b) in Figure 3.5, co-represented by trace (b). The cell was then flushed with pure Ar at 300 mL/min, giving a linear velocity of over 70 cm/s, and the OCV during this flush is shown in (d) of Figure 3.5. The voltage stayed nearly constant at about 1 V for several seconds until the gas tubes had been flushed of propane, and then abruptly dropped as the propane was flushed away from the cell. By 100 s after the gases had been switched, the voltage had leveled at 0.7 V and stayed constant for a further 600 s. This shows that the propane is certain to have been removed from the cell in only a few minutes. The anode gas was then switched to CO_2 under which the cell generated greater than 0.85 V for two minutes after the Ar had been flushed away. Therefore the cell was capable of voltage generation using pyrolytically deposited carbon as fuel, in both Ar and CO_2 gases.

After an identical carbon deposition and argon flush, current was recorded while the cell was held at 0.4 V, approximately half the OCV which was recorded with CO_2 gas flow over the pyrolytically deposited carbon. The cell produced a current density greater than 14 mA/cm^2 and power of 5.65 mW/cm^2 for about sixty seconds, before the soot started to become depleted, as seen in Figure 3.6. Although the power generated with solid carbon fuel is only about 10% of that generated with hydrogen or hydrocarbon fuels, it is consistent with the early results of other groups [45], and is a reasonable value for the first fabrication of this type of cell. Subsequent tests can be expected to increase power by varying the anode thicknesses, composition, porosity, or sintering schedules.

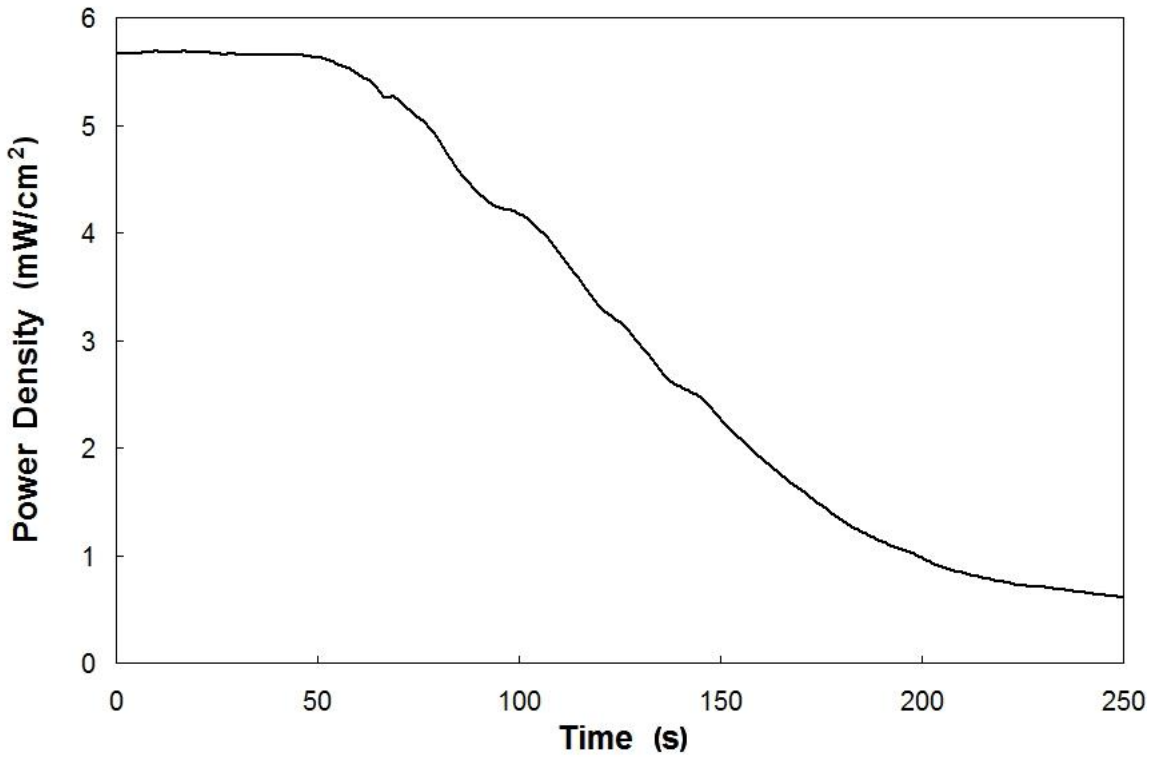

Figure 3.6. Area specific power of cell in operation with CO_2 over anode after 7 minutes OCV operation in propane and 10 minutes Ar flush.

The linear slope of the decrease from 5.6 mW/cm^2 to 0.5 mW/cm^2 between 75 seconds and 175 seconds was probably the result of the consumption of carbon at the most active areas of the anode first, those areas of three phase boundary closest to the electrolyte [47]. As the carbon closest to the electrolyte was consumed, oxygen ions were required to travel a longer distance through the ionic conductor in the anode to gain proximity to fuel at a three phase boundary. This longer ionic conduction distance increased the overpotential and decreased the power.

However, recent studies indicated that little pyrolytic carbon was deposited on the more active interior portions of the anode [43], so a more important aspect might be that the generation point of the CO gas moved farther away from the electrolyte, further increasing the overpotential due to gas transport issues. The effect of increasing conduction distance and the effect of increased gas transport distance would both be expected to decrease the produced power in a linear fashion.

Two more subsequent tests showed near identical performance, with only minor decrease attributable to electrolyte aging, indicating that at least three short 10-minute deposition/utilization cycles are possible. Although longer testing times and more deposition/utilization cycles may reveal anode deterioration, longevity can be improved in subsequent tests by varying anode thickness, porosity, and particle size. The results presented here indicate that this simply fabricated cell was capable of power generation with a variety of fuels, including hydrocarbons and solid carbon, on par with cells fabricated by means of more elaborate and expensive methods.

The polarization profile shown in Figure 3.7 reveals linear, ohmic behavior without sudden decrease at high current, which shows that the reactions at the anode do not excessively hinder the cells operation. Excess porosity or cracking in the electrolyte, such as from a YSZ-GDC interaction, would exhibit in the polarization profile as a decrease in voltage at higher current density due to an increased electrolyte overpotential. From (a) to (e) was about 6 hours of operation of a single cell. A small decrease in voltage at higher current density is evident in (e), however the Cole-Cole impedance plot in Figure 3.8 shows that this increase in overpotential is from the anode and because the lower overpotential can be restored by allowing current through the cell to consume

carbon, this likely is due to carbon buildup, which limits gas transport to the active area of the anode.

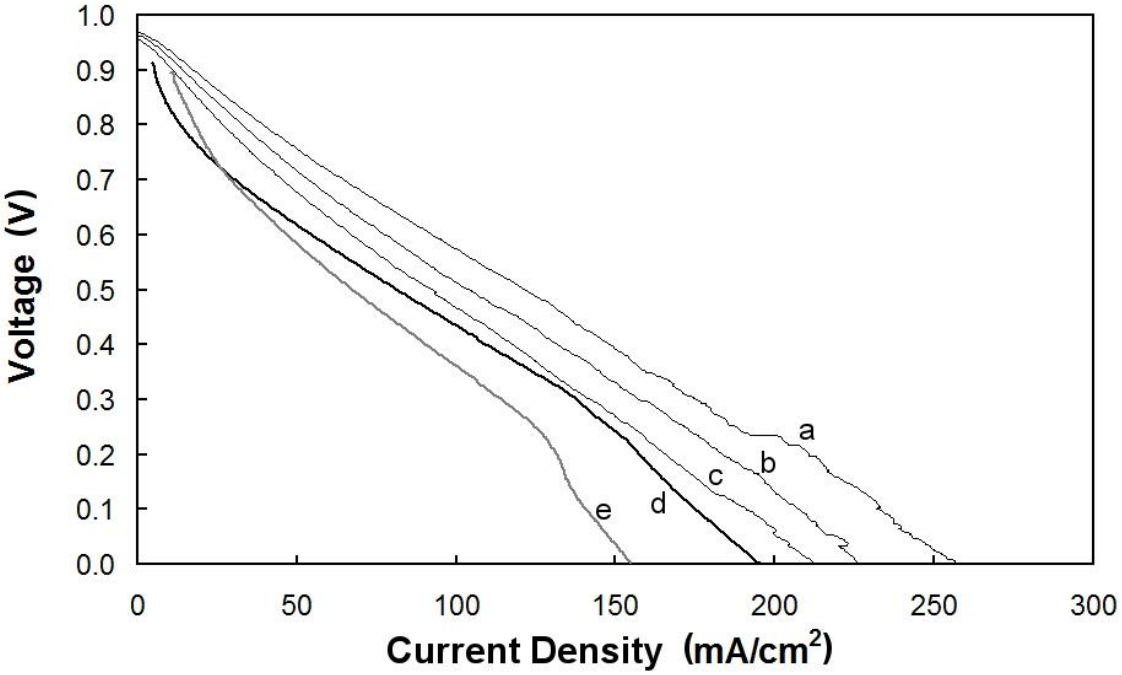

Figure 3.7. Polarization graph of three subsequent tests in 5% H_2 (a-c) and two subsequent tests in propane (d,e).

The Cole-Cole plot showing the impedance of the SOFC in operation is shown in Figure 3.8 for four tests spanning about 8 hours of operation in heavily-sooting propane. The first test is labeled (a), the fourth test is (b), the sixth (c) and the eighth test is labeled (d). Each test was about an hour apart, during which time other tests were run, including OCV and potentiostatic tests.

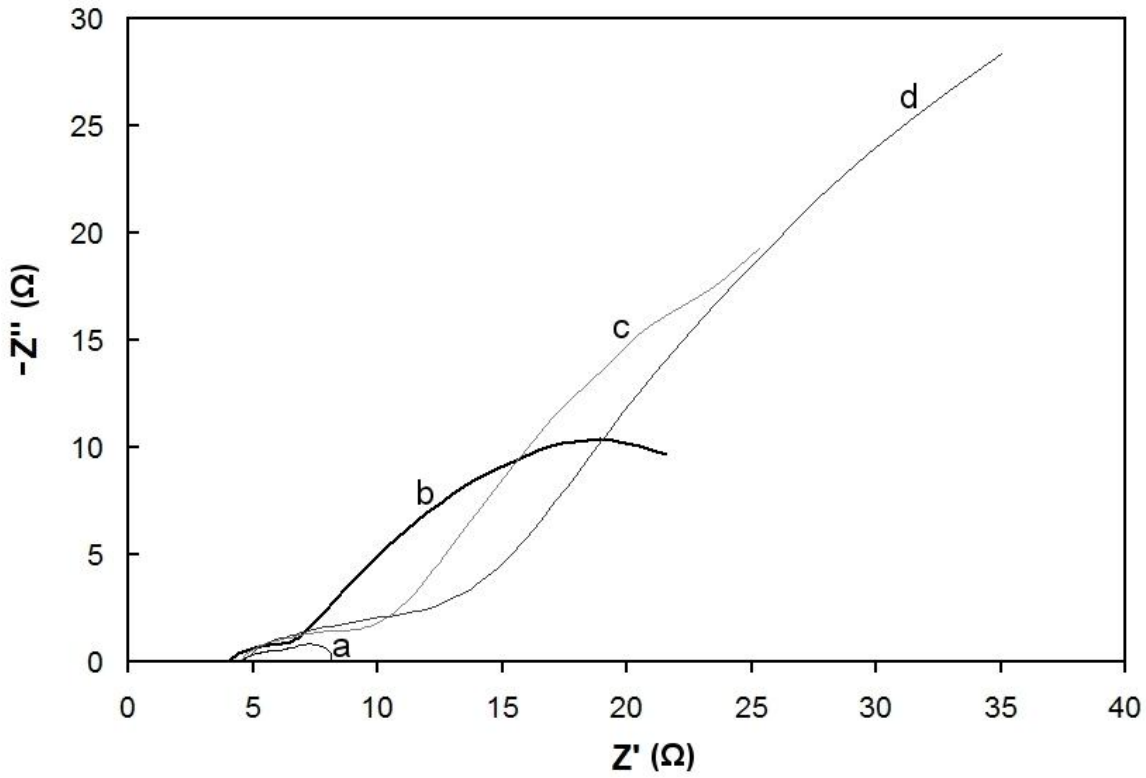

Figure 3.8. Cole-Cole plot showing the impedance of the SOFC in operation with propane fuel after (a) 1 hour, (b) 4 h, (c) 6 h, (d) 8 h.

It should be noted that the electrolyte resistance (the distance on the Z' axis between the 0 mark and the intersection of the impedance curve with the Z' axis) remains fairly constant, changing only about 10% over the course of four hours, only slightly decreasing from 5 to 4.5. This is attributable to aging of the electrolyte as it allows more electron leakage that decreases both the cell resistance and the OCV. The cathode equivalent resistance (the size of the leftmost, high frequency semicircle of the impedance curve) remains approximately the same as well. However, the anode equivalent resistance (size of the rightmost, low frequency semicircle) increases

dramatically from (a) to (d). This is because the anode overpotential increases as the anode becomes clogged with solid carbon, increasing the resistance of gas transport to the active area of the anode.

3.4. SUMMARY AND CONCLUSIONS

A simple method for applying a GDC bearing anode to a YSZ electrolyte was demonstrated, and power in excess of 60 mW/cm^2 was recorded with both hydrogen fuel and propane fuel, and an amount of power similar to the first solid carbon fuelled cells developed by other groups was recorded with pyrolytically deposited carbon fuel. Cell performance indicated no detrimental effects of YSZ/GDC adjacency, and SEM revealed no voids or other indications of the problems typical of YSZ/GDC interactions. The method presented here is significantly simpler than the methods which rely on complex oxide mixtures, and more effective than the methods which rely on higher Ni content in the GDC anode. This allows for easier fabrication of carbon-deposition resistant cells or cells which can collect and utilize soot from a diesel engine exhaust stream to decrease particulate pollution and increase fuel efficiency both by removing the necessity of filter regeneration and by secondary power generation which can decrease the power consumption requirements of the alternator.

4. SOLID OXIDE FUEL CELL UTILIZING SIMULATED DIESEL SOOT AS FUEL

4.1. BACKGROUND

Diesel engines are the primary power plant for most cargo shipping in the United States and much of the world, as well as local small-scale power generation and heavy-duty personal transportation. In recent years, heightened environmental awareness has led to increasing regulation of these historically sooty engines [54,56]. In addition to more stringent fuel purity standards and higher efficiency engine designs, diesel particulate filters (DPF) are used to capture particulate material (PM) from the exhaust.

Studies on the size and structure of particulates [53,52] have increased the understanding of what is necessary for a DPF to be effective. Research continues into more effective and durable materials such as aricular mullite [59] or high temperature metal foam [58]. Structural changes in the DPF are also being studied, such as growing ceramic "whiskers" on a standard porous ceramic filter [60].

Any filter eventually will become clogged and need replacement or cleaning, and a DPF in operation accumulates enough soot to increase the backpressure of the exhaust system enough that fuel economy suffers [61,58]. A DPF is typically too expensive and becomes clogged too quickly for easy replacement, so cleaning is accomplished by a process called regeneration, typically through "post-injection" of fuel into the exhaust stream combined with changing engine control parameters to increase air in the exhaust, which burns on a catalyst near the DPF to raise the temperature high enough to burn off the carbon accumulated in the DPF [59].

While regeneration does clear the DPF and lower the backpressure on the exhaust system to original levels, it presents another set of problems. Regeneration decreases average fuel economy because it consumes significant amounts of fuel which is not used to run the engine. For this reason, there is research into alternative methods of regeneration, such as microwave heating of the DPF [63] or injection into the DPF of highly active oxidizing species such as ozone from plasma reactors [64]. Other research focuses on lower temperature regeneration by direct injection of plasma into the DPF [65] or by addition of a catalyst to the diesel fuel [66], which may open up new lower-temperature materials for possible DPF use.

During operation of a diesel engine equipped with a DPF, fuel economy drops continuously as the DPF becomes clogged, increases back pressure of the exhaust, and changes the filtering ability as well as regeneration characteristics [62]. Therefore research has been directed toward continuous regeneration [64] to maintain low exhaust back pressure.

Unfortunately, regeneration itself increases pollution; for traditional post-injection regeneration the amount of particulates exiting the exhaust is increased by 1000 to 10,000 times [56], but all pollutants including unburned hydrocarbons are increased [57]. Modern diesel engine requirements decrease the mass of particulates in the exhaust but actually increase the number of nanoparticles [54], which are more dangerous to health.

However, new solid oxide fuel cell (SOFC) technology exists which can directly utilize solid carbon, including pyrolytic soot, for fuel to generate small amounts of electricity, around 50-60 mW/cm^2 [45,49]. This type of SOFC can electrochemically

oxidize solid carbon or use the Boudouard reaction (equation 9) to gasify the carbon in-situ within the anode to produce carbon monoxide gas which is then used as fuel.

A DPF has been tested which uses electrical current to electrochemically consume soot in what is essentially a SOFC with externally applied current [72]. A combination of these two technologies offers the possibility of a DPF constructed from a SOFC with continuous regeneration and simultaneous power generation. Partial oxidation of nano-sized particulates may be induced in the gaseous state [47] by injection of small amounts of air, to consume particulates which are routinely missed by the DPF.

An initial cell has been constructed with this ultimate goal in mind. Acetylene soot, a close simulator of diesel engine soot as shown in Figure 4.1 [76,52], was used as fuel in an atmosphere of CO_2 to analyze the possibility of using a future cell of this lineage as a DPF.

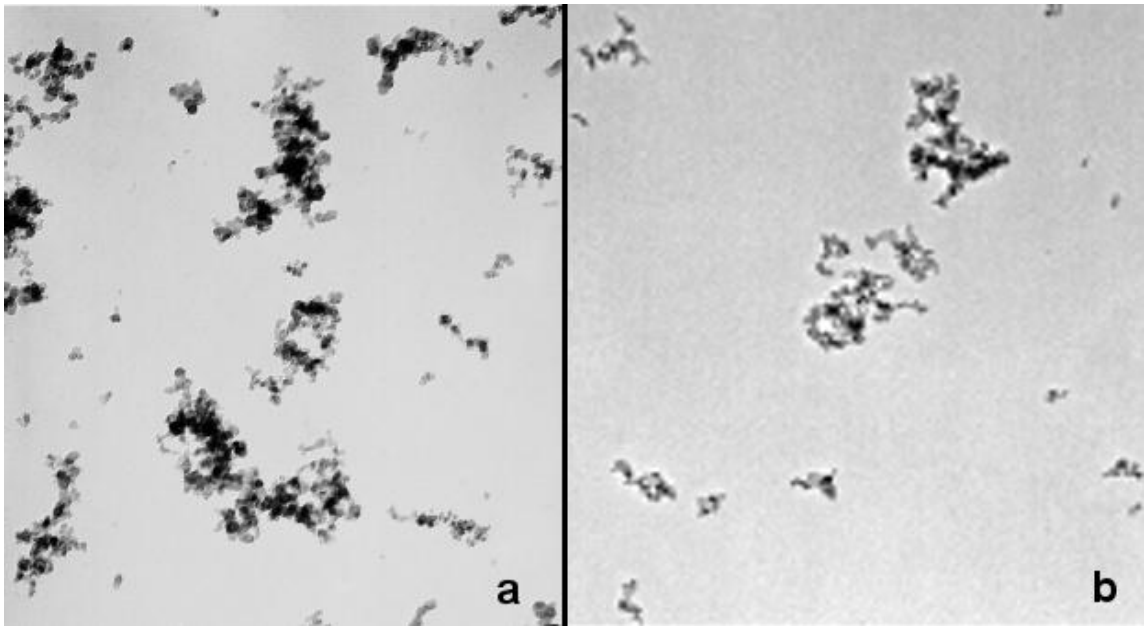

Figure 4.1. (a) Acetylene soot [76] and (b) diesel engine soot [52].

4.2. EXPERIMENTAL METHODS

4.2.1. Sample Fabrication. The cells for these tests were electrolyte supported, with a 300 μm thick fully-dense electrolyte composed of 8 mol% Y_2O_3 stabilized zirconia (8YSZ), tape cast from Tosoh TZ-8Y powder. The anode was composed of NiO (Aldrich, USA) and GDC (Praxair, USA) as these materials work well in cells intended for use with solid carbon fuel. However, due to negative interactions with YSZ, a porous buffer anode layer composed of NiO and YSZ (TZ-8Y, Tosoh, Japan) was used to prevent undesirable porosity in the electrolyte, as discussed in the previous chapter. Therefore, two anode inks were prepared, denoted as Anode 1 and Anode 2. The anode component powders were combined with an equal amount by weight of Ferro B-75000, a commercial screen printing binder and mixed in mortar and pestle, the compositions are given in Table 1 by weight percent.

Table 4.1. Bi-layer anode compositions by weight for soot fueled cell

Layer	NiO	YSZ	GDC
Anode 1	60 wt%	40 wt%	0 wt%
Anode 2	65 wt%	0 wt%	35 wt%

Anode 1 ink was first painted onto an electrolyte disk and allowed to dry at room temperature. Anode 2 ink was then painted over Anode 1 and also allowed to dry at room temperature. The anodes were then sintered in air at 1350 °C for 4 hours, resulting in a sintered anode with a thickness of between 3 and 5 μm, as measured from SEM

micrographs. This configuration is identical to that shown in Figure 3.3, but with both anode layers thinner to limit gas diffusion overpotential.

Screen printing binder and $La_{0.8}Sr_{0.2}Fe_{0.8}Co_{0.2}$ oxide powder were combined and mixed in mortar and pestle to make the cathode ink, which was painted onto each electrolyte disk opposite the anode. The cells were then sintered in air at 900 °C for one hour.

Some cells were held over a laminar non-premixed sooting acetylene flame in order to deposit soot on the anodes. Each cell was dipped into the post-flame gas stream for half of a second, sixty times, leaving a black layer of soot about 150 µm in thickness, as measured with SEM, on the anode. Other cells were sooted for a single dip in the same acetylene flame, to apply a very thin layer of carbon PM, less than 3 µm.

4.2.2. Test Procedures. Both sooted and bare cells were mounted in a furnace and heated to temperatures between 600 °C and 900 °C at a rate of 5 °C/min while the cathode was exposed to low flow rates (60 mL/min) of air to prevent undesirable reduction of the cathode materials, and the anode was exposed to low flow rates of 5% H_2 in N_2, to prevent the soot from being oxidized by air before the measurement temperature was reached. All measurements were taken at this furnace temperature, but the actual cell temperature was 5-10 °C higher, as indicated before, depending on the type of test being performed, due to the exothermic reactions taking place at the electrodes.

During testing, the cathode was exposed to a flow of preheated air at a flow rate of 300 mL/min, and the anode was exposed to various preheated fuel gases at 300 mL/min, including 5% H_2 in N_2, CO_2, and propane. All gas flows unless otherwise specified were at a rate of 300 mL/min. When operated with propane fuel, solid carbon

was deposited on the anode by pyrolysis of the propane. Any remaining fuel gas was flushed from the test chamber with Ar for sufficiently long times to ensure no gaseous fuels remained in the system [45,47], which was verified by OCV measurements. Any solid carbon on the anode, whether externally applied from acetylene or diesel engine, or applied in situ from pyrolytic propane decomposition, was used as indirect fuel by flowing CO_2 gas over the anode. CO_2 was used because it is found with soot in diesel engine exhaust, and because it gasifies the solid carbon to CO according to the Boudouard reaction, equation (9).

$$C + CO_2 \rightarrow 2CO \tag{9}$$

Temperature measurements were taken with a type R thermocouple. Gas flow was measured with Cole-Parmer 112-02-N ball flow meters calibrated for nitrogen. Correction factors for the ball flow meters were determined by flowing gas through a Tylan FC-260 electronic mass flow controller and then through the ball flow meters. Electrical tests were taken by four-point probe with a Solartron CellTest 1470 system, and recorded by CorrWare and Zplot software. Impedance was measured from 1 Hz to $1x10^6$ Hz at an amplitude of 20 mV AC. SEM micrography was performed with a Hitachi S-4700 scanning electron microscope.

4.2.3. Error Analysis. Voltage measurements are accurate to within 1%, current density and impedance measurements to within 5%, for a 95% confidence interval. Details on uncertainty analysis can be found in the appendix.

4.3. RESULTS AND DISCUSSION

4.3.1. Acetylene Soot Deposition. In order to ensure sufficient fuel to last through the furnace warmup and the testing procedures, a thick layer of soot from an acetylene torch, about 150 µm, was applied to each cell by dipping the cell into the flame for ½ second sixty times. The cells were then examined under both an optical microscope and a scanning electron microscope to determine the characteristics of the soot deposits.

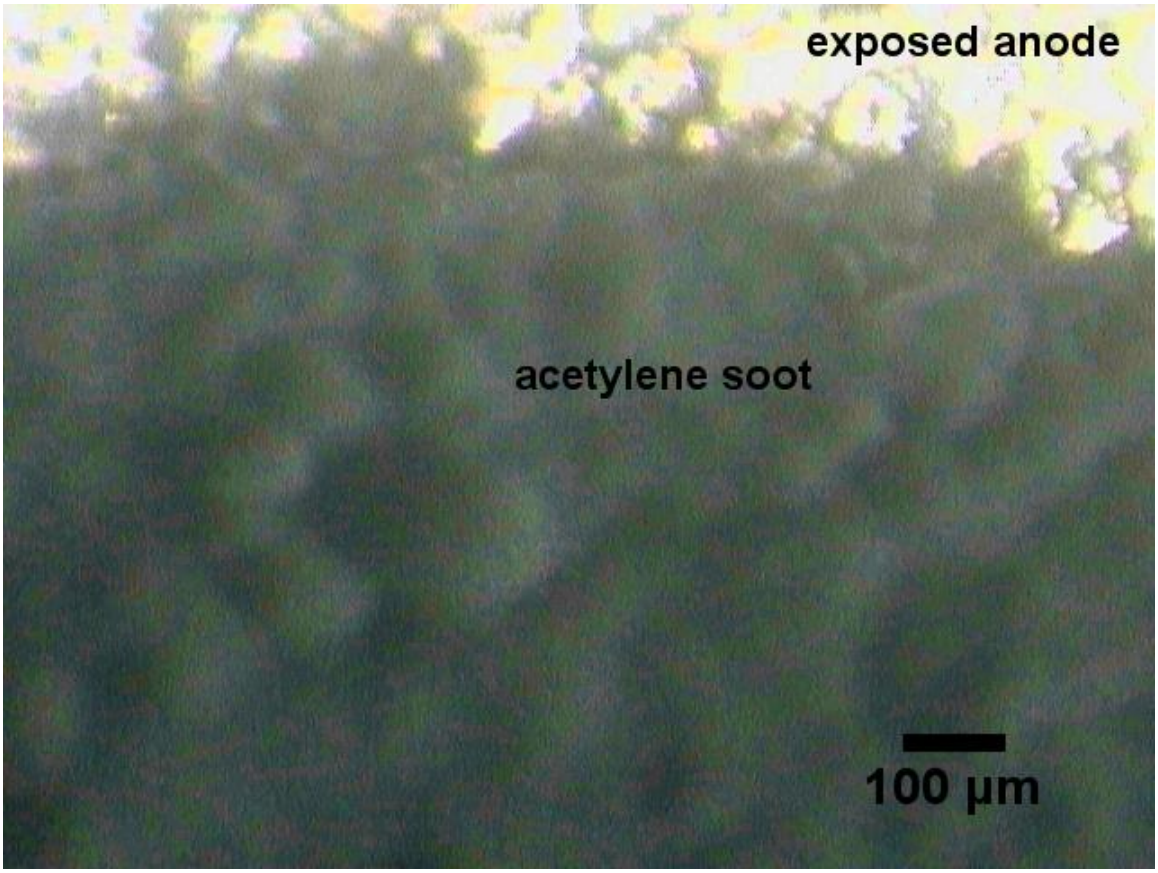

Figure 4.2. Optical microscope image of the thick acetylene soot deposit on the anode, and the edge of the reduced Ni-GDC anode.

Figure 4.2 is a photograph taken through an optical microscope, showing the anode of a cell with this thick acetylene soot deposit, and a small portion of the bare anode visible at the top edge where the alumina fiber mask covered the rest of the cell. The center of the cell is visible in Figure 4.3, covered in a thick layer of soot with a very smooth, nearly featureless, dense appearance, visibly lacking any macroscopic porosity which would aid the necessary gas diffusion into the anode. When contrasted with a corresponding photograph of pyrolytically deposited soot in Figure 4.10, it becomes clear that gas transport through this layer would be severely hindered.

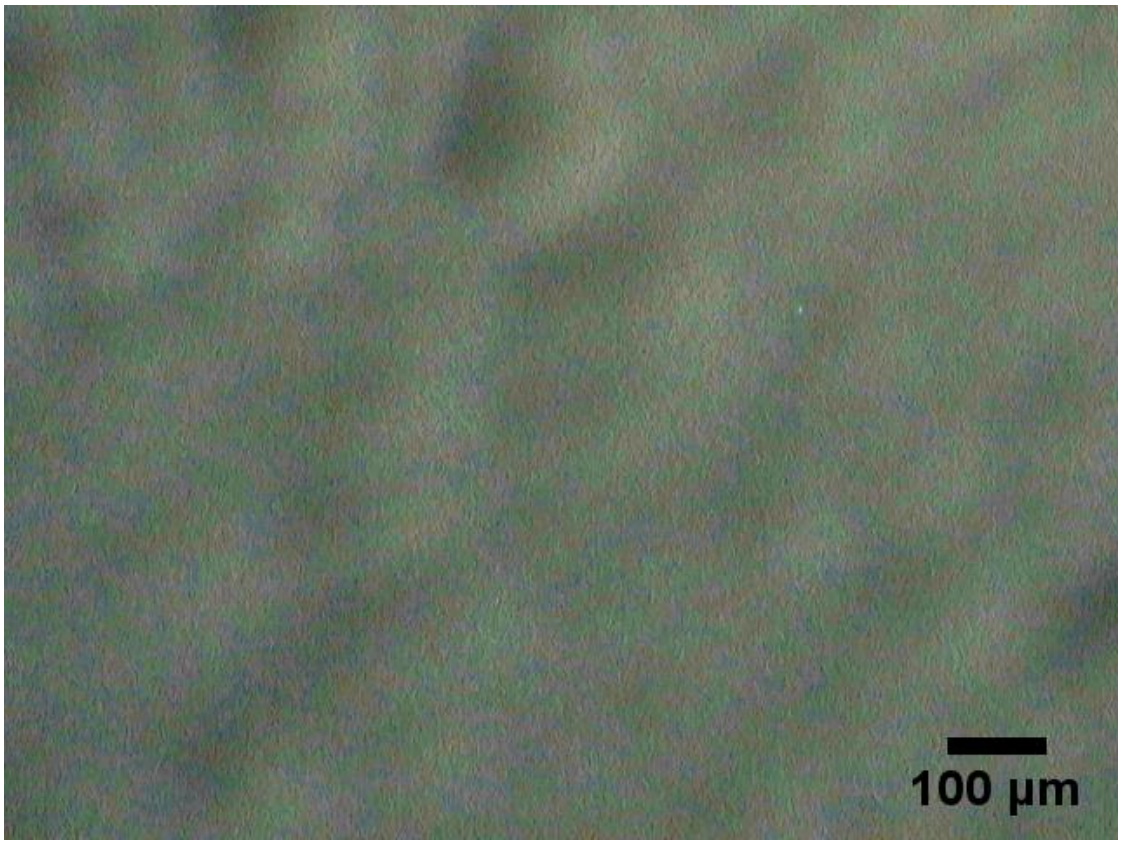

Figure 4.3. Optical microscope image of the thick, smooth acetylene soot deposit on the center of the anode.

The edge of a fractured cell is visible under the SEM in Figure 4.4 where the 100 µm thick layer of soot is visible on top of the thin anode. This soot layer is 3-4 times thicker than a typical electrolyte-supported SOFC anode, and 20 times thicker than the thin anode used in the present study. The material below the cathode is the conductive tape used to secure the sample to the SEM pedestal.

Figures 4.5 and 4.6 show higher magnification images of the same soot, revealing a lack of micrometer scale porosity, which would be expected to greatly hinder gas diffusion into the anode. Because gas diffusion into the anode is very important [77], often the rate limiting step in a solid carbon fuel SOFC [43], this in turn decreases the power output of the cell by an order of magnitude or more beyond the low power typically produced by solid carbon fuel.

Tiny particles as small as 50 µm are visible on the bulk soot in Figure 4.6, which are likely aggregates of the nanoparticles known to be produced by an acetylene flame, though some individual nanoparticles may be visible as the size of these primary particles varies from 15 to 50 nm [76], the same as primary particles from an internal combustion engine [52,53,54]. There is little to no visible open porosity in this photograph, which effectively provides a gas seal over the anode, preventing the necessary gas diffusion from taking place. This limits the reaction mechanism to the much slower direct oxidation of carbon at the three-phase boundary [11] rather than the faster Boudouard gasification [47] which significantly increases fuel mobility.

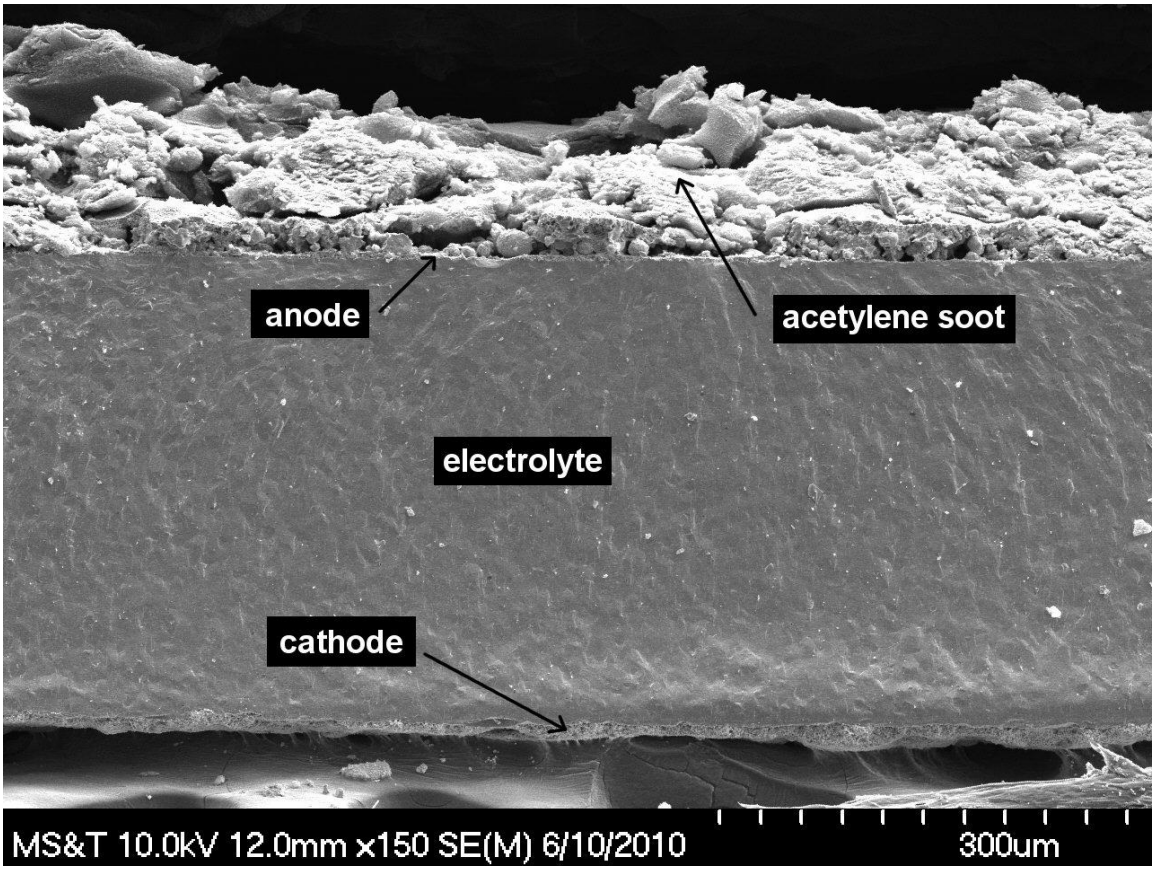

Figure 4.4. SEM image of the fracture cross section of the cell showing thick acetylene soot deposit on top of the anode.

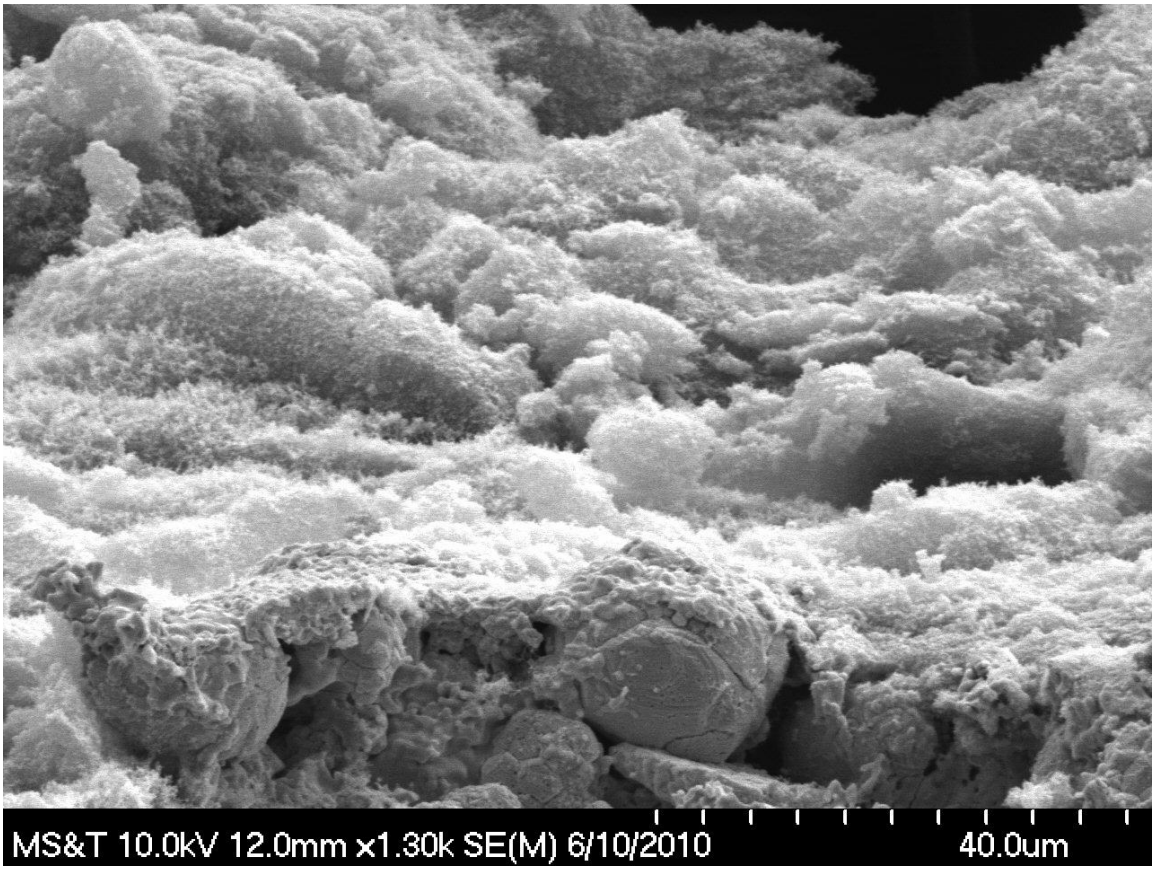

Figure 4.5. SEM image of thick acetylene soot deposit on the anode.

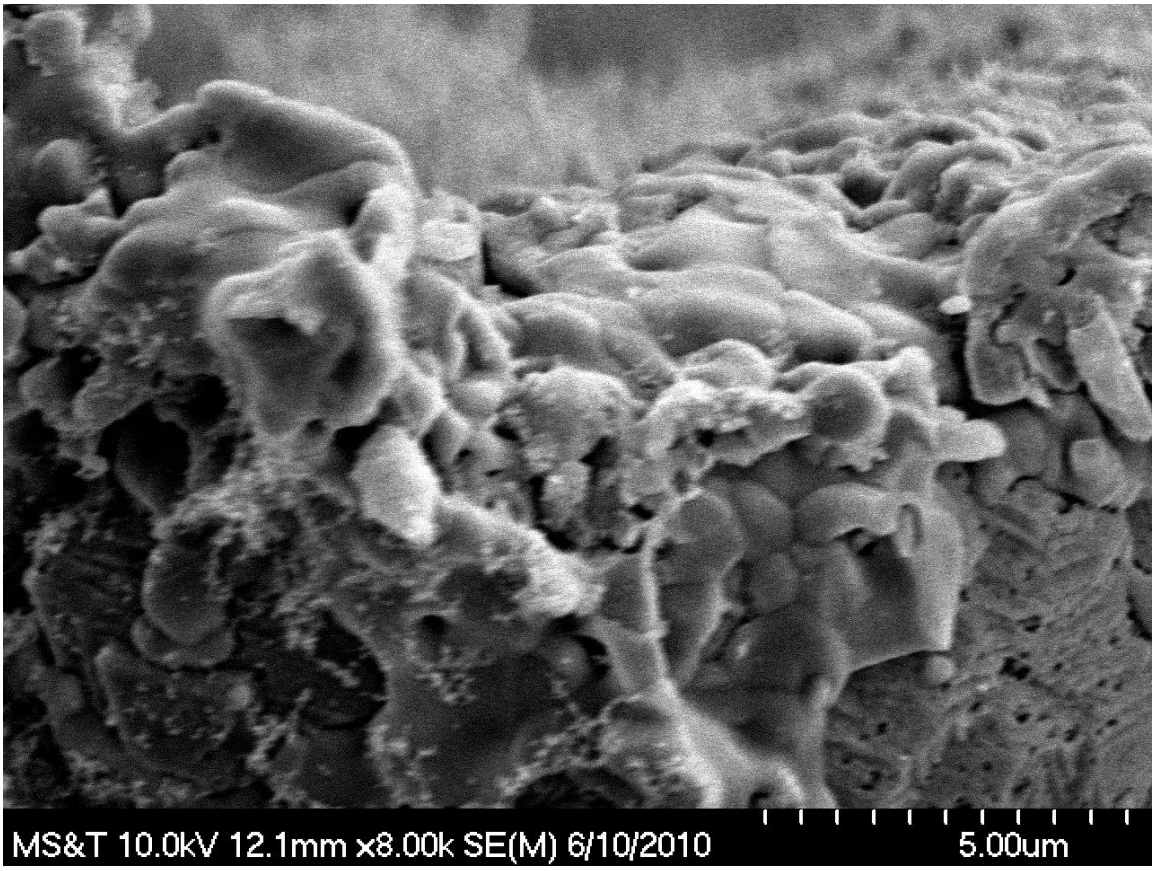

Figure 4.6. High magnification SEM image of thick acetylene soot deposit on the anode.

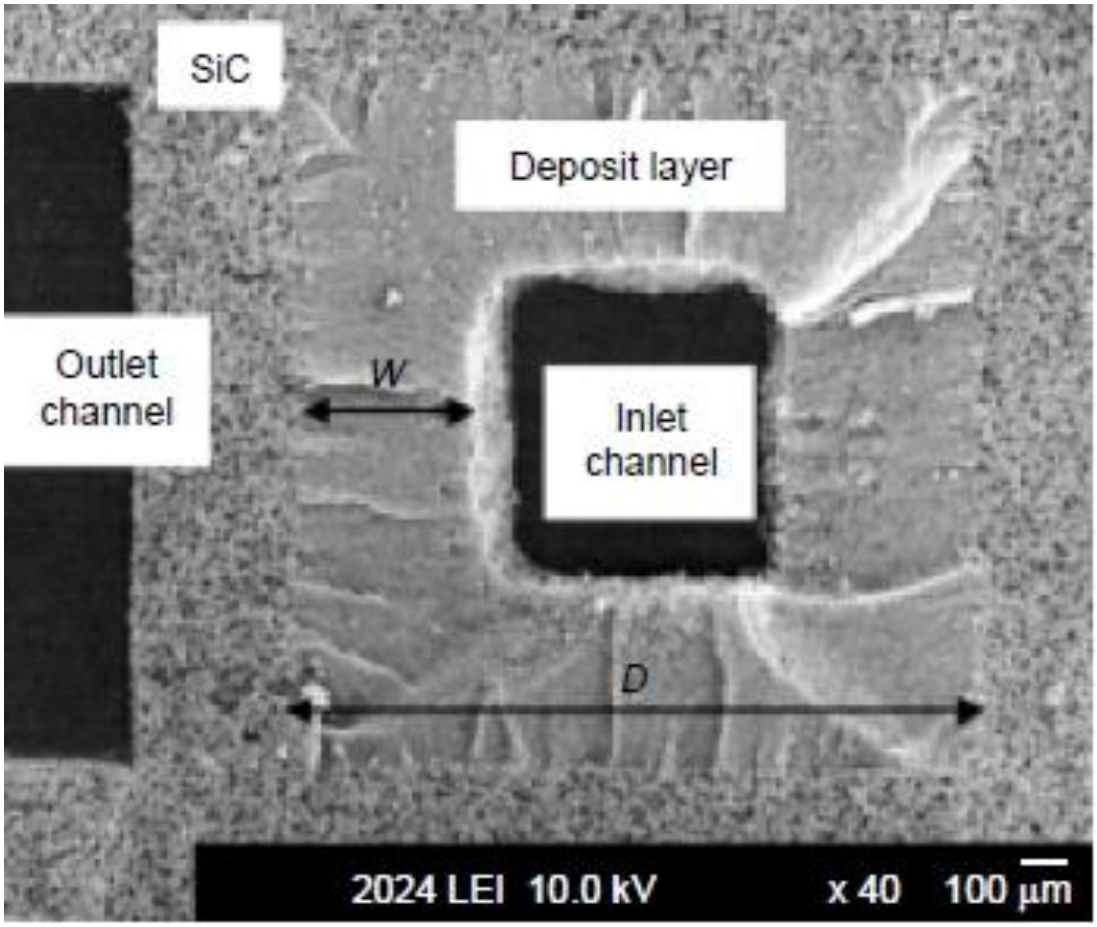

Figure 4.7. SEM image of thick diesel soot deposit on diesel particulate filter [66].

The dense layer of acetylene soot built up on the anode is very similar to that found in a DPF, such as the SEM image in Figure 4.7 from Millet et. al. [66]. The problem of limited gas transport through the thick layer of carbon is common to SOFC and DPF uses, as the structure of the deposit affects DPF regeneration [62] and gas flow through the filter itself during operation [61], which is why much research is focused on decreasing pressure drop through the DPF.

Because of the difficult gas diffusion through the thick acetylene soot, some cells were sooted with only a single ½ second dip into the acetylene flame. Examination under optical microscope revealed a thin, discontinuous layer which should permit more gas diffusion to the porous anode, as shown in Figure 4.8, where part of the electrolyte is seen with a thin film of soot, as well as the edge of the anode with green NiO visible through the soot.

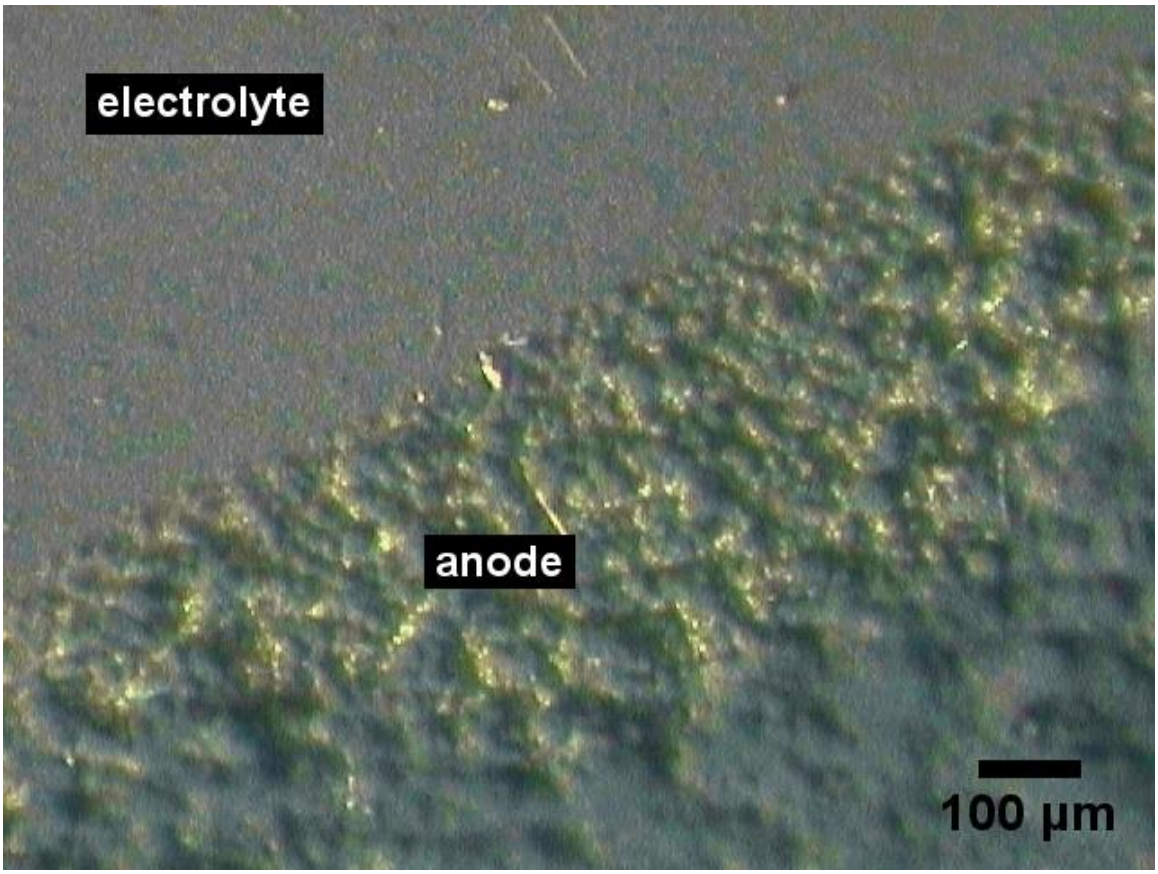

Figure 4.8. Optical microscope image of thin single-dip acetylene soot deposit on electrolyte and edge of the anode.

4.3.2. Pyrolytic Soot Deposition. After each cell was tested with externally applied acetylene soot, the soot was consumed in-situ by allowing current to flow through the cell [47], then the anode was exposed to propane for 120 seconds and immediately flushed with Ar for 5 minutes. Some cells were tested with this pyrolytic soot as fuel while other cells were exposed to hydrogen to prevent oxidation of the soot while the furnace cooled. These cells were examined under both an optical microscope and SEM. Figure 4.9 shows the edge of an anode covered in pyrolytic soot from the decomposition of propane, revealing a macroscopic porosity which appears likely to allow gas transport to the anode.

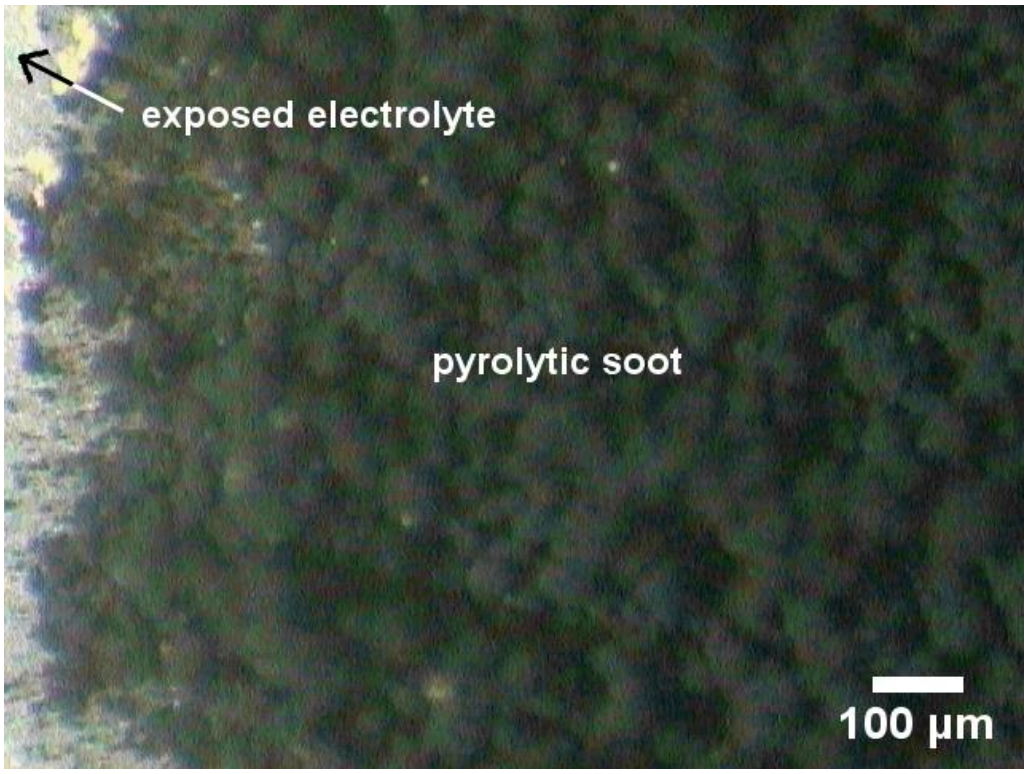

Figure 4.9. Optical microscope image of pyrolytic soot deposit on edge of the anode after cell operation in propane.

Shiny specks are visible in Figure 4.10 which are flakes of Ni metal spalled off of the surface of the anode as the soot particles grew from within the porosity of the anode. Damage to porous anodes from pyrolytic decomposition of hydrocarbons is known to occur by this method when the carbon is deposited within the porous anode [40,41], but a solid carbon fuelled SOFC which uses externally applied soot would not suffer from this problem, making externally applied soot a more attractive method for recharging SOFC capable of use with carbon fuel.

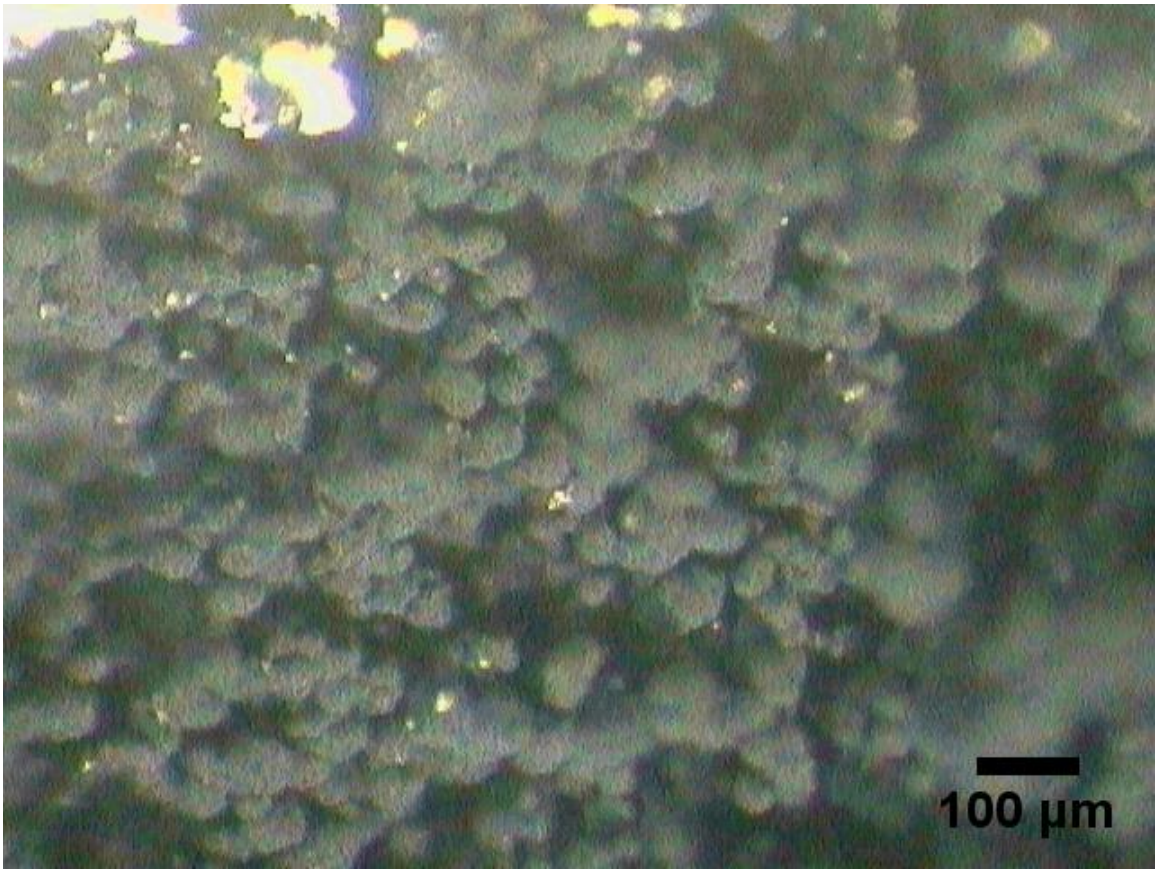

Figure 4.10. Optical microscope image of pyrolytic soot deposit on center of the anode after cell operation in propane.

For visual scale, a particle of pyrolytic soot is shown on the edge of a steel ruler with 1mm scale in Figure 4.11, composed of nodules as small as 10 µm in diameter.

An SEM image of the cell with pyrolytic soot is shown in Figure 4.12, and like the acetylene soot, the pyrolytic soot is much thicker than a traditional anode. However, in this case the soot appears to be less monolithic, composed of individual spherules of about 20 to 50 µm, and may allow more gas diffusion than the acetylene soot. The strip on the top of the photograph is a conductive tape to secure the sample to the SEM pedestal.

More evidence of anode spalling is visible in Figure 4.13, where the pyrolytic soot appears to be layered directly on the electrolyte and the porous anode is gone. Unlike the soot from the acetylene torch, this soot deposit appears to be more porous.

Figure 4.11. Optical microscope image of pyrolytic soot particle from anode, which rubbed off onto the edge of a 1mm ruler.

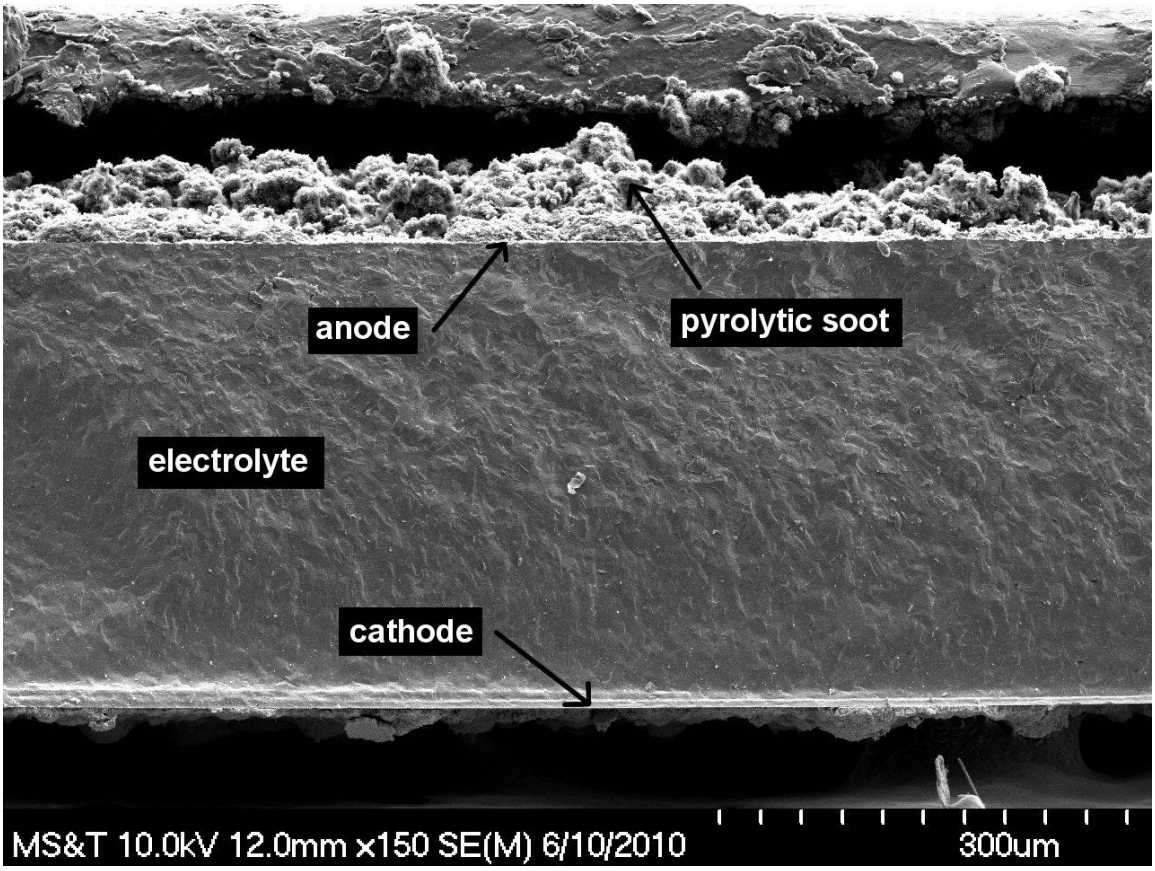

Figure 4.12. SEM image of fracture cross-section of the cell, showing pyrolytic soot deposited onto the anode.

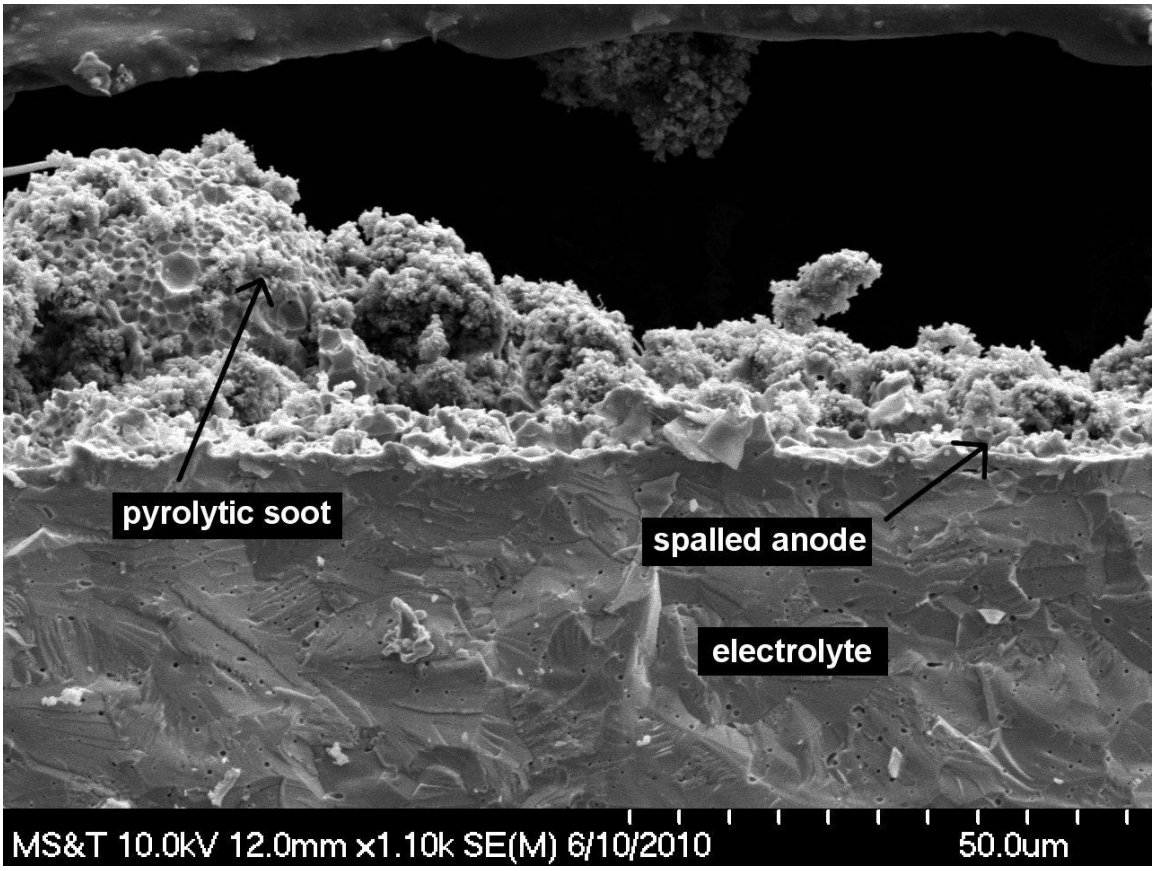

Figure 4.13. SEM image of pyrolytic soot deposited on the anode side, and the lack of an intact anode as evidence of the spalling action.

4.3.3. Electronic and Performance Tests. During furnace warmup, the anode was exposed to 5% H_2 in N_2 to preserve the soot until operating temperature was reached. When the furnace operating temperature of 800 °C was achieved, the cells produced about 1 V in open circuit.

Figure 4.14 shows the open circuit voltage (OCV) recorded during the subsequent switch from H_2 to Ar, then from Ar to CO_2. The first small downward spike at about 10 seconds is the decrease in voltage due to decreased flow rate when a gas hose was

disconnected during the gas switching process, but the immediate subsequent increase is due to the freshly connected Ar pushing the remaining H_2 through the gas hose to the cell for a few seconds. Once the Ar reached the cell, the voltage quickly dropped again and leveled off at around 0.35 V, and after a quick spike due to higher pressure in the CO_2 regulator, the cell returned to the same voltage and maintained that voltage for up to five minutes before other tests began.

The results of potentiodynamic tests are shown as area specific power in Figure 4.15 for 5% H_2 fuel and pyrolytic soot. While the focus of this study is not the use of hydrogen fuel, the area specific power of the cells in 5% hydrogen is typical for a thick electrolyte supported cell in such diluted fuel, demonstrating that the cells are functional in the simplest possible fuel. The spread from Figure 4.15 (a) to (c) as the temperature decreases from 800 °C to 600 °C demonstrates the ineffectiveness of the SOFC components at lower temperatures, as the electrolyte becomes less conductive and the electrodes lose their catalytic effectiveness. The highest temperature available in a diesel engine is about 600 °C at the exhaust valves, though most DPF operate farther downstream around 400-500 °C. For comparison, Figure 4.15 (d) shows the power produced by the cell when utilizing pyrolytic soot as fuel at 800 °C. The power produced by solid carbon is lower than that produced by hydrogen due to several factors [78], including the higher activation energy of carbon oxidation than the oxidation of hydrogen, the increased resistance to gas diffusion into the anode [77], decreased mobility of the fuel, and the addition of extra reaction steps such as the Boudouard reaction that must take place before the bulk of the fuel can be reacted.

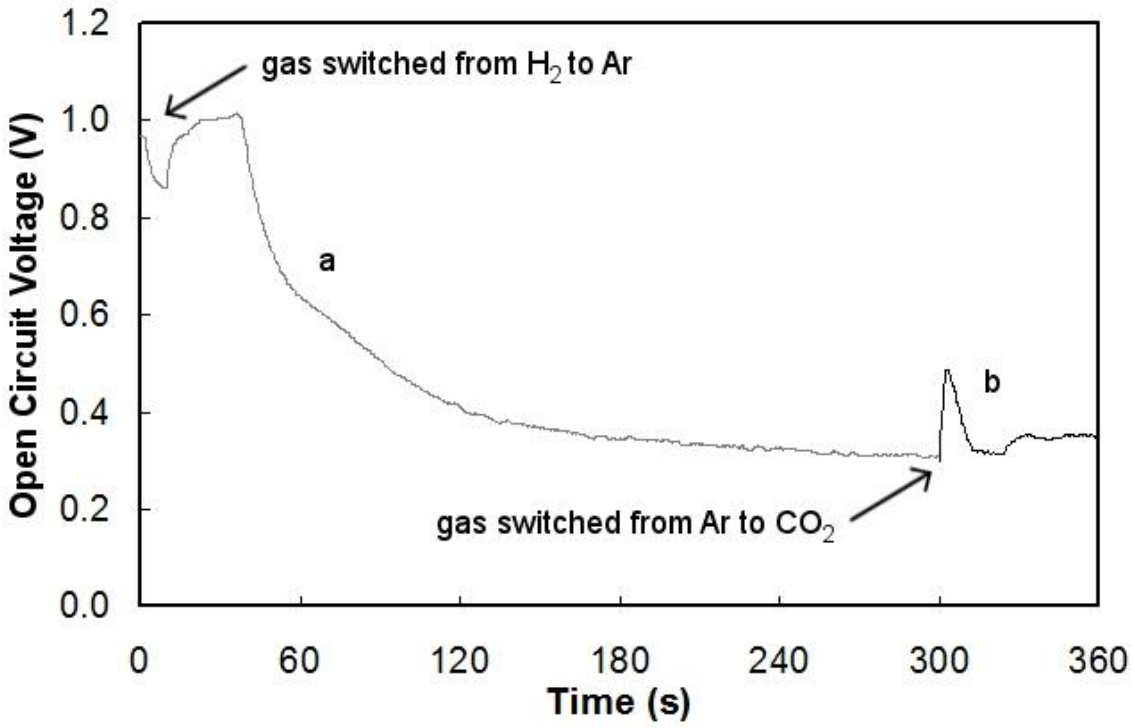

Figure 4.14. Typical OCV of cell with acetylene soot at 800 °C (a) being flushed with Ar and (b) as CO_2 gas is applied.

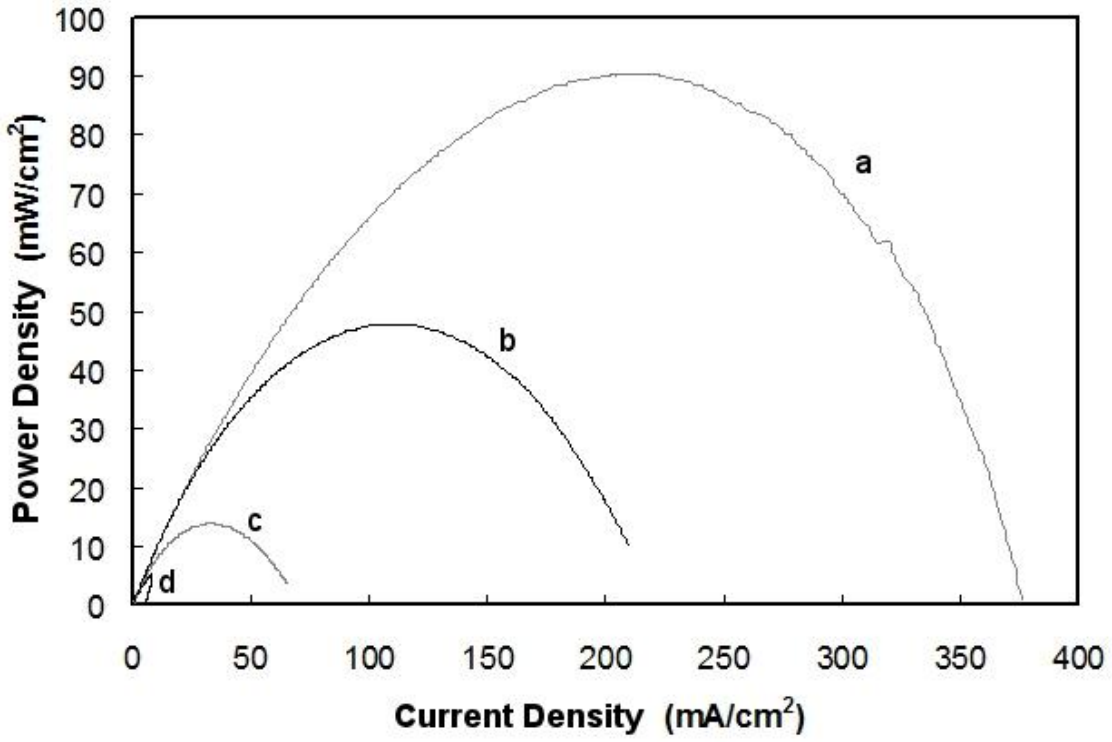

Figure 4.15. Area specific power of cell with 300 mL/min 5% H_2 fuel at (a) 800 °C, (b) 700 °C, (c) 600 °C, and (d) with CO_2 gas over pyrolytically deposited soot at 800 °C.

The power produced by the cell using both pyrolytic and acetylene soot (with CO_2 gas) is shown in Figure 4.16. The pyrolytic soot in (a) produced higher power most likely due to higher porosity in the soot which allowed more gas transport both within the soot and through the soot to the anode. Unlike the hydrogen or acetylene soot power curves, the power curve (a) is cut off, because the soot is consumed faster as the current increases [47] during the course of the test, and the fuel began to run out partway through the measurement, leaving an incomplete arc.

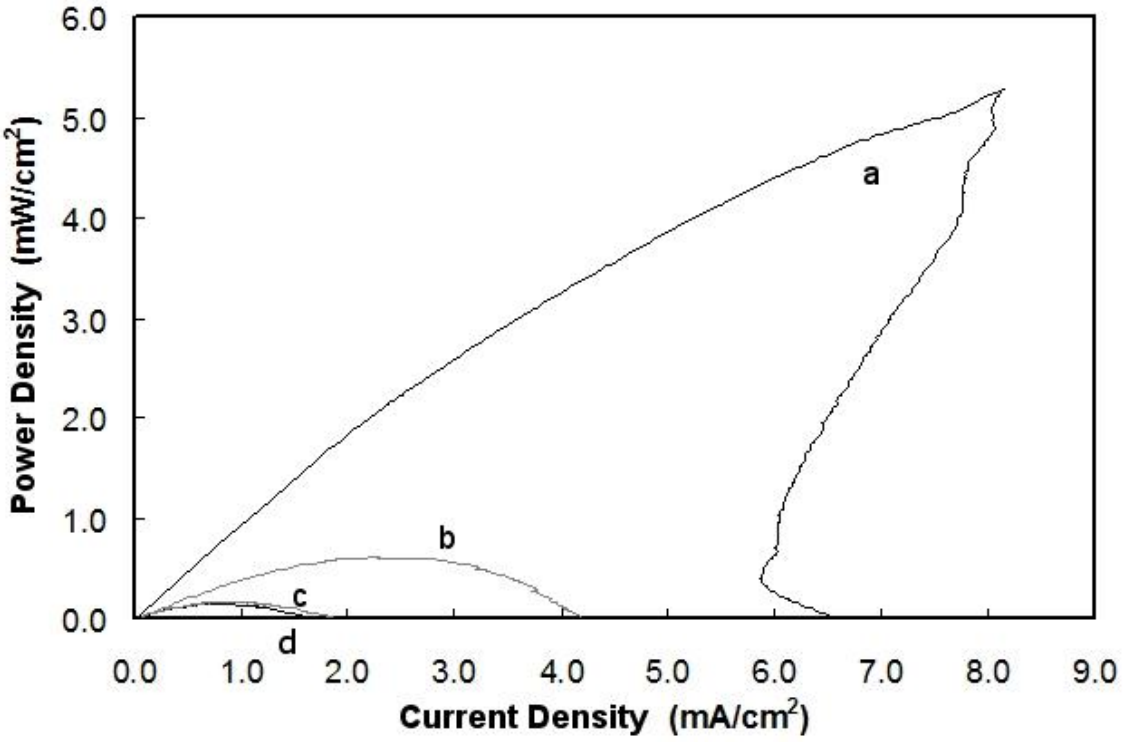

Figure 4.16. Area specific power of cell with CO_2 gas over (a) pyrolytically deposited soot at 800 °C, (b) acetylene soot at 900 °C, (c) thin acetylene soot at 800 °C and (d) thick acetylene soot at 800 °C.

Increasing the furnace temperature to 900 °C allowed the cell to generate more power from the acetylene soot, Figure 4.16 (b), due to increased electrolyte conductivity, increased anode catalytic activity, and increased thermal energy available to activate the carbon oxidation reaction. At 800 °C, the cell with a thin layer of soot produced 13% more power (c) than the cell with a thick layer of soot (d), despite having 98% less fuel available to consume oxygen. This is due entirely to the increased gas transport to the anode, as demonstrated by the impedance spectra seen in Figure 4.17.

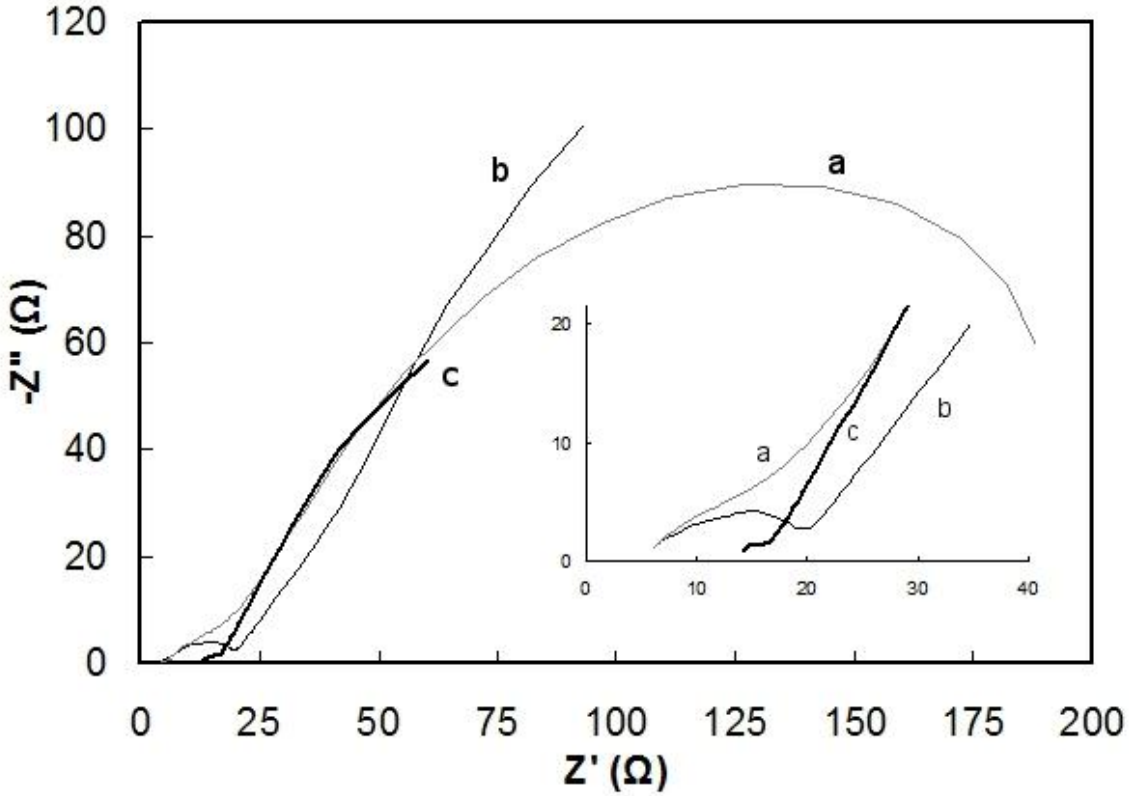

Figure 4.17. Impedance spectrum of cell at 800 °C with CO_2 over (a) pyrolytically deposited soot (b) thick acetylene soot and (c) thin acetylene soot. Inset shows high frequency response.

Figure 4.17 shows the impedance spectra for three cells fuelled by soot at 800 °C, (a) is soot deposited from pyrolytically decomposed propane in-situ, (b) is a thick layer of externally applied acetylene flame soot, and (c) is a very thin layer of acetylene soot. The two depressed semicircles in a typical impedance spectrum are considered to be the overpotentials of the electrodes, with the cathode overpotential represented by the high frequency semicircle on the left and the anode on the right as the low frequency semicircle [15]. In this case, gas diffusion is the dominant contributor to the anode

overpotential [43] and the thick acetylene soot cell (b) overpotential, though not a complete semicircle, is visibly much larger than the pyrolytic soot cell (a) anode overpotential. However, the cell with a thin layer of acetylene soot matches the overpotential of the pyrolytic soot cell much more closely, demonstrating that it does not restrict gas diffusion as it would if the layer was thicker. The thinner acetylene soot layer does not add conductivity to the anode as the thicker acetylene and pyrolytic soot layers do [14], as seen in the inset of figure 4.17 where the spectra of the more heavily sooted samples is shifted toward lower resistance.

4.4. SUMMARY AND CONCLUSIONS

Diesel engine soot was simulated with soot from an acetylene flame and used as fuel in a solid oxide fuel cell. Although the recorded power was only about 5% that of a SOFC powered with pyrolytic solid-carbon, this demonstrates that with more research into better materials and more suitable and optimum operating conditions, the use of diesel engine soot to fuel a SOFC is feasible.

The importance of gas diffusion through the soot layer was affirmed by comparing the power output from two cells with different thicknesses of acetylene soot. The lightly-sooted cell produced 13% more power even though it had less than 2% of the fuel available to the heavily-sooted cell, which is due entirely to the lack of porosity in the thicker soot layer which blocked gas diffusion into the anode, as verified by impedance measurements and SEM micrography. The results presented here, including the lack of gas transport in thick layers of soot and the resultant decrease in power

production, highlight a problem common to both SOFC and DPF. If a SOFC is to be used as a DPF, it is important that it is capable of consuming soot fast enough that the soot does not build up to a thickness which limits gas diffusion.

5. SUMMARY AND CONCLUSIONS

Solid oxide fuel cells are a promising technology which can be a part of the green energy solution by both utilizing conventional fuels more efficiently and using a wider variety of fuels, including fuels from renewable or sustainable energy sources. However, there are several significant hurdles preventing the implementation of commercially viable SOFCs in the transportation and electricity generation markets. To increase the power generating capabilities of SOFCs, it is necessary to determine the effectiveness of a particular material for use as an electrode, but no methods to measure this were discovered in an exhaustive search of the available literature. This study presents a method by which the effectiveness of an individual electrode can be determined independent of the other electrode, as well as initial results from a set of these tests. Because this method allows separate observation of the effects of the individual electrodes, phenomena which affect one electrode can be isolated and studied. One such phenomenon was examined in this study; the cyclic variation in open circuit voltage measured in mixed fuel and air was determined to be the result of a Ni/NiO redox cycle within the anode.

Anodes containing gadolinia-doped ceria have been found to be about 9 times more effective for use with solid carbon fuel, but application of GDC to an electrolyte of YSZ is problematic at best. Solutions proposed in the available literature were less than fully effective or required specialty components or fabrication techniques. This study developed a simple method for applying a GDC anode to a YSZ electrolyte, without any negative interactions between the two materials, and successfully operated the cell with

pyrolytically deposited solid carbon as fuel in a gas similar in composition to diesel engine exhaust.

Diesel engine particulate filters are required for modern diesel engines in order to decrease particulate pollution released to the atmosphere, but the filters themselves are far from perfected. Filters become quickly clogged with soot and require a cleaning process called regeneration, which consumes large amounts of fuel to increase the DPF temperature hot enough to burn off the soot clogging the filter. This wastes fuel and momentarily increases pollution by three to four orders of magnitude. This study demonstrated a cell which was capable of utilizing simulated diesel engine soot as fuel, which is the first step toward a continuously self-cleaning DPF which, rather than consuming extra fuel, could generate electrical power and decrease the horsepower load on the alternator, thereby increasing gas mileage in diesel engines.

5.1. RECOMMENDATIONS FOR FUTURE RESEARCH

For further improvement of SOFC technology based on the research presented here, further investigation into the following areas is recommended:

1. Wider and deeper exploration into single chamber SOFC anode and cathode materials, to decrease overpotential of the electrode reactions. Although many materials have already been characterized, there are thousands of variations in chemical composition, crystal structure, and microstructure of ceramic, metal, and cermet electrodes which can be thoroughly characterized by the methods presented here.

2. Optimization of Ni-GDC bi-layer anodes for use with pyrolytic solid carbon fuel, including variations of both the upper layer and the interlayer in terms of composition,

microstructure, and thickness, as well as optimization of conditions for pyrolytic deposition of the carbon fuel. Similar optimization research on other anodes has increased power production by factors of up to 100.

3. Further exploration into the use of SOFCs in the exhaust stream of a sooting internal combustion engine, including a test method which can apply externally-generated flame or diesel engine soot to the fuel cell in-situ in order to determine the deposition and consumption rates. This information would be important for the development of a DPF which constantly generates electricity and prevents clogging.

4. Investigation into a SOFC anode which is sufficiently catalytic toward the oxidation of carbon that it can be used at the lower temperatures experienced in diesel engine exhaust, without the necessity of further heating the SOFC to sustain the reaction.

5. Development of a SOFC which is capable of functioning as a DPF within an actual diesel engine, which will require novel solutions to the problems of shock resistance, long ion conduction distance, lower operating temperature, and other unforeseen issues. This could be a critical technology in light of increasing EPA and state-level regulations for both fuel efficiency and particulate emission.

APPENDIX A.

UNCERTAINTY ANALYSIS

Uncertainty interval of measured quantities.

Estimation of the uncertainty of measured values is done according to the methods presented in [79] by taking 20 to 30 repeated observations for a diagnostic sample. Voltage, current, resistance and impedance were analyzed under the assumption that the replication level is of Nth order. Therefore, the uncertainty interval $\delta x_{i,N}$ of measured value x_i of replication level order N is found by equation A.1, where $\delta x_{i,1}$ is the first order replication level stochastic uncertainty interval from timewise variation and $\delta x_{i,cal}$ is the uncertainty interval for the calibrations of the measuring instrument. This uncertainty interval is equal to twice the standard deviation centered around the average value, with a 95% confidence interval.

$$\delta x_{i,N} = \sqrt{\left(\delta x_{i,cal}\right)^2 + \left(\delta x_{i,1}\right)^2} \tag{A.1}$$

Voltage:

$$\delta V = \sqrt{\left(-2.55\times10^{-6}\right)^2 + \left(2.55\times10^{-3}\right)^2}$$

$$\frac{\delta V}{V} = 5.44\times10^{-3} = 0.54\%$$

Current:

$$\delta I = \sqrt{\left(-2.16\times10^{-10}\right)^2 + \left(8.25\times10^{-10}\right)^2}$$

$$\frac{\delta I}{I} = 1.64\times10^{-4} = 0.016\%$$

Impedance:

$$\delta Z = \sqrt{(0.01)^2 + (330.625)^2}$$

$$\frac{\delta Z}{Z} = 5.49\times10^{-3} = 0.55\%$$

Uncertainty interval of calculated quantities

For a quantity Y which is a function f(X_1, X_2, …, X_N) of N variables, the propagation of uncertainty δY is given equation A.2 which is the Constant Odds Combination presented in [79].

$$\delta Y = \sqrt{\sum_{i=1}^{N}\left(\frac{\partial f}{\partial x_i}\right)^2 (\delta x_i)^2} \tag{A.2}$$

Resistance:

Resistance was calculated by measuring current at a constant voltage and using the simple equation for Ohm's Law, equation A.3.

$$R = \frac{V}{I} \tag{A.3}$$

$$\delta R = \sqrt{\left(\frac{\partial R}{\partial V}\right)^2 (\delta V)^2 + \left(\frac{\partial R}{\partial I}\right)^2 (\delta I)^2} = \sqrt{\left(\frac{1}{I}\right)^2 (\delta V)^2 + \left(\frac{-R}{I^2}\right)^2 (\delta I)^2}$$

$$\frac{\delta R}{R} = 5.44 \times 10^{-3} = 0.54\%$$

Area Specific Resistance:

Area Specific Resistance was calculated by multiplying the resistance of the cell by the area, according to equation A.4.

$$ASR = R \times A \tag{A.4}$$

$$\delta ASR = \sqrt{\left(\frac{\partial ASR}{\partial R}\right)^2 (\delta R)^2 + \left(\frac{\partial ASR}{\partial A}\right)^2 (\delta A)^2} = \sqrt{(A)^2 (\delta R)^2 + (R)^2 (\delta A)^2}$$

$$\frac{\delta ASR}{ASR} = 1.13 \times 10^{-1} = 11.3\%$$

Power:

Power was calculated by multiplying the current and resistance, equation A.5.

$$P = I \times V \tag{A.5}$$

$$\delta P = \sqrt{\left(\frac{\partial P}{\partial I}\right)^2 (\delta I)^2 + \left(\frac{\partial P}{\partial V}\right)^2 (\delta V)^2} = \sqrt{(V)^2(\delta I)^2 + (I)^2(\delta V)^2}$$

$$\frac{\delta P}{P} = 5.44 \times 10^{-3} = 0.54\%$$

Table A.1. Summary of experimental certainties.

	V	I	Z	R	ASR	P
Uncertainty Source	measurement	measurement	measurement	V, I	R, A	I, V
Uncertainty	0.54%	0.016%	0.55%	0.54%	11.3%	0.54%

APPENDIX B.

THESIS RESEARCH PUBLISHED IN THE INTERNATIONAL JOURNAL OF HYDROGEN ENERGY

INTERNATIONAL JOURNAL OF HYDROGEN ENERGY 34 (2009) 5138–5143

Available at www.sciencedirect.com

ScienceDirect

journal homepage: www.elsevier.com/locate/he

Effectiveness of anode in a solid oxide fuel cell with hydrogen/oxygen mixed gases

Isaiah D. Kellogg[a,b,*], *Umit O. Koylu*[a], *Vladimir Petrovsky*[b], *Fatih Dogan*[b]

[a]*Department of Mechanical and Aerospace Engineering, Missouri University of Science & Technology, Rolla, MO, USA*
[b]*Department of Materials Science and Engineering, Missouri University of Science & Technology, Rolla, MO, USA*

ARTICLE INFO

Article history:
Received 5 September 2008
Received in revised form
6 February 2009
Accepted 14 February 2009
Available online 7 May 2009

Keywords:
Hydrogen
Fuel cell
SOFC
Single chamber
Anode
NiO
Voltage oscillation
Redox

ABSTRACT

A porous Ni/YSZ cermet in mixed hydrogen and oxygen was investigated for its ability to decrease oxygen activity as the anode of a single chamber SOFC. A cell with a dense 300 μm YSZ electrolyte was operated in a double chamber configuration. The Ni–YSZ anode was exposed to a mixture of hydrogen and oxygen of varying compositions while the cathode was exposed to oxygen. Double chamber tests with mixed gas on the anode revealed voltage oscillations linked to lowered power generation and increased resistance. Resistance measurements of the anode during operation revealed a Ni/NiO redox cycle causing the voltage oscillations. The results of these tests, and future tests of similar format, could be useful in the development of single chamber SOFC using hydrogen as fuel.

1. Introduction

Single chamber solid oxide fuel cells (SC-SOFC) are immersed in a flow of mixed fuel and oxygen, relying on the selectivity of the respective electrode catalysts to create a difference in oxygen ion activity across the thickness of the electrolyte [1,2]. In order to increase the effectiveness of SC-SOFC, previous research has explored various possibilities including quantification of electrode catalytic activity [3,4] and detailed studies of oxygen reduction in the cathode [5] as well as enhancing electrode performance by adding new dopants [6]. Other studies investigated improved electrolyte fabrication [7–9] and use of electrolyte supported cells [10–12], alternative electrolyte materials [13,14] or improving existing electrolyte materials with added oxide layers [15], and increasing the conductivity and chemical stability of potential proton-conducting perovskite electrolytes [16]. Efficiency could be significantly improved with a thermally self-sustaining cell heated only by the exothermic reaction at the anode [17].

In a traditional double chamber SOFC, the fuel and oxygen are separated by the electrolyte. The oxygen ions (O^{2-}) diffuse through the electrolyte due to the high O^{2-} activity on the cathode side and low O^{2-} activity on the anode side. The fuel simply prevents a buildup of O^{2-} on the anode side by consuming the O^{2-}. In a single chamber SOFC, the same mixed gas is flowing over both electrodes, so the anode must

* Corresponding author. 111 Toomey Hall, 400 West 13th St, Missouri University of Science and Technology, Rolla, MO 65409-0050, USA. Tel.: +1 573 465 1803; fax: +1 573 341 6934.
E-mail address: ikellogg@mst.edu (I.D. Kellogg).
0360-3199/$ – see front matter © 2009 International Association for Hydrogen Energy. Published by Elsevier Ltd. All rights reserved.
doi:10.1016/j.ijhydene.2009.02.086

decrease the O^{2-} activity by effectively catalyzing the consumption of O^{2-} by the fuel without catalyzing the ionization of O_2. Likewise the cathode must have the opposite catalytic effects [2]. The ability of the electrode to create or sustain a difference in O^{2-} activity across the electrolyte is measured by the open circuit voltage (OCV).

In order to separately observe the effectiveness of the anode in a single chamber fuel cell, the OCV of an SOFC was measured with the anode exposed to varying gas compositions while the cathode was exposed to a standard double chamber oxidizing environment. Hydrogen was used as a fuel for simulating a single chamber SOFC. Although there is no substantial improvement in cell design or operation in this study, it may be one of the first studies in which the effectiveness of the individual electrodes have been measured in this way, and it contributes to the understanding of the way in which the anode reacts to its environment. Future studies may enable better design and selections of anode materials to further increase power density.

2. Experimental

A sample was fabricated from a dense 300 μm thick 8% yttria-stabilized zirconia (YSZ) electrolyte substrate with tape cast porous NiO–YSZ anode and painted with 25% $(La,Sr)(Co,Fe)O_3$ (LSCF)/75% Ag porous cathode. This cell composition was chosen because similar cells have been successfully tested in single chamber tests with other fuels [18].

The double chamber sample holder was constructed so that both anode and cathode gas compositions could be controlled separately. As illustrated in Fig. 1, the double chamber sample holder consisted of two concentric tubes within a tubular furnace. The gas flow rates were controlled by electronic mass flow meters calibrated for the respective gases. Both the anode and cathode gases were flowed at a rate of 300 ml min^{-1}. The anode experienced significantly higher gas velocity than the cathode due to the much smaller tube.

In order to record data, the anode was exposed to a mixed fuel–oxidizer gas while the cathode was exposed to pure oxidizer. This was to simulate a single chamber configuration for the anode while the cathode was operated in the well-characterized double chamber configuration. The fuel selected was dry hydrogen, and in order to avoid the explosion limits, all gases were diluted with 95% argon. All gas mixtures are stated as a percentage of the remaining 5% of reactive gas. The anode gas compositions were varied from pure fuel (double chamber configuration) through the stoichiometric mixture (66% H_2/33% O_2) to being slightly oxygen rich (60% H_2/40% O_2). No gases were bubbled through water.

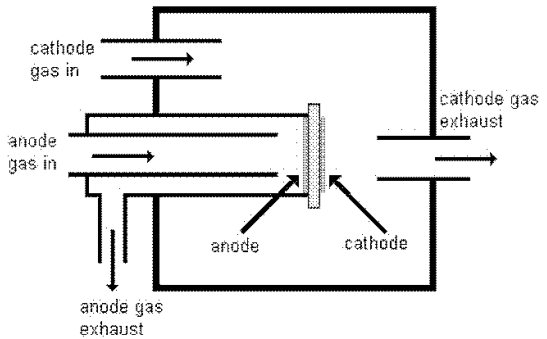

Fig. 1 – Double chamber sample holder.

All measurements were taken for the furnace temperature range from 400 to 700 °C in 50 °C increments. Note that the actual cell temperature was in most cases slightly higher due to the exothermic reactions taking place on the surface of the electrodes. For each gas composition, impedance and open circuit voltage (OCV) were measured at each temperature in order to determine the effectiveness of the anode. The OCV was measured for 20 min at each condition to ensure that a stable voltage was achieved. Other measurements including potentiodynamic measurements were conducted but the results were not included in this paper. All data were recorded with commercial data collection software (CorrWare) and analyzed with the corresponding analysis software (CorrView or Zview).

Voltage measurements are accurate to within 1% and area specific resistance measurements are accurate to within 11%, for a 95% confidence interval.

3. Results and discussion

The open circuit voltage for the double chamber cell with mixed gas on the anode is shown in Fig. 2. Based on a comparison of single and double chamber SOFC performance in the available literature, a standard double chamber SOFC performs better at higher temperatures and offers higher open circuit voltage and area specific power compared to a single chamber SOFC. As expected, the anode was most effective when tested closest to double chamber configuration and at higher temperatures.

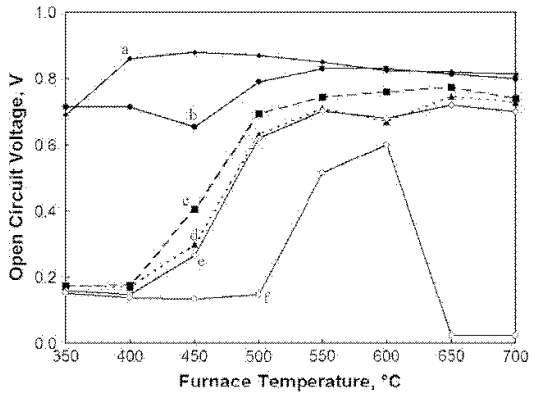

Fig. 2 – Anode exposed to various mixtures of fuel and oxidizer gases (diluted with 95% Ar – mixtures stated as percentage of remainder) in double chamber configuration: (a) 93% fuel (balance oxidizer); (b) 87%; (c) 80%; (d) 73%; (e) 67% (stoichiometric); (f) 60%, while cathode was exposed to constant oxidizer gas.

In gas mixtures of 80% fuel and below (Fig. 2c–f), at low temperatures, the reaction between O^{2-} from the electrolyte and the increasingly dilute fuel was occurring too slowly to remove the O^{2-} which had diffused through the electrolyte, leading to a lower OCV. As the temperature or fuel concentration was increased, the reaction occurred faster, decreasing the oxygen activity at the anode and causing the increase in OCV between 400 and 550 °C seen in Fig. 2c–f.

It is known that mixed hydrogen and oxygen gases in the absence of a catalyst will react to complete consumption of reactants at temperatures above 500 °C with a residence time of several minutes [19], but the mixed gas in this study was only exposed to high temperatures for a time on the order of 5 s before reaching the cell. However, Ni is known to be a catalyst for this reaction [20], and above 600 °C in the 60% fuel mixture (Fig. 2f), the Ni allowed the oxygen gas to consume a significant portion of the H_2 before it was able to diffuse farther into the anode to reach the O^{2-} ions from the electrolyte. This led to a buildup of O^{2-} ions which further decreased the OCV and also increased the overpotential.

The equilibrium gases contained water vapor and oxygen, which readily oxidized the part of the Ni anode to which it was exposed. The partially oxidized Ni anode lowered the available catalytic surface area and did not allow the anode to make effective use of what fuel remained in the gas under these conditions [21]. The oxidized portion of the anode also decreased in porosity [22], slowing the diffusion of fuel into the anode. The Ni anode did not completely oxidize, as complete oxidation of the anode would decrease its conductivity by more than three orders of magnitude [23,24].

The impedance spectra of the sample was measured from 10^6 to 10^{-1} Hz and analyzed with both Bode and Nyquist plots, then the data was fitted to an equivalent circuit (Fig. 3). The electrolyte is represented by a resistor while the anode and cathode are each represented by a resistor and constant phase element (CPE) in parallel (a Cole element), with all three in series. The resistance of the individual electrolyte, cathode, and anode can be determined by the equivalent circuit approach.

Zview software was used to calculate values for each component of the equivalent circuit based on the measured spectra to determine the electrical properties under each tested condition. The impedance spectrum of the equivalent circuit was calculated and compared to the measured spectrum. Fig. 4 shows the impedance spectrum of the cell at 700 °C with the anode exposed to 93% fuel, as well as the spectrum of the equivalent circuit based on the calculated values of the components. Two Cole-element semicircles are visible. Although there was no reference electrode for this experiment, de-convolution of the impedance spectra was achieved by a method similar to that used by Boillot et al. for

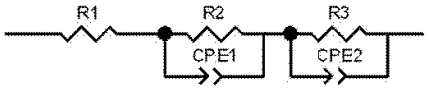

Fig. 3 – Equivalent circuit diagram representing the electrolyte (R1), cathode (R2 and CPE1 in parallel) and anode (R3 and CPE2 in parallel).

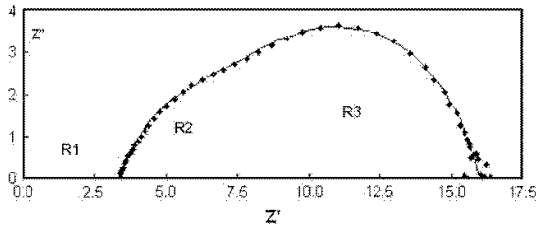

Fig. 4 – An example of impedance spectra: (♦) experimental data (—) line fitting by equivalent circuit which gives the following values: R1, 3.4, R2, 4.3, R3, 8.3 Ohms.

a PEM fuel cell [25]. As the anode gas mixture changed, features on the Bode plot which correspond to the higher frequency semicircle (R2) remained unchanged. However, features on the Bode plot which correspond to the low frequency semicircle (R3) experienced significant phase shift, indicating that the anode reaction corresponds to the semicircle labeled R3 in Fig. 4. A similar test was performed by changing conditions on the cathode side while keeping the anode conditions constant, and these tests showed that cathode effects on the R3 semicircle were minimal. Changes in cathode conditions showed changes in the R2 semicircle while the R3 semicircle remained unchanging.

The calculated values for the resistance of the anode were used to calculate the area specific resistance (ASR) of the anode, shown in Fig. 5 for the different gas mixtures. Note the significantly higher resistance for 60% fuel at 650 and 700 °C. The low frequency semicircle in this case represented by R3 is typically associated with gas transport in an electrode. However, in this case the increase is likely due to oxidation of part of the Ni within the anode, rather than a change in gas transport as the gas flow conditions and anode porosity were constant.

Although the power generated by this cell was low due to the highly diluted gases and thick electrolyte, the purpose of

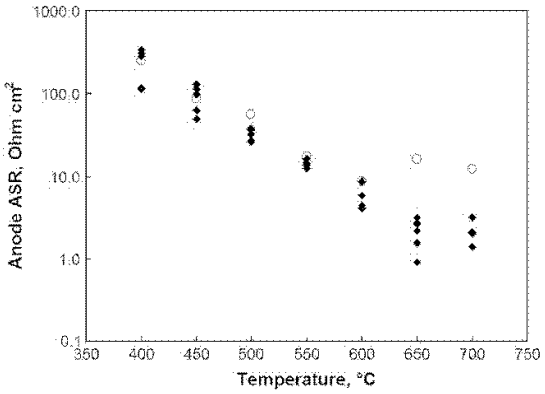

Fig. 5 – Area specific resistance of the anode when it was exposed to gas mixtures; (○) 60% fuel mixture, (♦) all other mixtures.

these tests was not to directly increase the power density of a cell. The present tests were designed to study the ability of the anode to create and sustain a difference in oxygen activity across the electrolyte in a single chamber environment. With a greater understanding of the way in which the individual electrodes behave, fuel cells with higher power density may be achieved.

Some open circuit voltage (OCV) measurements also showed significant periodic voltage oscillations, an example of which is shown in Fig. 6. These voltage oscillations appeared to coincide with lower power curves and the higher ASR measurements in Fig. 5. Impedance measurements for these gas mixtures were taken during intervals with stable voltage. These oscillations were detected in various gas mixtures but were most pronounced and most frequent in the stoichiometric mixture of 66% fuel. Carbon deposition has been previously studied for its role in anode degradation [26] both by blocking pores and by volume expansion to create micro-cracks [27]. However, based on a survey of relevant literature, carbon has not been found to act in a cyclic manner which could cause voltage oscillations. More importantly, hydrogen was exclusively used as fuel in these tests; the lack of any hydrocarbon in the system precludes the possibility of any carbon deposition.

A mechanism by which the cell generates voltage oscillations is proposed: the Ni anode consumes fuel during normal operation, leading to a locally oxygen rich atmosphere. The Ni anode then oxidizes in this local atmosphere, lowering its catalytic effectiveness which lowers the voltage. The decrease in fuel concentration would also increase the anode overpotential, further contributing to lowering of cell voltage. Partial oxidation of the anode also significantly decreases its conductivity. While the oxidized anode is not consuming fuel, more mixed gas diffuses into the porous anode which restores the concentration of fuel. The surplus oxygen simultaneously diffuses out of the anode. The anode is now exposed to

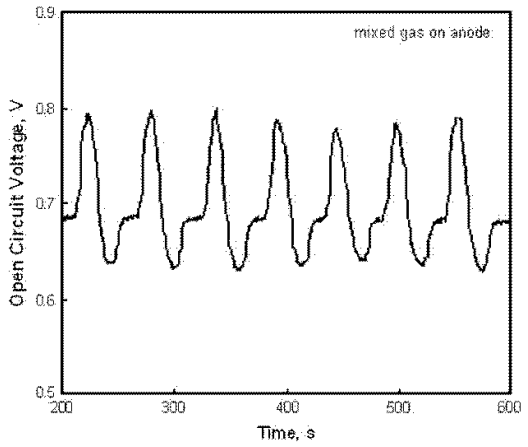

Fig. 6 – Typical open circuit voltage oscillations detected at 600 °C in double chamber with stoichiometric gas mixture (66% H_2/33% O_2 diluted with 95% Ar) on the anode, and pure diluted oxidizer (O_2 diluted with 95% Ar) on the cathode.

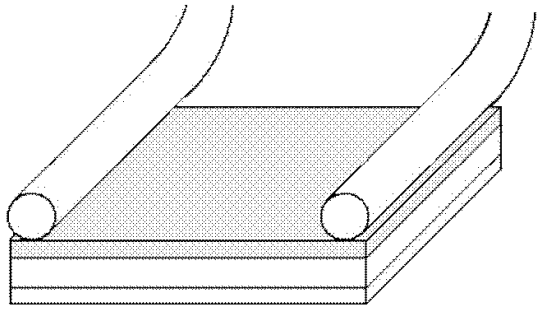

Fig. 7 – Au sensing wires mounted on the anode (gray layer) for measuring ASR.

a reducing atmosphere and reduces to Ni and becomes catalytically effective once again, while the restored fuel concentration decreases the anode overpotential. The anode is in the same condition as when the cycle began, except for microcracking due to volume changes [20].

The resistance of the Ni anode was measured during normal fuel cell operating conditions by laying two Au sensing wires along opposing edges of the anode (Fig. 7). The entire width of the anode was measured in this method. An oscillation in the resistance was detected (Fig. 8). This indicates a cyclic change in the oxidation state of the anode, as NiO is far less conductive than Ni. These oscillations, with a period of around 70 s, were in the same period range as the voltage oscillations recorded under the same conditions, which varied from 45 to 90 s. The anode resistance oscillations were of only a few percent magnitude compared to the voltage oscillation magnitude of about 20%. However, due to the large measured area, the change in resistance signifies a large change in the volume of oxidized Ni within the anode. This would cause a correspondingly large change in the catalytic ability of the anode.

An oxidized anode would lower the voltage due to both a decreased available catalytic surface area and an increased

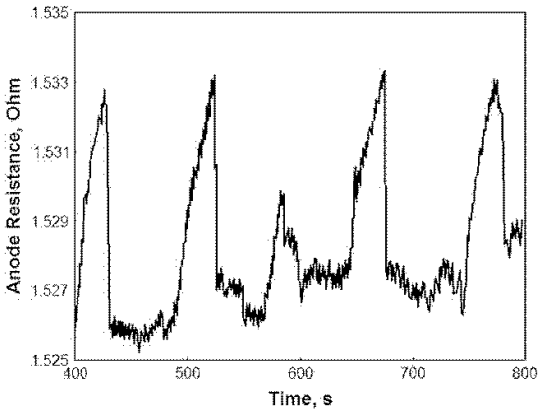

Fig. 8 – Typical anode resistance oscillations detected at 550 °C in single chamber conditions with stoichiometric gas mixture (66% H_2/33% O_2 diluted with 95% Ar).

internal resistance of the cell as a whole. This mechanism is further supported by the OCV oscillations which were detected when the anode was exposed to a single chamber atmosphere, including single chamber tests, but not when the anode was exposed to a pure fuel environment. No OCV oscillations were detected when the test was reversed and the cathode was exposed to mixed gases while the anode was exposed to only fuel.

Tikekar et al. [22] determined that the oxidation kinetics of a porous Ni/YSZ anode are governed by gas diffusion into the pores. The rate limiting mechanism for the voltage oscillation cycle is probably gas diffusion into the porous anode. The gas flow rate in these tests was fast enough to ensure that the gas immediately outside of the anode was constantly flushed and replaced with fresh gas. The anode particles were on the order of 1 μm as measured by SEM micrography, likely small enough that oxidation and reduction occur relatively quickly compared to the period of the oscillations.

4. Conclusions

The effect of different hydrogen–oxygen gas compositions on the anode's ability to effect and sustain a decrease in O^{2-} activity was investigated. A dense YSZ electrolyte supported SOFC with NiO–YSZ anode and Ag/LSCF cathode was tested with mixed gas on the anode. The Ni anode was unable to sufficiently lower the O^{2-} activity in fuel-lean mixtures. These tests and future tests of similar format may aid in the development of new electrodes which would be better suited for single chamber use.

The hydrogen–oxygen mixture may have reacted before reaching the active area of the anode, and fuel-lean mixtures then caused the Ni anode to partially oxidize to NiO which is both less catalytic and less conductive. The lower voltage and conductivity would result in lowered power density if a single chamber SOFC with this anode were to be operated in such a gas mixture. The NiO anode was able to reduce again to Ni upon exposure to a gas mixture richer in fuel, with only a miniscule drop in performance due to known volume expansion cracking issues in the porous Ni–YSZ matrix.

Voltage oscillations were observed in several of the tests, which could not have been caused by a carbon deposition/burnoff cycle due to the absence of carbon in the hydrogen/oxygen system. These oscillations were not detected when the anode was exposed only to fuel. A redox cycle in the Ni anode was proposed which is believed to cause a periodic change in the catalytic effectiveness and resistance of the cell, leading to voltage oscillations that corresponded to lower power densities. This redox cycle was measured under SC-SOFC operating conditions where carbon-based reactions and related mechanisms did not exist. Future research on development of more redox-stable anode materials may help resolve this issue.

Acknowledgements

The authors would like to thank the US Department of Education GAANN fellowship for financially supporting I.D. Kellogg, as well as Nathaniel Goss for his assistance in preparing and testing samples.

REFERENCES

[1] Reiss I. On the single chamber solid oxide fuel cells. J Power Sourc 2008;175:325–37.
[2] Yano M, Tomita A, Sano M, Hibino T. Recent advances in single-chamber solid oxide fuel cells: a review. Solid State Ionics 2007;177:3351–9.
[3] Suzuki T, Jasinski P, Petrovsky V, Anderson HU, Dogan F. Performance of a porous electrolyte in single-chamber SOFCs. J Electrochem Soc 2005;152:A527–31.
[4] Hibino T, Hashimoto A, Inoue T, Tokuno J, Yoshida S, Sano M. Single-chamber solid oxide fuel cells at intermediate temperatures with various hydrocarbon–air mixtures. J Electrochem Soc 2000;147:2888–92.
[5] Adler SB. Factors governing oxygen reduction in solid oxide fuel cell cathodes. Chem Rev 2004;104. 4791–84.
[6] Hibino T, Wang S, Kakimoto S, Sano M. Single chamber solid oxide fuel cell constructed from an yttria-stabilized zirconia electrolyte. Electrochem Solid State Lett 1999;2:317–9.
[7] Jasinski P, Petrovsky V, Suzuki T, Petrovsky T, Anderson HU. Electrical properties of YSZ films prepared by net shape technology. J Electrochem Soc 2005;152:A454–8.
[8] Babilo P, Haile SM. Enhanced sintering of yttrium-doped barium zirconate by addition of ZnO. J Am Ceram Soc 2005;88:2362–8.
[9] Guentes R, Baker R. Synthesis and properties of gadolinium-doped ceria solid solutions for IT-SOFC electrolytes. Int J Hydrogen Energ 2008;33:3480–4.
[10] Suzuki T, Jasinski P, Anderson HU, Dogan F. Single chamber electrolyte supported SOFC module. Electrochem Solid State Lett 2004;7:A391–3.
[11] Moon H, Kim S, Park E, Hyun S, Kim H. Characteristics of SOFC single cells with anode active layer via tape casting and co-firing. Int J Hydrogen Energ 2008;33:2826–33.
[12] Moon H, Kim S, Hyun S, Kim H. Development of IT-SOFC unit cells with anode-supported thin electrolytes via tape casting and co-firing. Int J Hydrogen Energ 2008;33:1758–68.
[13] Asahara S, Michiba D, Hibino M, Yao T. Single chamber SOFC using BaLaIn2O5.5 solid electrolyte. Electrochem Solid State Lett 2005;8:A449–51.
[14] Uda T, Boysen DA, Chisholm CRI, Haile SM. Alcohol fuel cells at optimal temperatures. Electrochem Solid State Lett 2006;9:A261–4.
[15] Hibino T, Tsunekawa H, Tanimoto S, Sano M. Improvement of a single-chamber solid-oxide fuel cell and evaluation of new cell designs. J Electrochem Soc 2000;147:1338–43.
[16] Haile SM, Staneff G, Ryu KH. Non-stoichiometry, grain boundary transport and chemical stability of proton conducting perovskites. J Mater Sci 2001;36:1149–60.
[17] Suzuki T, Jasinski P, Petrovsky V, Anderson HU, Dogan F. Anode supported single chamber solid oxide fuel cell in CH_4–air mixture. J Electrochem Soc 2004;151:A1473–6.
[18] Shao Z, Haile SM, Ahn J, Ronney PD, Zhan Z, Barnett SA. A thermally self-sustained micro solid-oxide fuel-cell stack with high power density. Nature 2005;435:795–8.
[19] Hustad J, Sonju O. Experimental studies of lower flammability limits of gases and mixtures of gases at elevated temperatures. Combust Flame 1988;71:283–94.
[20] Tao S, Irvine J. A redox-stable efficient anode for solid-oxide fuel cells. Nat Mater 2003;2:320–3.
[21] Jacques-B'edard X, Napporn TW, Roberge R, Meunier M. Performance and ageing of an anode-supported SOFC operated in single-chamber conditions. J Power Sourc 2006;153:108–13.

[22] Tikekar NM, Armstrong TJ, Virkar AV. Reduction and reoxidation kinetics of nickel-based SOFC anodes. J Electrochem Soc 2006;153:A654–63.
[23] Petrovsky V, Suzuki T, Jasinski P, Anderson HU. Low-temperature processed anode for solid oxide fuel cells. Electrochem Solid State Lett 2005;8:A341–3.
[24] Jasinski P, Suzuki T, Petrovsky V, Anderson HU. Nanocomposite nickel ceria cermet with low nickel content for anode-supported SOFCs. Electrochem Solid State Lett 2005;8:A219–21.
[25] Boillot M, Bonnet C, Didierjean S, Lapicque F. Investigation of the response of separate electrodes in a polymer electrolyte membrane fuel cell without reference electrode. J Appl Electrochem 2007;37:103–10.
[26] Iida T, Kawano M, Matsui T, Kikuchi R, Eguchi K. Carbon deposition on fuel electrode and subsequent deteriorationof cell. J Electrochem Soc 2007;154:B234–41.
[27] Lin Y, Zhan Z, Liu J, Barnett S. Direct operation of solid oxide fuel cells with methane fuel. Solid State Ionics 2005;176: 1827–35.

APPENDIX C.

THESIS RESEARCH PUBLISHED IN THE JOURNAL OF POWER SOURCES

Journal of Power Sources 195 (2010) 7238–7242

Contents lists available at ScienceDirect

Journal of Power Sources

journal homepage: www.elsevier.com/locate/jpowsour

Short communication

Solid oxide fuel cell bi-layer anode with gadolinia-doped ceria for utilization of solid carbon fuel

Isaiah D. Kellogg[a,b,*], Umit O. Koylu[a], Fatih Dogan[b]

[a] Department of Mechanical and Aerospace Engineering, Missouri University of Science and Technology, 290A Toomey Hall, 400 West 13th Street, Rolla, MO 65409, USA
[b] Department of Materials Science and Engineering, Missouri University of Science and Technology, 223 McNutt Hall, 1400 N. Bishop, Rolla, MO 65409, USA

ARTICLE INFO

Article history:
Received 7 April 2010
Received in revised form 27 May 2010
Accepted 27 May 2010
Available online 1 June 2010

Keywords:
Solid oxide fuel cell
YSZ
Gadolinia-doped ceria
Anode
Soot
Carbon

ABSTRACT

Pyrolytic carbon was used as fuel in a solid oxide fuel cell (SOFC) with a yttria-stabilized zirconia (YSZ) electrolyte and a bi-layer anode composed of nickel oxide gadolinia-doped ceria (NiO–GDC) and NiO–YSZ. The common problems of bulk shrinkage and emergent porosity in the YSZ layer adjacent to the GDC/YSZ interface were avoided by using an interlayer of porous NiO–YSZ as a buffer anode layer between the electrolyte and the NiO–GDC primary anode. Cells were fabricated from commercially available component powders so that unconventional production methods suggested in the literature were avoided, that is, the necessity of glycine–nitrate combustion synthesis, specialty multicomponent oxide powders, sputtering, or chemical vapor deposition. The easily-fabricated cell was successfully utilized with hydrogen and propane fuels as well as carbon deposited on the anode during the cyclic operation with the propane. A cell of similar construction could be used in the exhaust stream of a diesel engine to capture and utilize soot for secondary power generation and decreased particulate pollution without the need for filter regeneration.

1. Introduction

Solid oxide fuel cells (SOFC) are capable of directly converting chemical energy from a wide variety of liquid and gaseous fuels into electrical energy. The high temperature necessary to enable oxygen ion diffusion through the ceramic electrolyte makes even the direct use of solid carbon fuel possible [1,2]. Solid carbon may come from internal pyrolysis of hydrocarbon fuel or as soot from the exhaust gas of an internal combustion engine. Diesel engine exhaust soot has been removed from an exhaust filter with an electrochemical reaction [3] but it may be possible to recover energy rather than expend energy while consuming the unwanted soot particulate pollution, similar to carbon particulate filter regeneration downstream from thermal partial oxidation reformers intended to feed hydrogen to a SOFC [4]. SOFCs capable of using solid carbon fuel could recover a significant amount of unused energy while simultaneously decreasing particulate pollution from diesel engine exhaust stream. The amount of electricity recovered from this soot can reduce the load on the alternator and remove the need for filter regeneration, both of which would increase fuel efficiency.

Utilization of solid carbon fuel may be by direct oxidation or by Boudouard gasification [5], which are both made more practical by the correct choice of anode material to catalyze the carbon oxidation reaction [5–7], which in turn makes hydrocarbon fuels more practical by oxidizing the deposited solid carbon before it builds up to the point of hindering cell performance.

An SOFC requires the use of an ion conducting ceramic both as the electrolyte and as one component of a cermet anode. High ionic conductivity is necessary to allow oxygen ion transport and minimize internal cell resistance, and for the electrolyte a low electronic conductivity is necessary to minimize electron leakage. When the ionic conductor is used as part of the anode cermet, it should also have high catalytic activity toward oxidation of the selected fuel.

Two ceramic materials commonly used as ion conductors in SOFCs are yttria-stabilized zirconia (YSZ) and gadolinia-doped ceria (GDC). GDC is more catalytically active than YSZ, performing more than eight times better as a catalyst for oxidation of solid carbon than does YSZ [8], and the reaction zone in a GDC anode extends significantly beyond the three-phase boundary [9]. These characteristics make GDC more favorable as the anode ion conductor for the use of solid carbon fuel in a SOFC [5,10]. YSZ provides the low electrical conductivity which is desirable in an electrolyte material, but as an anode material suffers from lower catalytic activity for fuel oxidation than ceria. GDC has higher ionic conductivity than YSZ but suffers from higher electronic conductivity, which makes it less suitable for use as an electrolyte; however YSZ has been used

* Corresponding author at: Department of Mechanical and Aerospace Engineering, Missouri University of Science and Technology, 290A Toomey Hall, 400 West 13th Street, Rolla, MO 65409-0050, USA. Tel.: +1 573 341 6601; fax: +1 573 341 4607.
E-mail address: ikellogg@mst.edu (I.D. Kellogg).

0378-7753/$ – see front matter © 2010 Elsevier B.V. All rights reserved.
doi:10.1016/j.jpowsour.2010.05.055

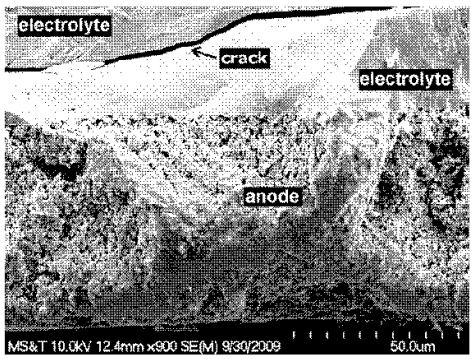

Fig. 1. YSZ electrolyte (top) and Ni/GDC anode (bottom) showing voids and a crack.

as a thin layer to block electronic conduction with a GDC electrolyte [11].

An SOFC composed of a YSZ electrolyte combined with a GDC anode would have less electron leakage and higher catalytic activity. GDC also shows increased electronic conductivity in the low oxygen partial pressure environment of the anode, further decreasing anode resistance. However, when GDC and YSZ are sintered as adjacent layers, there are significant chemical compatibility problems [12], including excessive diffusion of Y ions into the GDC causing bulk shrinkage and voids which lead to decreased overall cross-sectional area and lower ionic conductivity, as well as lower mechanical strength. Adding Ni to the anode somewhat suppresses the undesirable solid-state reaction [13], but does not eliminate the problem, as illustrated in Fig. 1, which shows voids and a crack caused by a Ni/GDC anode sintered onto a YSZ electrolyte. An interlayer of $Ce_{0.43}Zr_{0.43}Gd_{0.10}Y_{0.04}O_{1.93}$ can be used to slow the solid-state reaction so a GDC anode can be sintered onto a YSZ electrolyte [13] but this cannot be done with commercially available materials, requiring combustion synthesis or other unconventional methods.

Previous cell construction using GDC anode directly applied to the YSZ electrolyte revealed several problems after sintering, consistent with results from other groups [12,13]. Excess diffusion of Y from the YSZ electrolyte into the GDC anode caused void formation and bulk shrinkage, which in turn led to subsurface cracking. Fig. 2a shows the surface of the electrolyte after the anode flaked off. Fig. 2b shows some of the anode flakes on both the front anode surface and the rear where a thin layer of electrolyte is still visible.

Commercial cells with a YSZ electrolyte and GDC anode are available and do well in testing, both in terms of power production and resistance to carbon fouling [6], while experimental cells of similar composition have successfully used solid carbon as fuel [10]. However, few researchers have discussed the methods used to overcome the difficulties in applying a GDC anode to a YSZ electrolyte. The methods which have been presented are less than completely effective or require specialty multicomponent oxide materials or unconventional synthesis methods such as glycine–nitrate combustion synthesis [13]. The first objective of this paper is to present a simple and effective method to fabricate a functional SOFC using a GDC cermet anode and a YSZ electrolyte using only the commercially available oxide powders necessary to make either a YSZ or a GDC based anode. The second objective is to successfully demonstrate the utilization of not only hydrogen and a hydrocarbon fuel but also solid carbon fuel and this bi-layer SOFC anode for their applications in power generation and pollution control.

Table 1
Anode compositions by weight.

Layer	NiO (wt%)	YSZ (wt%)	GDC (wt%)
Anode 1	60	40	0
Anode 2	55	15	30

2. Experimental methods

2.1. Fabrication

Several cells were fabricated for testing. Electrolytes were 300 μm thick, fully-dense 8 mol% Y_2O_3 stabilized zirconia (8YSZ) disks tape cast from Tosoh TZ-8Y powder. In order to promote oxidation of solid carbon as well as increase anode conductivity, GDC was chosen as the ionic conductor for the anode. Two anode inks were prepared, denoted as Anode 1 and Anode 2. Each anode ink was mixed from commercial off-the-shelf component powders; NiO (Aldrich, USA), GDC (Praxair, USA), and YSZ (TZ-8Y, Tosoh, Japan); then combined with an equal amount by weight of Ferro B-75000, a commercial pre-prepared screen printing binder, and mixed in mortar and pestle. Anode compositions are given in Table 1 by weight percent according to industry standard.

Anode 1 ink was first painted onto an electrolyte disk and allowed to dry at room temperature. Anode 2 ink was then painted over Anode 1 and also allowed to dry at room temperature. The anodes were then sintered in air at 1350 °C for 4 h, resulting in a sintered anode with a thickness of between 25 and 30 μm, as measured with SEM micrography.

This anode fabrication method is much simpler or less expensive than many of the methods mentioned in the literature. No combustion synthesis or chemical vapor deposition was necessary, and

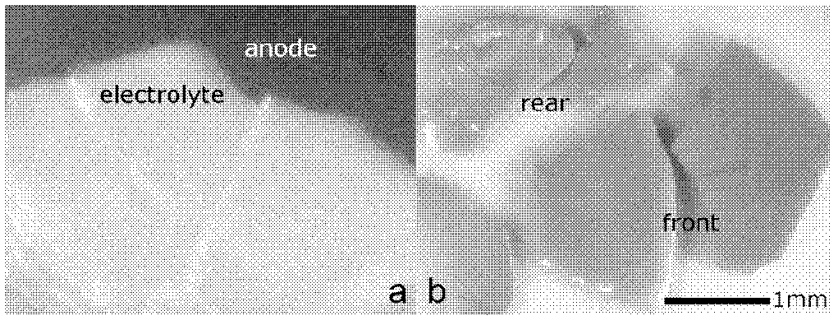

Fig. 2. (a) YSZ electrolyte surface after GDC anode flaked off; (b) GDC anode flakes showing a thin layer of electrolyte remaining on the rear surface.

no equipment more complicated than a simple sintering furnace was used for fabrication. Commercial samples by this method could be manufactured with a simple screen printing or inkjet process, which would be both simpler and much less expensive than vapor deposition, while laboratories can make effective fuel cell samples without the cost of specialty multicomponent oxides.

Cathode ink was prepared by combining $La_{0.8}Sr_{0.2}Fe_{0.8}Co_{0.2}$ oxide powder with the same screen printing binder and mixing in mortar and pestle. The cathode was painted onto each electrolyte disk opposite the anode and sintered in air at 900 °C for 1 h.

2.2. Test procedures

Cells were mounted in a furnace and heated to 800 °C at a rate of 5 °C min^{-1}, and all measurements were taken at this furnace temperature. The actual cell temperature was 5–15 °C higher due to the exothermic reactions taking place at the electrodes. The actual temperature increase depended on the type of test being performed. The cathode was exposed to a flow of preheated air at 300 mL min^{-1}, and the anode was exposed to various preheated fuel gases at 300 mL min^{-1}, including 5% H_2 in Ar, 10% H_2 in N_2, and propane. All gas flows unless otherwise specified were at a rate of 300 mL min^{-1}. When operated with propane fuel, solid carbon was deposited on the anode by pyrolysis of the propane. Any remaining fuel gas was flushed from the test chamber with Ar for sufficiently long times to ensure no gaseous fuels remained in the system [8,5]. The solid carbon remaining on the anode was used as indirect fuel by flowing CO_2 gas, which is a major component of hydrocarbon combustion exhaust and found with soot in diesel engine exhaust, over the anode to gasify the carbon via the Boudouard reaction, converting it to CO which can be directly utilized by the anode as fuel, according to $C + CO_2 \rightarrow 2CO$.

Temperature measurements were taken with a type R thermocouple. Gas flow was measured with Cole-Parmer 112-02-N ball flow meters calibrated for nitrogen. Correction factors for the ball flow meters were determined by flowing gas through a Tylan FC-260 electronic mass flow controller and then through the ball flow meters. Electrical tests were taken by four-point probe with a Solartron CellTest 1470 system, and recorded by CorrWare and Zplot software. Impedance was measured from 1 Hz to 1×10^6 Hz at an amplitude of 20 mV AC. Voltage measurements are accurate to within 1%, current density and impedance measurements to within 5%, for a 95% confidence interval. SEM micrography was performed with a Hitachi S-4700 scanning electron microscope.

3. Results and discussion

3.1. Electron microscopy

A representative sample SOFC identical to the ones used in these tests was fractured and examined under SEM. Fig. 3 shows the cross-section, with a thin porous bi-layer anode on the bottom firmly bonded to the dense electrolyte on the top of each picture, revealing that the electrolyte is intact and has no voids. If detrimental interactions between the GDC and YSZ had occurred, there would be significant bulk shrinkage evidenced by voids or cracking in the electrolyte layer near the porous anode, as shown in Fig. 1. The adjacency of the GDC and YSZ is located in the anode, where porosity is necessary for gas transport, and where bulk shrinkage normally takes place during sintering.

3.2. Electrical tests

Fig. 4 shows the results of the open circuit voltage (OCV) tests with the anode exposed to various fuels, including 5% H_2 in Ar and 10% H_2 in N_2, which produce identical voltage around 1.0 V, both

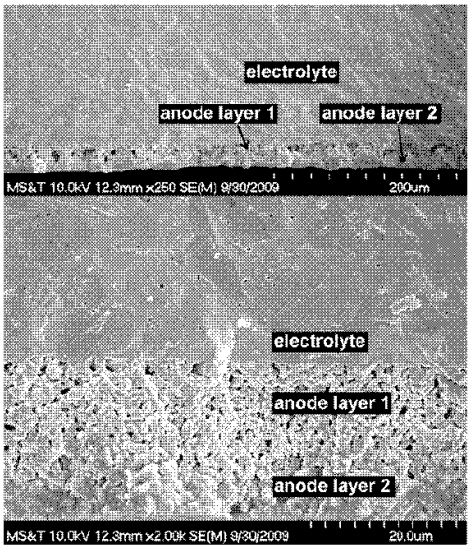

Fig. 3. SEM photos of the SOFC cross-section showing the anode and proximate electrolyte.

represented on trace (a), revealing that the SOFC was capable of producing about 1 V in hydrogen which is consistent with the value predicted by the Nernst equation. Trace (b) in Fig. 4 shows the OCV as the cell is first exposed to propane after operating with H_2 fuel, and trace (c) shows the voltage in propane after an hour of propane operation and then 300 s of potentiostatic operation at 0.5 V, which allows oxide ion current to flow through the electrolyte and consume the solid carbon which clogged the anode porosity. Trace (d) shows the voltage recorded when the gas was switched to argon at 0 s, after 420 s of open circuit operation in propane to pyrolytically deposit solid carbon on the anode.

It is interesting to note that after operating the sample in propane for <60 s, the OCV had dropped by about 0.075 V from its initial value, but after increasing the current and operating in potentiostatic mode at 0.5 V, the voltage increased initially, but slowly decreased again. This is consistent with results from other groups [5] that the open circuit condition tends to allow carbon

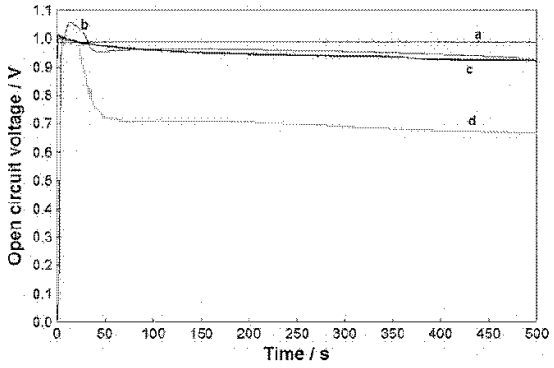

Fig. 4. OCV of the SOFC when operated with (a) 5% H_2 and 10% H_2 (b) initial propane, (c) propane after 1 h of propane and 5 min of potentiostatic operation at 0.5 V, (d) Ar after 7 min of propane on a new cell.

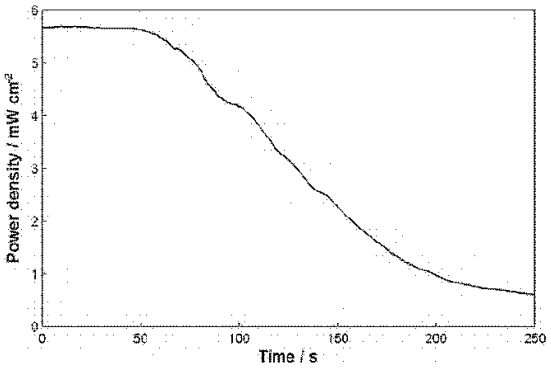

Fig. 5. Area specific power of cell in operation with CO_2 over anode after 7 min OCV operation in propane and 10 min Ar flush.

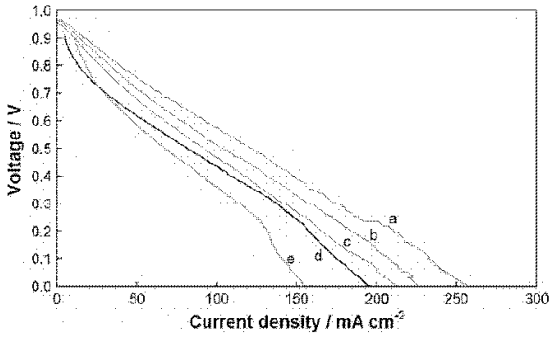

Fig. 6. Polarization graph of three subsequent tests in 5% H_2 (a–c) and two subsequent tests in propane (d and e).

build-up which decreases the OCV, while an increased current consumes some of the deposited carbon and restores some porosity to the anode, restoring the high OCV.

The cell initially produced a maximum power of about 65.6 mW cm^{-2} using 5% H_2 as fuel, but after about an hour the cell had degraded slightly and only produced 61.6 mW cm^{-2} with 10% H_2 fuel, and subsequently 61.8 mW cm^{-2} with propane fuel. This amount of power is lower than current thin-electrolyte technology cells, but it is quite respectable when the thicker 300 μm electrolyte is taken into account.

A new identical cell was exposed to propane fuel gas stream at 300 mL min^{-1} for 420 s, achieving identical voltage performance to (b) in Fig. 4, co-represented by trace (b). The cell was then flushed with pure Ar at 300 mL min^{-1} as seen in (d) of Fig. 4. The voltage stayed nearly constant at about 1 V for several seconds until the gas tubes had been flushed of propane, and then abruptly dropped as the propane was flushed away from the cell. By 100 s after the gases had been switched, the voltage had leveled and stayed about the same for a further 600 s. This shows that the propane is certain to have been removed from the cell in only a few minutes. The anode gas was then switched to CO_2 under which the cell generated >0.85 V for 2 min after the Ar had been flushed away. Therefore the cell was capable of voltage generation using pyrolytically deposited carbon as fuel, in both Ar and CO_2 gases.

After an identical carbon-deposition and argon flush, current was recorded while the cell was held at 0.4 V, approximately half the OCV which was recorded with CO_2 gas flow over the pyrolytically deposited carbon. The cell produced a current density >14 mA cm^{-2} and power of 5.65 mW cm^{-2} for about 60 s, before the soot started to become depleted, as seen in Fig. 5. Although the power generated with solid carbon fuel is much lower than that generated with hydrogen or hydrocarbon fuels, it is consistent with the early results of other groups [8], and is a reasonable value for the first fabrication of this type of cell. Subsequent tests can be expected to increase power by varying the anode thicknesses, composition, porosity, or sintering schedules.

The linear slope of the decrease from 75 to 175 s is probably the result of the consumption of carbon at the most active areas of the anode first, those areas of three-phase boundary closest to the electrolyte [5]. As the carbon closest to the electrolyte was consumed, oxygen ions were required to travel a longer distance through the ionic conductor in the anode to gain proximity to fuel at a three-phase boundary. This longer ionic conduction distance increased the overpotential and decreased the power. However, recent studies indicate that little pyrolytic carbon is deposited on the more active interior portions of the anode [14], so a more important aspect may be that the generation point of the CO gas moved farther away from the electrolyte, further increasing the overpotential due to gas transport issues. The effect of increasing conduction distance and the effect of increased gas transport distance would both be expected to decrease the produced power in a linear fashion.

Two more subsequent tests showed near identical performance, with only minor decrease attributable to electrolyte aging, indicating that at least three short 10-min deposition/utilization cycles are possible. Although longer testing times and more deposition/utilization cycles may reveal anode deterioration, longevity can be improved in subsequent tests by varying anode thickness, porosity, and particle size. The results presented in this paper indicate that this simply fabricated cell is capable of power generation with a variety of fuels, including hydrocarbons and solid carbon, on par with cells fabricated by means of more elaborate and expensive methods.

The polarization profile shown in Fig. 6 reveals fairly ohmic behavior, which shows that the reactions at the anode and cathode do not excessively hinder the cells operation. Excess porosity or cracking in the electrolyte, such as from a YSZ–GDC interaction, would exhibit in the polarization profile as a decrease in voltage at higher current density due to an increased electrolyte overpotential. From (a) to (e) was about 6 h of operation of a single cell. A small decrease in voltage at higher current density is evident in (e), however the Cole–Cole impedance plot in Fig. 7 shows that this increase in overpotential is from the anode and is due to carbon build-up, which limited gas transport to the active area of the anode.

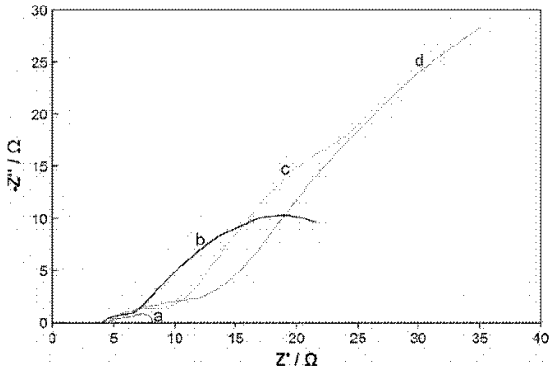

Fig. 7. Cole–Cole plot showing the impedance of the SOFC in operation with propane fuel after (a) 1 h, (b) 4 h, (c) 6 h, and (d) 8 h.

The Cole–Cole plot showing the impedance of the SOFC in operation is shown in Fig. 7 for four tests spanning about 8 h of operation in heavily-sooting propane. The first test is labeled (a), the fourth test is (b), the sixth (c) and the eighth test is labeled (d). Each test was about an hour apart, during which time other tests were run, including OCV and potentiostatic tests.

It should be noted that the electrolyte resistance (the distance on the Z' axis between the 0 mark and the intersection of the impedance curve with the Z' axis) remains fairly constant over the course of 4 h, only slightly decreasing from 5 to 4.5. This is attributable to aging of the electrolyte as it allows more electron leakage that decreases both the cell resistance and the OCV, as noted in Fig. 2. The cathode equivalent resistance (the size of the leftmost semicircle of the impedance curve) remains approximately the same as well. However, the anode equivalent resistance (size of the rightmost semicircle) increases dramatically from (a) to (d). This is because the anode overpotential increases as the anode becomes clogged with solid carbon, increasing the resistance of gas transport to the active area of the anode.

4. Conclusions

A simple method for applying a GDC bearing anode to a YSZ electrolyte was demonstrated, and power in excess of 60 mW cm^{-2} was recorded with both hydrogen fuel and propane fuel, and a reasonable power was recorded with pyrolytically deposited carbon fuel. Cell performance indicated no detrimental effects of YSZ/GDC adjacency, and SEM revealed no voids or other indications of the problems typical of YSZ/GDC interactions. The method presented in this paper is significantly simpler than the methods which rely on complex oxide mixtures, and more effective than the methods which rely on higher Ni content in the GDC anode. This allows for easier fabrication of carbon-deposition resistant cells or cells which can collect and utilize soot from a diesel engine exhaust stream to decrease particulate pollution and increase fuel efficiency both by removing the necessity of filter regeneration and by secondary power generation which can decrease the power consumption requirements of the alternator.

Acknowledgement

The authors would like to thank the US Department of Education GAANN fellowship for financial support of this research.

References

[1] S. Park, J.M. Vohs, R.J. Gorte, Lett. Nat. 404 (2000) 265–267.
[2] D. Cao, Y. Sun, G. Wang, J. Power Sources 167 (2007) 250–257.
[3] H. Christensen, J. Dinesen, H.H. Engell, K.K. Hansen, Soc. Auto. Eng. (1999), 1999-01-0472.
[4] A. Raimondi, D. Fino, G. Saracco, J. Power Sources 193 (2009) 338–341.
[5] S. Hasegawa, M. Ihara, J. Electrochem. Soc. 155 (2008) B58–B63.
[6] P. Hofmann, A. Schweiger, L. Fryda, K.D. Panopoulos, U. Hohenwarter, J.D. Bentzen, J.P. Ouweltjes, J. Ahrenfeldt, U. Henriksen, E. Kakaras, J. Power Sources 173 (2007) 357–366.
[7] T.J. Huang, C.H. Wang, J. Power Sources 163 (2006) 309–315.
[8] M. Ihara, K. Matsuda, H. Sato, C. Yokoyama, Solid State Ionics 175 (2004) 51–54.
[9] T. Nakamura, K. Yashiro, A. Kamai, T. Otake, K. Sato, T. Kawada, J. Mizusaki, J. Electrochem. Soc. 155 (2008) B1244–B1250.
[10] M. Ihara, S. Hasegawa, J. Electrochem. Soc. 153 (2006) A1544–A1546.
[11] Q.L. Liu, K.A. Khor, S.H. Chan, X.J. Chen, J. Power Sources 162 (2006) 1036–1042.
[12] T.L. Nguyen, K. Kobayashi, T. Honda, Y. Iimura, K. Kato, A. Neghisi, K. Nozaki, F. Tappero, K. Sasaki, H. Shirahama, K. Ota, M. Dokiya, T. Kato, Solid State Ionics 174 (2004) 163–174.
[13] A. Tsoga, A. Gupta, A. Naoumidis, P. Nikolopoulos, Acta Mater. 48 (2000) 4709–4714.
[14] X.Y. Zhao, Q. Yao, S.Q. Li, N.S. Cai, J. Power Sources 185 (2008) 104–111.

BIBLIOGRAPHY

[1] M. Yano, M. Nagao, K. Okamoto, A. Tomita, Y. Uchiyama, N. Uchiyama, T. Hibino, A Single-Chamber SOFC Stack Operating in Engine Exhaust, *Electrochemical and Solid-State Letters*, 11, B29-B33 (2008).

[2] T. Hibino, A. Hashimoto, T. Inoue, S. Tokuno, M. Sano, A Low-Operating-Temperature Solid Oxide Fuel Cell in Hydrocarbon-Air Mixtures, *Science*, 288, 2031-2033 (2000).

[3] T. Hibino, A. Hashimoto, M. Yano, M. Suzuki, S. Yoshida, S., M. Sano, A Solid Oxide Fuel Cell Using an Exothermic Reaction as the Heat Source, *Journal of the Electrochemical Society*, 148, A544-A549 (2001).

[4] I. Reiss, The Significance of Impeded Reactions in Solid State Electrochemistry, *Solid State Ionics*, 176, 1667-1674 (2005).

[5] M.A. Priestnall, V.P. Kotzeva, D.J. Fish, E.M. Nilsson, Compact Mixed-Reactant Fuel Cells, *Journal of Power Sources*, 106, 21-30 (2002).

[6] S. Tao, J. Irvine, A Redox-Stable Efficient Aanode for Solid-Oxide Fuel Cells, *Nature Materials*, 2, 320-323 (2003).

[7] N.M. Tikekar, T.J. Armstrong, A.V. Virkar. Reduction and Reoxidation Kinetics of Nickel-Based SOFC Anodes, *Journal of the Electrochemical Society*, 153, A654-A663 (2006).

[8] I. Riess, P.J. van der Put, J. Schoonman, Solid Oxide Fuel Cells Operating on Uniform Mixtures of Fuel and Air, *Solid State Ionics*, 82, 1-4 (1995).

[9] T. Suzuki, P. Jasinski, V. Petrovsky, H.U. Anderson, F. Dogan, Performance of a Porous Electrolyte in Single-Chamber SOFCs, *Journal of the Electrochemical Society*, 152, A527-A531 (2005).

[10] T. Hibino, A. Hashimoto, T. Inoue, J. Tokuno, S. Yoshida, M. Sano, Single-Chamber Solid Oxide Fuel Cells at Intermediate Temperatures with Various Hydrocarbon-Air Mixtures, Journal of the Electrochemical Society, 147, 2888-2892 (2000).

[11] S.B. Adler, Factors Governing Oxygen Reduction in Solid Oxide Fuel Cell Cathodes, *Chemical Reviews*, 104, 4791-484 (2004).

[12] T. Hibino, S. Wang, S. Kakimoto, M. Sano, Single Chamber Solid Oxide Fuel Cell Constructed from an Yttria-Stabilized Zirconia Electrolyte, *Electrochemical and Solid-State Letters*, 2, 317-319 (1999).

[13] T. Hibino, A. Hashimoto, M. Yano, M. Suzuki, S. Yoshida, M. Sano, High Performance Anodes for SOFCs Operating in Methane-Air Mixture at Reduced Temperatures, *Journal of the Electrochemical Society*, 149, A133-A136 (2002).

[14] R.J. Gorte, J.M. Vohs, S. McIntosh, Recent Developments on Anodes for Direct Fuel Utilization in SOFC, *Solid State Ionics*, 175, 1-6 (2004).

[15] P. Jasinski, T. Suzuki, F. Dogan, H.U. Anderson, Impedance Spectroscopy of Single Chamber SOFC, *Solid State Ionics*, 175, 35-38 (2004).

[16] T.W. Napporn, F. Morin, M. Meunier, Evaluation of the Actual Working Temperature of A Single-Chamber SOFC, *Electrochemical and Solid-State Letters*, 7, A60-A62 (2004).

[17] P. Jasinski, V. Petrovsky, T. Suzuki, T. Petrovsky, H.U. Anderson, Electrical Properties of YSZ Films Prepared by Net Shape Technology, *Journal of the Electrochemical Society*, 152, A454-A458 (2005).

[18] P. Babilo, S.M. Haile, Enhanced Sintering of Yttrium-Doped Barium Zirconate by Addition of ZnO, *Journal of the American Ceramic Society*, 88, 2362–2368 (2005).

[19] R. Guentes, R. Baker, Synthesis and Properties of Gadolinium-Doped Ceria Solid Solutions for IT-SOFC Eelectrolytes, *International Journal of Hydrogen Energy*, 33, 3480-3484 (2008).

[20] T. Suzuki, P. Jasinski, H.U. Anderson, F. Dogan, Single Chamber Electrolyte Supported SOFC Module, *Electrochemical and Solid-State Letters*, 7, A391-A393 (2004).

[21] T. Hibino, A. Hashimoto, M. Suzuki, M. Yano, S. Yoshida, M. Sano, A Solid Oxide Fuel Cell with a Novel Geometry That Eliminates the Need for Preparing a Thin Electrolyte Film, *Journal of the Electrochemical Society*, 149, A195-A200 (2002).

[22] H. Moon, S. Kim, S. Hyun, H. Kim, Development of IT-SOFC Unit Cells With Anode-Supported Thin Electrolytes via Tape Casting and Co-Firing, *International Journal of Hydrogen Energy*, 33, 1758-1768 (2008).

[23] T. Suzuki, P. Jasinski, V. Petrovsky, H.U. Anderson, F. Dogan, Anode Supported Single Chamber Solid Oxide Fuel Cell in CH4-Air Mixture, Journal of the Electrochemical Society, 151, A1473-A1476 (2004).

[24] T.W. Napporn, X. Jacques-Bedard, F. Morin, M. Meunier, Operating Conditions of a Single-Chamber SOFC, *Journal of the Electrochemical Society*, 151, A2088-A2094 (2004).

[25] S. Asahara, D. Michiba, M. Hibino, T. Yao, Single Chamber SOFC Using $BaLaIn_2O_{5.5}$ Solid Electrolyte, *Electrochemical and Solid-State Letters*, 8, A449-A451 (2005).

[26] T. Uda, D.A. Boysen, C.R.I. Chisholm, S.M. Haile, Alcohol Fuel Cells at Optimal Temperatures, *Electrochemical and Solid-State Letters*, 9, A261-A264 (2006).

[27] T. Hibino, H. Tsunekawa, S. Tanimoto, M. Sano, Improvement of a Single-Chamber Solid-Oxide Fuel Cell and Evaluation of New Cell Designs, *Journal of the Electrochemical Society*, 147, 1338-1343 (2000).

[28] S.M. Haile, G. Staneff, K.H. Ryu, Non-Stoichiometry, Grain Boundary Transport and Chemical Stability of Proton Conducting Perovskites, *Journal of Materials Science*, 36, 1149-1160 (2001).

[29] Z. Shao, S.M. Haile, J. Ahn, P.D. Ronney, Z. Zhan, S.A. Barnett, A Thermally Self-Sustained Micro Solid-Oxide Fuel-Cell Stack With High Power Density, *Nature*, 435, 795-798 (2005).

[30] X. Jacques-B'edard, T.W. Napporn, R. Roberge, M. Meunier, Performance and Ageing of an Anode-Supported SOFC Operated in Single-Chamber Conditions, *Journal of Power Sources*, 153, 108-113 (2006).

[31] B.C.H. Steele, Survey of Materials Selection for Ceramic Fuel Cells, *Solid State Ionics*, 86-88, 1223-1234 (1996).

[32] V. Petrovsky, T. Suzuki, P. Jasinski, H.U. Anderson, Low-Temperature Processed Anode for Solid Oxide Fuel Cells, *Electrochemical and Solid-State Letters*, 8, A341-A343 (2005).

[33] P. Jasinski, T. Suzuki, V. Petrovsky, H.U. Anderson, Nanocomposite Nickel Ceria Cermet with Low Nickel Content for Anode-Supported SOFCs, *Electrochemical and Solid-State Letters*, 8, A219-A221 (2005).

[34] H. Moon, S. Kim, E. Park, S. Hyun, H. Kim, Characteristics of SOFC Single Cells With Anode Active Layer via Tape Casting and Co-Firing, *International Journal of Hydrogen Energy*, 33, 2826-2833 (2008).

[35] T. Suzuki, P. Jasinski, H. Anderson, F. and Dogan, Role of Composite Cathodes in Single Chamber SOFC, *Journal of the Electrochemical Society*, 151, A1678-A1682 (2004).

[36] Z. Shao, C. Kwak, S.M. Haile, Anode-Supported Thin-Film Fuel Cells Operated in a Single Chamber Configuration 2T-I-12, *Solid State Ionics*, 175, 39-46 (2004).

[37] Z. Shao, S.M. Haile, A High Performance Cathode for the Next Generation of Solid Oxide Fuel Cells, *Nature*, 431, 170-173 (2004).

[38] R. Chiba, F. Yoshimura, Y. Sakurai, Y. Tabata, M. Arakawa, A Study of Cathode Materials for Intermediate Temperature SOFCs Prepared by the Sol-gel Method, *Solid State Ionics*, 175, 23-27 (2004).

[39] S. Park, J.M. Vohs, R.J. Gorte, Direct Oxidation of Hydrocarbons in a Solid-Oxide Fuel Cell, *Letters to Nature*, 404, 265-267 (2000).

[40] T. Iida, M. Kawano, T. Matsui, R. Kikuchi, K. Eguchi, Carbon Deposition on Fuel Electrode and Subsequent Deterioration of Cell, *Journal of the Electrochemical Society*, 154, B234-B241 (2007).

[41] Y. Lin, Z. Zhan, J. Liu, S. Barnett, Direct Operation of Solid Oxide Fuel Ccells With Methane Fuel, *Solid State Ionics*, 176, 1827-1835 (2005).

[42] C.Y. Sheng, A.M. Dean, Importance of Gas-Phase Kinetics Within the Anode Channel of a Solid-Oxide Fuel Cell, *Journal of Physical Chemistry A*, 108, 3772-3783 (2004).

[43] X.Y. Zhao, Q. Yao, S.Q. Li, N.S. Cai, Studies on the Carbon Reactions in the Anode of Deposited Carbon Fuel Cells, *Journal of Power Sources*, 185, 104-111 (2008).

[44] D. Cao, Y. Sun, G. Wang, Direct Carbon Fuel Cell: Fundamentals and Recent Developments, *Journal of Power Sources*, 167, 250-257 (2007).

[45] M. Ihara, K. Matsuda, H. Sato, C. Yokoyama, Solid State Fuel Storage and Utilization Through Reversible Carbon Deposition on an SOFC Anode, *Solid State Ionics*, 175, 51-54 (2004).

[46] T.J. Huang, C.H. Wang, Factors in Forming CO and CO_2 Over a Cermet of Ni-Gadolinia-Doped Ceria With Relation to Direct Methane SOFCs, *Journal of Power Sources*, 163, 309-315 (2006).

[47] S. Hasegawa, M. Ihara, Reaction Mechanism of Solid Carbon Fuel in Rechargeable Ddirect Carbon SOFCs With Methane for Charging, *Journal of the Electrochemical Society*, 155, B58-B63 (2008).

[48] T. Nakamura, K. Yashiro, A. Kamai, T. Otake, K. Sato, T. Kawada, J. Mizusaki, Determination of Reaction Zone in Gadolinia-Doped Ceria Anode for Solid Oxide Fuel Cell, *Journal of the Electrochemical Society*, 155, B1244-B1250 (2008).

[49] M. Ihara, S. Hasegawa, Quickly Rechargeable Direct Carbon Solid Oxide Fuel Cell With Propane for Recharging, *Journal of the Electrochemical Society*, 153, A1544-A1546 (2006).

[50] A. Tsoga, A. Gupta, A. Naoumidis, P. Nikolopoulos, Gadolinia-Doped Ceria and Yttria Stabilized Zirconia Interfaces: Regarding Their Application for SOFC Technology, *Acta Materialia*, 48, 4709-4714 (2000).

[51] P. Hofmann, A. Schweiger, L. Fryda, K.D. Panopoulos, U. Hohenwarter, J.D. Bentzen, J.P. Ouweltjes, J. Ahrenfeldt, U. Henriksen, E. Kakaras, High Temperature Electrolyte Supported Ni-GDC/YSZ/LSM SOFC Operation on Two-Stage Viking Gasifier Product Gas, *Journal of Power Sources*, 173, 357-366 (2007).

[52] M.F. Chandler, Y. Teng, U.O. Koylu, Diesel Engine Particulate Emissions: A Comparison of Mobility and Microscopy Size Mmeasurements, *Proceedings of the Combustion Institute*, 31, 2971-2979 (2007).

[53] A. Neer, U.O. Koylu, Effect of Operating Conditions on the Size, Mmorphology, and Concentration of Submicrometer Particulates Emitted Ffrom a Diesel Engine, *Combustion and Flame*, 146, 142-154 (2006).

[54] D.B. Kittelson, Engines and Nanoparticles: A Review, *Journal of Aerosol Science*, 29, 575-588 (1998).

[55] R.A. Yapaulo, E. Wirojsakunchai, T. Orita, D.E. Foster, M. Akard, L.R. Walker, M.J. Lance, Impact of Filtration Velocities and Particulate Matter Characteristics on Diesel Particulate Filter Wall Loading, *International Journal of Engine Research*, 10, 287-304 (2009).

[56] M. Bergmann, U. Kirchner, R. Vogt, T. Benter, On-Road and Laboratory Iinvestigation of Low-Level PM Emissions of a Modern Diesel Particulate Filter Equipped Diesel Passenger Car, *Atmospheric Environment*, 43, 1908-1916 (2009).

[57] G. Bikas, E. Zervas, Regulated and Non-Regulated Pollutants Emitted during the Regeneration of a Diesel Particulate Filter, *Energy and Fuels*, 21, 1543-1547, (2007).

[58] J. Lee, N. Sung, G. Cho, K. Oh, Modeling of Filtration for a Metal Foam Diesel Particulate Filter, *Key Engineering Materials*, 326-328, 1153-1156, (2006).

[59] A.J. Pyzik, C.G. Li, New Design of a Ceramic Filter for Diesel Emission Control Applications, *International Journal of Applied Ceramic Technology*, 2, 440-451, (2005).

[60] D. Donijayaseelan, S. Ueno, h. Kita, N. Kondo, T. Ohji, Development of a Novel Design for Diesel Particulate Filter, *Journal of Porous Materials*, 12, 47-53 (2005).

[61] K. Yamamoto, S. Satake, H. Yamashita, Microstructure and Particle-Laden Flow in Diesel Particulate Filter, *International Journal of Thermal Sciences*, 48, 303-307 (2009).

[62] M. Kostoglou, A.G. Kostandopoulos, Effect of Soot Layer Microstructure on Diesel Particulate Filter Regeneration, AIChE Journal, 51, 2534-2546 (2005).

[63] S. Pallavkar, T.H. Kim, D. Rutman, J. Lin T. Ho, Active Regeneration of Diesel Particulate Filter Employing Microwave Heating, *Industrial and Engineering Chemistry Research*, 48, 69-79 (2009).

[64] M. Okubo, K. Yoshida, Continuous Regeneration of Ceramic Particulate Filter in Stationary Diesel Engine by Nonthermal-Plasma-Induced Ozone Injection, *IEEE Transactions on Industry Applications*, 45, 1568-1574 (2009).

[65] M. Okubo, T. Kuroki, Y. Miyairi, T. Yamamoto, Low-Temperature Soot Incineration of Diesel Particulate Filter Using Remote Nonthermal Plasma Induced by a Pulsed Barrier Discharge, *IEEE Transactions on Industry Applications*, 40, 1504-1512 (2004).

[66] C.N. Millet, P. Ménégazzi, B. Martin, H. Colas, Modeling of Diesel Particulate Filter Regeneration, with the Effect of Fuel-Borne Catalyst on Pressure Losses and Soot Oxidation Kinetics, *Oil and Gas Science and Technology - Revue de IFP*, 58, 151-162 (2003).

[67] I. Reiss, On the Single Chamber Solid Oxide Fuel Cells, *Journal of Power Sources*, 175, 325-337 (2008).

[68] M. Yano, A. Tomita, M. Sano, T. Hibino, Recent Advances in Single-Chamber Solid Oxide Fuel Cells: A Rreview, *Solid-State Ionics*, 177, 3351-3359 (2007).

[69] J. Hustad, O. Sonju, Experimental Studies of Lower Flammability Limits of Gases and Mixtures of Gases at Elevated Temperatures, *Combustion and Flame*, 71, 283-294 (1988).

[70] M. Boillot, C. Bonnet, S. Didierjean, F. Lapicque, Investigation of the Response of Separate Electrodes in a Polymer Electrolyte Membrane Fuel Cell Without Reference Electrode, *Journal of Applied Electrochemistry*, 37, 103-110 (2007).

[71] I.C. Stefan, C.P. Jacobson, S.J. Visco and L.C. De Jonghe, Single Chamber Fuel Cells: Flow Geometry, Rate, and Composition Considerations, *Electrochemical and Solid-State Letters*, 7, A198-A200 (2004).

[72] H. Christensen, J. Dinesen, H.H. Engell, K.K. Hansen, Electrochemical Reactor for Exhaust Gas Purification, *Society of Automotive Engineers*, 1999-01-0472 (1999).

[73] A. Raimondi, D. Fino, G. Saracco, New Concept for Soot Removal From a Syngas Mixture, *Journal of Power Sources*, 193, 338-341 (2009).

[74] Q.L. Liu, K.A. Khor, S.H. Chan, X.J. Chen, Anode-Supported Solid Oxide Fuel Cell With Yttria-Stabilized Zirconia/Gadolinia-Doped Ceria Bilayer Electrolyte Prepared by Wet Ceramic Co-Sintering Process, *Journal of Power Sources*, 162, 1036-1042 (2006).

[75] T.L. Nguyen, K. Kobayashi, T. Honda, Y. Iimura, K. Kato, A. Neghisi, K. Nozaki, F. Tappero, K. Sasaki, H. Shirahama, K. Ota, M. Dokiya, T. Kato, Preparation and Evaluation of Doped Ceria Interlayer on Supported Stabilized Zirconia Electrolyte SOFCs by Wet Ceramic Processes, *Solid State Ionics*, 174, 163-174 (2004).

[76] B. Yang, B. Hu, U.O. Koylu, Mean Soot Volume Fractions in Turbulent Hydrocarbon Flames: a Comparison of Sampling and Laser Measurements, *Combustion Science and Technology*, 177, 1603-1626 (2005).

[77] Y. Jinliang, B. Sunden, Analysis of Intermediate Temperature Solid Oxide Fuel Cell Transport Processes and Performance, *Transactions of the ASME*, 127, 1380-1390 (2005).

[78] P.W. Li, M.K. Chyu, Electrochemical and Transport Phenomena in Solid Oxide Fuel Cells, *Transactions of the ASME*, 127, 1344-1362, (2005).

[79] R.J. Moffat, Contributions to the Theory of Single-Sample Uncertainty Analysis, *Transactions of the ASME*, 104, 250-258 (1982).

VITA

Isaiah Daniel Kellogg, the son of Gary and Katty Kellogg, was born in Strafford, Missouri on January 17, 1982. After graduating from Strafford High School in 2000, he began attending the University of Missouri – Rolla. In 2003, Isaiah spent the summer working at the NASA Marshall Space Flight Center with the Undergraduate Student Research Program, but due to the recent crash of the Space Shuttle Columbia, he was put on the Return to Flight effort, helping to redesign part of the Space Shuttle External Tank. In 2005, Isaiah graduated with a Bachelor's degree in Mechanical Engineering.

In the same year, he was admitted into the PhD program at the University of Missouri – Rolla, now the Missouri University of Science and Technology, to study solid oxide fuel cells under the supervision of Dr. Umit O. Koylu and Dr. Fatih Dogan. In the course of his research, he has published papers in many venues, including International Journal of Hydrogen Energy, Journal of Power Sources, Electrochemical Society Transactions, the NATO Advanced Research Workshop, and several conferences.